



A SPREAD PLASTICITY FLEXURE-SHEAR INELASTIC FINITE ELEMENT FOR THE STUDY OF RC STRUCTURES

A Dissertation Submitted in Partial Fulfilment of the Requirements
for the Doctorate of Philosophy in

Urban and Territorial Risk Assessment and Mitigation

By

Mr. Vito Valotta

Tutor: Prof. Salvatore Caddemi

Supervisors: Prof. Ivo Calì

Prof. Enrico Spacone

Dr. Antonino Russo

July, 2017

Università degli Studi di Catania

The dissertation entitled “A SPREAD PLASTICITY SHEAR-FLEXURE FINITE ELEMENT FOR THE STUDY OF RC STRUCTURES”, by Mr. Vito Valotta, has been approved in partial fulfilment of the requirements for the Doctorate of Philosophy in Urban and Territorial Risk Assessment and Mitigation.

Prof. Salvatore Caddemi_____

ABSTRACT

The aim of this thesis is to achieve a new finite element formulation for framed RC structures capable to model the flexure-shear interaction both in terms of stiffness, strength and residual ductility. The objective is not the definition of an itemized model, rather an accurate model with a sustainable computational cost for the seismic vulnerability analysis of existing buildings. Especially for non slender structures, the contribution to the nonlinear behaviour due to flexure may be not sufficient and flexure-shear interaction changes deeply the structural response.

This new finite element is based on the adoption of Heaviside's distributions functions to model abrupt, both flexural and shear, stiffness discontinuities of the beam, by which it is possible to lead to the exact closed-form solution of the Timoshenko beam differential equations. The new frame element is composed by two sectional constitutive models, one for flexure and one for shear, that can interact by means of an empirical relation that relates curvature demand and shear strength degradation.

The flexure-shear model is verified against experimental tests on RC rectangular columns, walls and frames. Comparisons with experimental results on these shear-sensitive elements shows relatively good agreement.

Keywords: Nonlinear Analysis, Flexure-Shear Interaction (FSI), Shear Deformations

SUMMARY

In this thesis, a new finite element for framed RC structures capable to model the flexure-shear interaction both in terms of stiffness, strength and residual ductility is formulated. The model strategy that is used is the spread plasticity approach because is a great evolution of the concentrated plasticity models, and as such helps to improve results especially in cyclic non-linear analysis. A distributed plasticity model with a fiber discretization has the advantage to be self consistent from a P-Mz-My interaction but the model implies computational complexity and cost for relatively large structures with many elements. From this point of view the spread plasticity model has a convenient computational cost, because the constitutive laws are expressed in terms of sectional quantities.

The spread plasticity model is classically formulated using the principle of virtual work in order to determine the element flexibility matrix and this is equivalent to imposing equilibrium in the nodes (in the solution the stiffness matrix is used). There are alternatives methods that are not using the principle of virtual work, the one presented in section 6.1.1 makes use of the theory of distributions to solve the Timoshenko beam differential equations that directly govern the structural problem. In other words adopting Heaviside's distributions functions to model abrupt, both flexural and shear, stiffness discontinuities of the beam (see equations (6.2)), it is possible to lead to the exact closed-form solution because it is based on the differential equation associated (strong formulation). This alternative approach is the base of the proposed finite element.

The new frame element is composed by two sectional constitutive models, one for flexure and one for shear, that can interact by means of an empirical relation that relates curvature demand and shear strength degradation. The flexure-shear model is verified against experimental tests on RC rectangular columns, walls and frames. Comparisons with experimental results on these shear-sensitive elements shows relatively good agreement. Nevertheless, numerical complications are encountered, associated to the post-peak strength degradation that it is not fully captured if the shear strength degradation is dominant in the experimental test. Therefore, it seems that both at the element and sectional level additional improvements are required.

ACKNOWLEDGEMENTS

First of all I want to thank Prof. Salvatore Caddemi and Prof. Ivo Calìo for their support throughout the PhD program, for all the time they spent reviewing my thesis and especially for their competence.

Secondly this work is dedicated to all the components of the research group that is Prof. Enrico Spacone, Dr Antonino Russo, Prof. Annalisa Greco, Dr Francesco Cannizzaro, Dr Giuseppe Occhipinti that help me in this very intense period.

I want to acknowledge the reviewers Prof. Shing and Prof Mergos for their revision work that helps me to improve the thesis.

Finally I want to thank my wife and my parents for their sustenance.




TABLE OF CONTENTS

ABSTRACT	i
SUMMARY	ii
ACKNOWLEDGEMENTS	iii
1 INTRODUCTION	1
1.1 Research objectives	1
1.2 Organisation of the thesis	3
2 SHEAR IN BEAMS & COLUMNS	4
2.1 Shear in flexural members	4
2.2 Relations among moment, shear, and bond	6
2.2.1 Beam action and arch action	9
2.2.2 Internal forces in members with transverse reinforcement	10
2.2.3 Truss Model	12
2.2.4 Empirical Approach for Shear Strength of Beams and Columns	13
2.2.5 Strength of Members without Transverse Reinforcement	13
2.2.6 Members with Transverse Reinforcement	17
2.2.7 Effects of Inelastic Cyclic Loading	19
3 FINITE ELEMENT FORMULATIONS	25
3.1 Introduction	25
3.1.1 Lumped plasticity	28
3.1.2 Distributed plasticity	29
3.1.3 Spread plasticity	35
3.2 Final considerations	42
4 BEAM MODELS WITH MULTIPLE SINGULARITIES	43

4.1	Introduction	43
4.2	Euler–Bernoulli beams with multiple singularities	43
4.3	Final considerations.....	47
5	RC FRAME STRUCTURES ELEMENTS WITH SHEAR MODELLING	48
5.1	Introduction	48
5.2	Main approaches	48
5.2.1	Martinelli’s model.....	48
5.2.2	Ranzo and Petrangeli’s model	52
5.2.3	Petrangeli, Pinto and Ciampi’s model	55
5.2.4	Vecchio and Collins’ model.....	57
5.2.5	Marini and Spacone’s model	59
5.2.6	Ceresa et al. model.....	64
5.2.7	Mergos and Kappos’s model	68
6	THE PROPOSED FINITE ELEMENT.....	76
6.1	Introduction	76
6.1.1	Timoshenko beams with multiple singularities	77
6.1.2	Closed-form calculation of the Timoshenko stiffness matrix terms.....	83
6.1.3	Beam finite element with discontinuities.....	84
6.2	Formulation	86
6.2.1	Flexure constitutive law	88
6.2.2	Shear constitutive law	89
6.2.3	Flexure-Shear interaction.....	91
7	NUMERICAL VERIFICATIONS	93
7.1	Linear analysis.....	93
7.1.1	Portal frame with an horizontal force	93
7.2	Inelastic analysis	98
7.2.1	Lynn 1996	98
7.2.2	Dazio 2009.....	104
7.2.3	Duong 2007.....	117
8	CONCLUSIONS	126
	REFERENCES	128

LIST OF FIGURES

Figure 1 – Year of first seismic classification of Italian municipalities (ingvterremoti.wordpress.com).....	1
Figure 2 - percentage of dwellings built through the years (Censimento ISTAT 2001).	2
Figure 3 - Axial, flexural, and shearing actions on a column [Moe14].	5
Figure 4 - Cantilever beam with concentrated load [Moe14].	6
Figure 5 - Free-body diagram of short length of reinforcing bar [Moe14].	7
Figure 6 – Tested beams without stirrups [VS04].	8
Figure 7 - Theoretical beam action and arch action [Moe14].	9
Figure 8 - Practical conditions for beam action and arch action [Moe14].	10
Figure 9 - Internal forces in member with transverse reinforcement [Moe14].	11
Figure 10 – Ritter’s original drawing of the truss analogy (a) and shear forces (b) [CM97]. ...	12
Figure 11 – Truss model for simple supported beam [Moe14].	13
Figure 12 - Damage at failure in series of tests on beams without transverse reinforcement. (After leonhardt, 1962.)	14
Figure 13 - Shear at failure as function of aspect ratio for beams without transverse reinforcement [PP75].	15
Figure 14 - Nominal shear strength of beams without transverse reinforcement (After ACI-ASCE 326, 1962).	16
Figure 15 - Comparison of measured and calculated strengths as function of v_s provided (After ACI-ASCE 326, 1962).	18
Figure 16 - Idealized behaviour for yielding transverse reinforcement [Moe14].	19
Figure 17 - Surface deformations and cracks of beam in advanced stages of cyclic loading. Crack widths and deformations are amplified by factor 5.0 (After Popov, 1984).....	20
Figure 18 - Shear-displacement relations for (a) flexure-controlled column and (b) shear-controlled column. (After Higashi and Hirose, 1974.).....	20
Figure 19 - Elongation of flexural plastic hinge with cycling [LW03].	21
Figure 20 – γ parameter for V_c [PCK07].	22
Figure 21 – V_p contribution [PCK07].	23
Figure 22 - Shear strength degradation model [SM04].	24
Figure 23– Inelastic beam element, (a) lumped, (b) distributed [MID15].	26
Figure 24 – Curvature distribution along the element [IDA96].	27
Figure 25 - Two component beam model.	28
Figure 26 – Giberson one component beam model.	28

Figure 27 – One component element with rigid end zones.	29
Figure 28 – Finite element decrease of freedom.	29
Figure 29 – Fibers discretization of the element cross section [MID15].....	31
Figure 30 – Discretized rc cross section.	32
Figure 31 – Filament model (Taylor 1976).....	33
Figure 32 – Malerba-Bontempi's finite element; (a) coordinate system, nodal forces, nodal displacements, Gauss points; (b) section quadrilateral subdomain; (c) Shape functions [MB89].	34
Figure 33 Shape function of the element [SFT96].....	35
Figure 34 – Discrete Element models (a) [Po75] and (b) [TS76] from [OTA80].	36
Figure 35 – Takizawa's model [TAK73] from [OTA80].	36
Figure 36 – Park et al. model from [PRK87].....	37
Figure 37 – Spread models with constant (b) and linear (c) flexibility [RRL12].....	38
Figure 38 – Unit virtual force: (a) moments and (b) corresponding shears at the ends i and j [RRL12].	39
Figure 39 - Distribution of: (a) moment and (b) flexibility [RRL12].....	41
Figure 40– Type of distributions for different values of the power n at section i [RRL12].	42
Figure 41 – Beam with discontinuities in the Young modulus $E(x)$ and in the inertia moment $I(x)$ [BC07].	44
Figure 42-A beam with Dirac's delta singularities in the flexural stiffness, correspondent to (b) a beam with internal hinges and rotational springs with stiffnesses $k_{\phi,i}$. [BC07].	44
Figure 43– Nodal degrees of freedom of Martinelli's Fiber element [MAR98].	49
Figure 44 – (a) Inclined strut, (b) Mohr's circle used in arch action mechanism, and (c) assemblage used to model truss mechanism [MAR98].	49
Figure 45– Stress shape functions and element forces and deformations [RP98].	52
Figure 46– Section shear hysteretic model — skeleton and degraded curves [RP98].	53
Figure 47 – Beam segment truss idealization [RP98].....	53
Figure 48– Section and fiber mechanics [PPC99].	55
Figure 49 - Beam section discretization. Estimates of longitudinal strain gradient and shear flow distribution are required across section [VC88].	57
Figure 50– Dual section analysis: (a) scheme and free-body diagram for concrete layer k, and (b) solution procedure for beam analysis model [VC88].....	58
Figure 51 – Frame element forces and deformations [MS06].	59
Figure 52– Timoshenko element: section forces, deformations, and strain distributions [MS06].	59
Figure 53 – Section shear law: possible envelope curves. [MS06].	62
Figure 54– Section shear law: hysteretic rules [MS06].	62
Figure 55 - Element state determination of the developed Timoshenko fiber beam element from [CPPS09].....	66
Figure 56 – Uniaxial laws for reinforcement (a) and concrete (b) from [CPPS09].....	67
Figure 57- Flexural sub-element [MK08].....	69
Figure 58 - Primary curve without degradation for shear force vs shear deformation [MK08].	70

Figure 59 - Relationship between curvature ductility demand and strength of concrete shear resisting mechanisms [PSC96].	71
Figure 60 - Shear–flexure interaction procedure [MK08].	72
Figure 61 - Derivation of shear primary curve after modelling shear–flexure interaction effect: (a) flexural primary curve in terms of member shear force and curvature ductility demand of the critical cross section and (b) shear ($V-\gamma$) primary curve after modelling shear–flexure interaction [MK08].	73
Figure 62 - Shear sub-element: (a) dominant gravity loading and (b) dominant seismic loading.	74
Figure 63 - (a) A beam with Dirac’s delta singularities in the flexural stiffness, correspondent to (b) a beam with internal hinges and rotational springs with stiffnesses $k_{\phi,i}$ [BC07].	78
Figure 64 – First row/column stiffness matrix derivation.	83
Figure 65 – Finite element’s dof [RAP12].	84
Figure 66– The proposed finite element.	86
Figure 67 – Degraded hysteretic model [CBW65].	88
Figure 68 – $V_0-\gamma$ curve.	90
Figure 69 – Element state determination of the Timoshenko beam element.	92
Figure 70 – Frame with discontinuities.	93
Figure 71– Deformed shape Midas.	94
Figure 72 – Code deformed shape [mm].	95
Figure 73 – Code rotations.	95
Figure 74– Bending moment diagram Midas.	96
Figure 75– Code bending moment diagram.	96
Figure 76 – Shear diagram Midas.	97
Figure 77 – Code shear diagram.	97
Figure 78 – Setup of Lynn 1996 [LMMH96].	98
Figure 79 – Reinforcement details [LMMH96].	99
Figure 80 – Force-displacement comparison.	100
Figure 81 - Total vs displacement due to shear strain.	100
Figure 82 – Inelastic dimensionless extension zone time history.	101
Figure 83 – Hysteretic loops quantity.	101
Figure 84 – Displacement functions along the element $u(\xi)$.	102
Figure 85 – Rotation functions along the element $\phi(\xi)$.	102
Figure 86 – Curvature functions along the element $\chi(\xi)$.	103
Figure 87 – Shear strain functions along the element $\gamma(\xi)$.	103
Figure 88 – Setup of Dazio 09 [DBB09].	104
Figure 89 - Longitudinal reinforcement details [DBB09].	105
Figure 90 - Transversal reinforcement details of WSH3 [DBB09].	106
Figure 91 - Transversal reinforcement details of WSH4 [DBB09].	106
Figure 92 - Force-displacement comparison for WSH3.	107
Figure 93 – Total vs displacement due to shear strain for WSH3.	107
Figure 94 – Inelastic dimensionless extension zone time history for WSH3.	108
Figure 95 – Hysteretic loops quantity.	109

Figure 96 - Displacement functions along the element $u(\xi)$	110
Figure 97 – Rotation functions along the element $\phi(\xi)$	110
Figure 98 – Curvature functions along the element $\chi(\xi)$	111
Figure 99 – Shear strain functions along the element $\gamma(\xi)$	111
Figure 100 - Force-displacement comparison for WSH4.	112
Figure 101 - Total vs displacement due to shear strain for WSH4.	112
Figure 102 – Inelastic dimensionless extension zone time history for WSH4.	113
Figure 103 – Hysteretic loops quantity.	114
Figure 104 - Displacement functions along the element $u(\xi)$	115
Figure 105 – Rotation functions along the element $\phi(\xi)$	115
Figure 106 – Curvature functions along the element $\chi(\xi)$	116
Figure 107 – Shear strain functions along the element $\gamma(\xi)$	116
Figure 108 – Frame Reinforcement Layout [DSV07].	117
Figure 109 – Designed frame cross-sections [DSV07].....	118
Figure 110 – Full steel and partial formwork assembly [DSV07].....	119
Figure 111 – Test setup [DSV07].	119
Figure 112 – Force-displacement comparison.	120
Figure 113 - Force-displacement comparison.....	121
Figure 114 – Load step 40.	122
Figure 115 – Load Step 60.....	122
Figure 116 – Load step 80.	122
Figure 117 – Load step 92.	122
Figure 118 – Shear force diagram.....	124
Figure 119 – Bending moment diagram.	124
Figure 120 Rotation functions along the element $\phi(\xi)$	125
Figure 121 – Curvature functions along the element $\chi(\xi)$	125

1 INTRODUCTION

1.1 Research objectives

The aim of this thesis is to achieve a new finite element formulation for framed RC structures capable to model the flexure-shear interaction both in terms of stiffness, strength and residual ductility. The objective is not the definition of an itemized model, rather an accurate model with a sustainable computational cost for the seismic vulnerability analysis of existing buildings. Figure 1 shows the year of first seismic classification of Italian municipalities; the city of Catania was classified as seismic risk area in 1981.

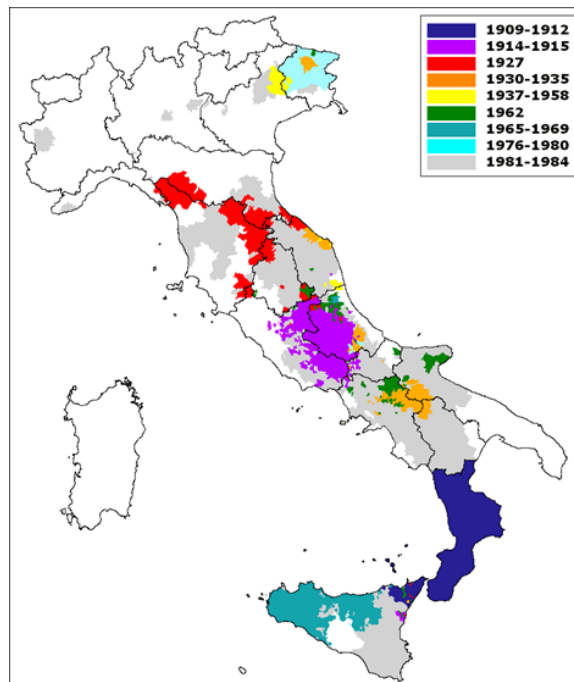


Figure 1 – Year of first seismic classification of Italian municipalities (ingvterremoti.wordpress.com).

Figure 2 shows the percentage of dwellings built through the years; so it is easy to see that at least 80% of the buildings in the city of Catania (and in his province) were designed without specific seismic provisions. This makes Catania extremely vulnerable from a seismic point of view.

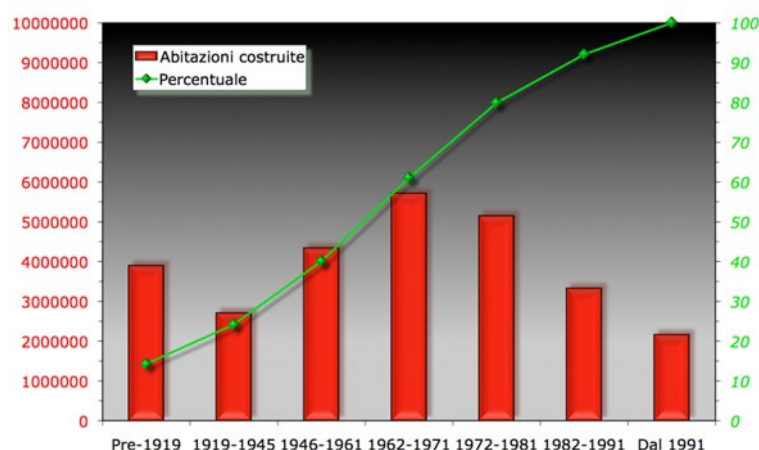


Figure 2 - percentage of dwellings built through the years (Censimento ISTAT 2001).

Therefore, it seems indispensable to consider this argument as of great importance in professional practice since buildings designed in absence of specific seismic provisions are particularly vulnerable to the fragile mechanisms. It is worth noting that the current approaches used in the professional, consistent with the seismic provisions requirements, in many cases, return the paradoxical response that the construction is expected to collapse even due to gravity loads only.

The shear failure mechanisms of reinforced concrete framed structures, on the contrary of the flexure mechanisms, are generally characterized to be brittle. For this reason in new buildings is necessary to ensure that such mechanisms do not become active, and this is achieved through a design that orients toward a more ductile collapse mechanisms according to the Capacity Design. However in buildings designed in the absence of specific seismic codes, as many existing buildings in Italy, often shear collapse manifests before the flexural one and it makes the building even more vulnerable (both in terms of resistance and ductility) especially for seismic actions. Therefore, there is the need to set analysis models capable of evaluating, for reinforced concrete elements, both the activation of any brittle failures or, more generally, the reduction of ductility capacity. The Italian code tends to separate the ductile mechanisms of flexure from those more fragile and, for the latter, require further limits through the introduction of safety coefficients that in many cases lead to unrealistic results by returning output in contrast with the physical sense.

1.2 Organisation of the thesis

The thesis is organised in eight chapters.

In Chapter 1, an introduction on the research field and on its importance is presented.

In Chapter 2 considers analysis and design for shear in flexural members, with emphasis on beams and columns. This chapter also introduces strut-and-tie models for low-aspect-ratio members and discontinuity regions.

In Chapter 3 an extensive description of the most used finite element formulations for framed structures is performed. Particular emphasis is given to the evolution of the formulations from the beginning to the most complex and recent.

Chapter 4 concerns the study of beam models with multiple singularities as a new approach to solve structural problems.

Chapter 5 is dedicated to the review of the main existing beam-column elements formulation with shear modelling, underling their characteristics and features.

In Chapter 6 the formulation of the novel finite element is performed.

Chapter 7 is dedicated to the elastic and inelastic numerical verification with benchmarks in order to validate the novel finite element.

The conclusions are inserted in Chapter 8.

2 SHEAR IN BEAMS & COLUMNS

2.1 Shear in flexural members

Structural elements such as beams, columns and wall designed to resist seismic loads are subjected to a combination of axial, flexural and shear actions. For example, in Figure 3, the internal actions on a column due to an earthquake are shown. Neglecting the body forces, shear and axial load are constant along the member. If the column was made of a homogeneous, isotropic material, shear and normal stresses would be as illustrated in Figure 3. Using the Mohr circle theory on infinitesimal elements at the ends and in the middle of the column it is possible to define the principal stresses directions. Cracks tend to form perpendicular to principal tensile stresses, suggesting crack orientations. First cracks occur near member ends, approximately perpendicular to the longitudinal axis and they are called flexure cracks. As loading continues, additional shear-flexural cracks initiate away from member ends, but shear causes these cracks to incline. In other words where the normal stresses are comparable with the shear stresses the principal tensile stresses deviate from the vertical direction.

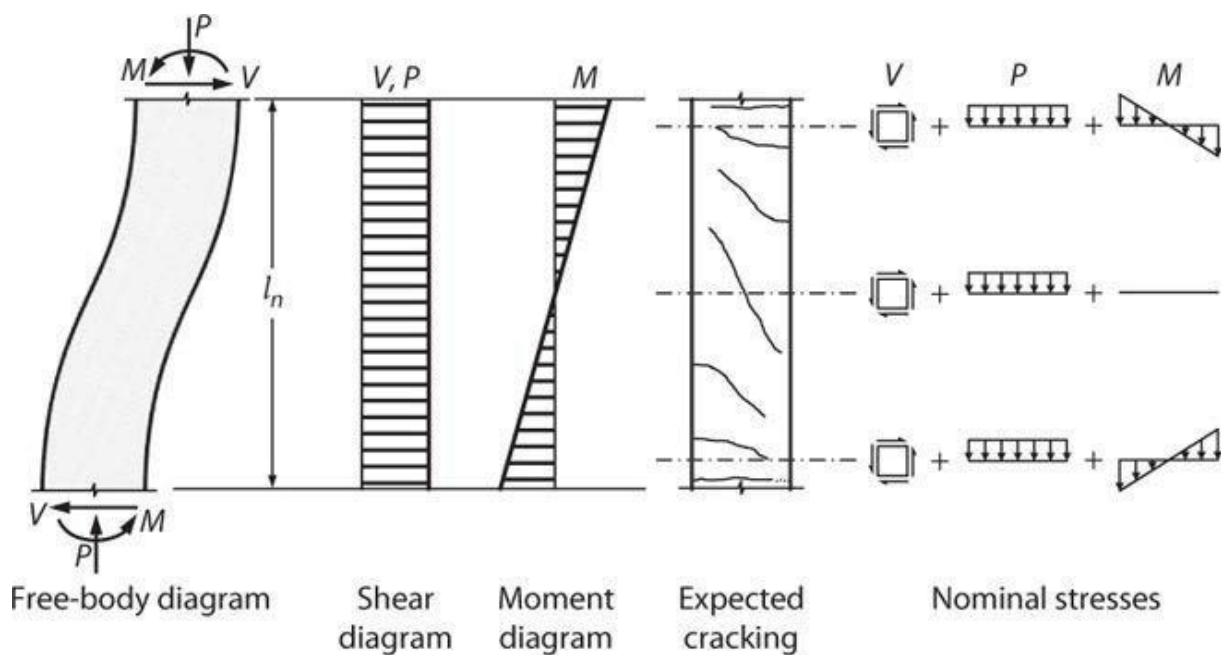


Figure 3 - Axial, flexural, and shearing actions on a column [Moe14].

This behavior is quite common in all the special moment framed structures, as it will be shown in the following sections.

2.2 Relations among moment, shear, and bond

From equilibrium, it is known that the shear is the first derivative of flexure respect to the x coordinate.

$$V = \frac{dM}{dx} \quad (2.1)$$

In members subjected to pure flexure $M = T_s j_d$, where T_s is the flexural tension force and j_d is the internal moment arm, substituting in eq. (2.1) we find

$$V = \frac{dM}{dx} = \frac{d(T_s j_d)}{dx} = \frac{d(T_s)}{dx} j_d + \frac{d(j_d)}{dx} T_s \quad (2.2)$$

The two terms on the right-hand side of eq. (2.2) represent two mechanisms by which shear can be resisted in structural concrete members without transversal reinforcement (Figure 4).

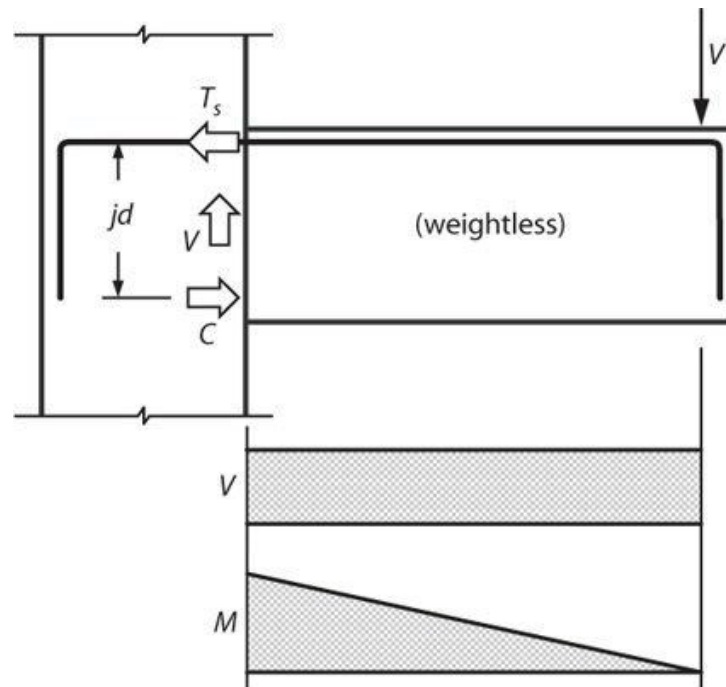


Figure 4 - Cantilever beam with concentrated load [Moe14].

Imposing that the internal moment arm j_d is constant, equation (2.2) simplifies to

$$V = \frac{d(T_s)}{dx} j_d \quad (2.3)$$

Equation (2.3) expresses *beam action* for a fully cracked beam where the flexural tension force T_s varies linearly along the span. If, instead, flexural tension force T_s is constant equation (2.2) simplifies to

$$V = \frac{d(j_d)}{dx} T_s \quad (2.4)$$

Equation (2.4) expresses *arch (or truss) action*, where the internal moment arm j_d varies linearly along the span. The physical meaning of these two resisting mechanisms will be explained in section 2.2.1 .

Recalling eq. (2.3) can be noted that beam action requires to be directly proportional to the shear force V . Thus, in a short length Δx of the beam, longitudinal reinforcing steel is subjected to a change in tensile force equal to $\frac{dT_s}{dx} \Delta x$. Figure 5 shows the forces T_s and $\frac{dT_s}{dx} \Delta x$ acting on a reinforcing bar of length Δx . In order to respect horizontal equilibrium, a bond stress u acting between the surface of the bar and the surrounding concrete is required.

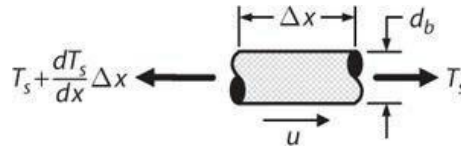


Figure 5 - Free-body diagram of short length of reinforcing bar [Moe14].

Horizontal force equilibrium requires

$$u \sum^{n \text{ bars}} (\pi d_b) \Delta x = \frac{dT_s}{dx} \Delta x \quad (2.5)$$

Rearranging eq. (2.5), bond stress is

$$u = \frac{dT_s}{dx} \frac{1}{\sum^{n \text{ bars}} (\pi d_b)} = \frac{V}{\sum^{n \text{ bars}} (\pi d_b) j_d} \quad (2.6)$$

This can prove that bond stress u between longitudinal reinforcement and surrounding concrete also is directly proportional to applied shear V . This somewhat explains why some members subjected to high shear and showing signs of shear failure may also show signs of bond failure. An example of this phenomenon can be found in [VS04] where the beams without stirrups experienced extensive cracks and in some cases bond failure (Figure 6).

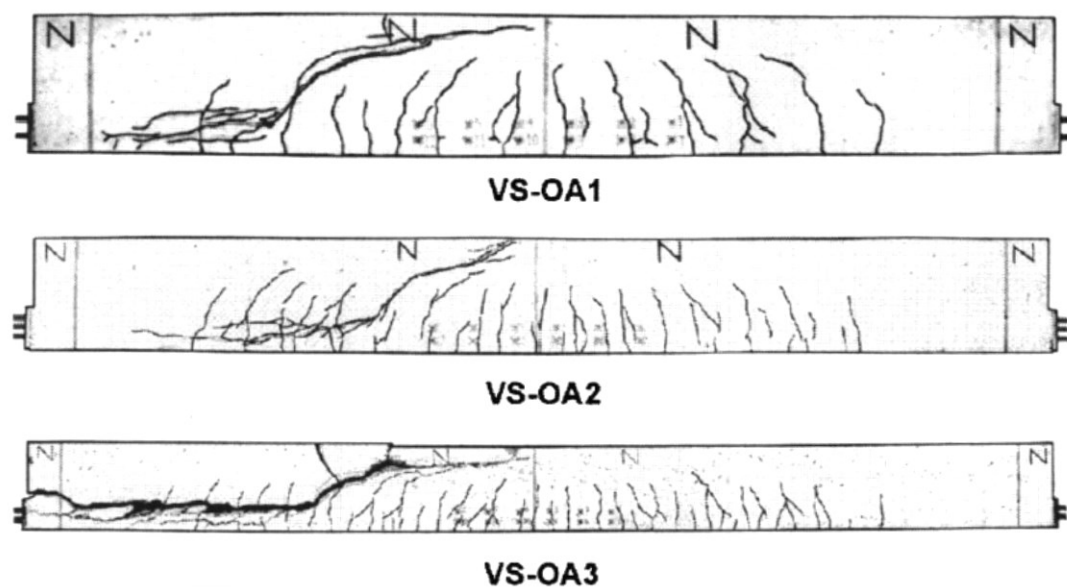


Figure 6 – Tested beams without stirrups [VS04].

Especially in beam OA3 splitting cracks due to bond slip are evident and bond failure is coupled with shear producing a brittle collapse mode.

2.2.1 Beam action and arch action

Equations (2.3) and (2.4) define mathematically the concepts of *beam action* and *truss action*, which are two distinct methods for resisting applied shear and moment. It is important to understand the physical meaning of these two equations. Figure 7a shows beam action, by which shear and moment are resisted through a couple between tensile and compressive forces at constant internal moment arm jd . Beam action results in flexural tension force T_s and flexural compression force C that vary in proportion with the applied moment. Basic flexural design is in accordance with the assumptions of beam action. Figure 7b illustrates arch (or truss) action, where shear and moment are resisted through constant tensile force T_s acting with the variation of the internal lever arm jd . In other words, the beam is acting as a truss **abc**.

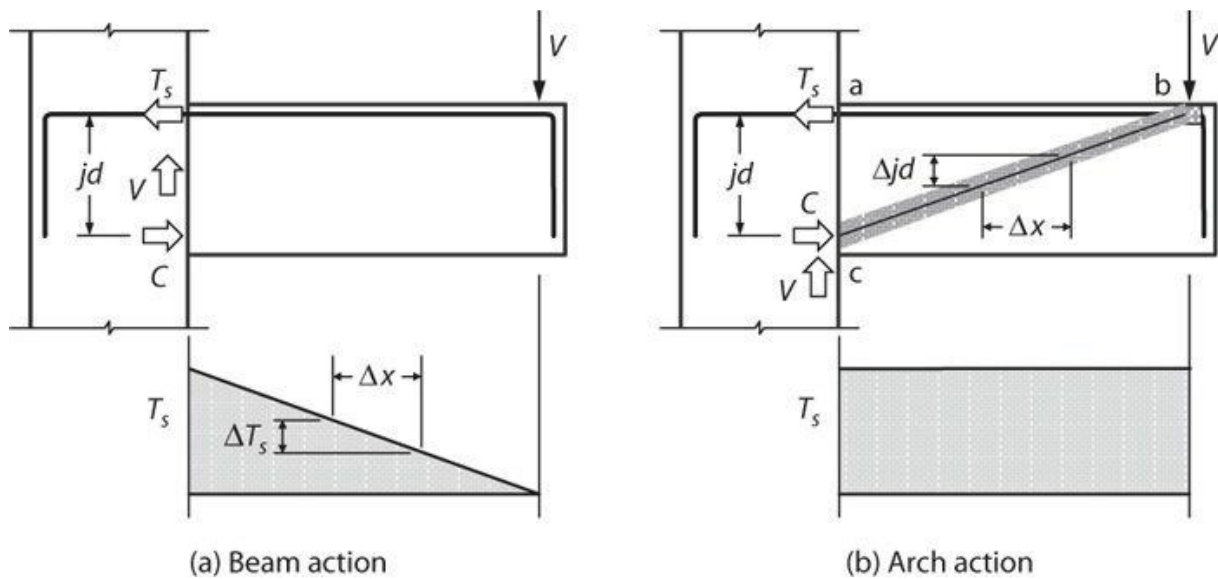


Figure 7 - Theoretical beam action and arch action [Moe14].

In typical members both mechanisms are existent, with one possibly more dominant than the other depending on member geometry.

In a relatively slender beam (Figure 8a), tests show that beam action predominates, with flexural tension force varying nearly linearly along the span.

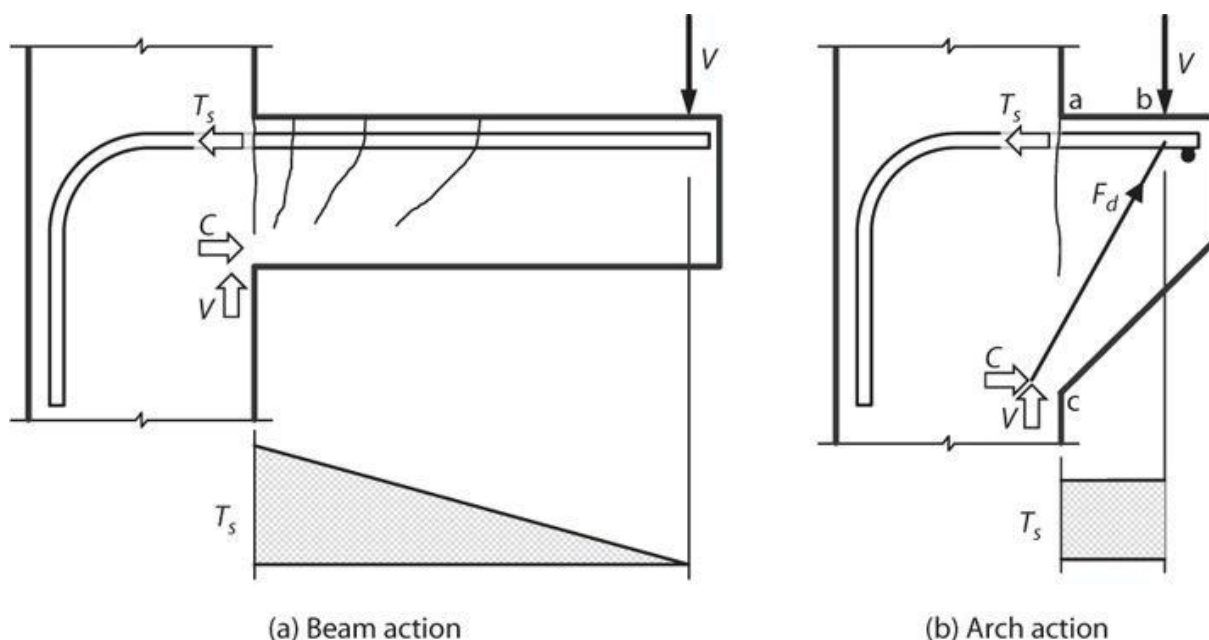


Figure 8 - Practical conditions for beam action and arch action [Moe14].

Whereas, in a deep beam, as in the corbel in Figure 8b, the stiffest force path is a compression strut along **bc**, equilibrated by tension T_s along **ab**. Thus, this member resists shear primarily through arch or truss action. For this reason, in all the cases where the aspect ratio between length and height of the member is less than 2.5 is preferred to design the reinforcing steel with the limit analysis approach using the static theorem and a truss analogy model.

2.2.2 Internal forces in members with transverse reinforcement

In members with transverse reinforcement subjected to shear, it is convenient to construct an idealized force path to approximate internal stresses. Consider the weightless cantilever shown in Figure 9a imagine two idealized cracks, a vertical crack along **ac** and an inclined crack along **bc**. Figure 9b shows a free-body diagram of **abc**. Tension in top reinforcement is assumed to increase along **ba** by amount ΔT_s . The crack surface along **bc** can be presumed to be rough, such that any movement parallel to the crack produces aggregate interlock shear V_a . It is assumed that there is no tension perpendicular to the crack, which is not necessarily correct but which is a reasonable approximation for the present discussion. Crack opening along **bc** will also result in tensile force F_t in the transverse reinforcement. Vertical movement at point **b** will result in a dowel shear V_d acting on the longitudinal reinforcement. Near ultimate strength, the dowel shear

is likely to cause concrete splitting cracks along the longitudinal reinforcement, the occurrence of which will reduce the dowel force. Therefore, for the present discussion, it is assumed $V_d \sim 0$. Finally, a portion of the total shear V and a compressive force C' will act on the vertical face **ac**. The line of action of force V_a passes approximately through point **c**. Therefore, moment equilibrium about **c** is preserved mainly by the opposing moments due to forces F_t and ΔT_s .

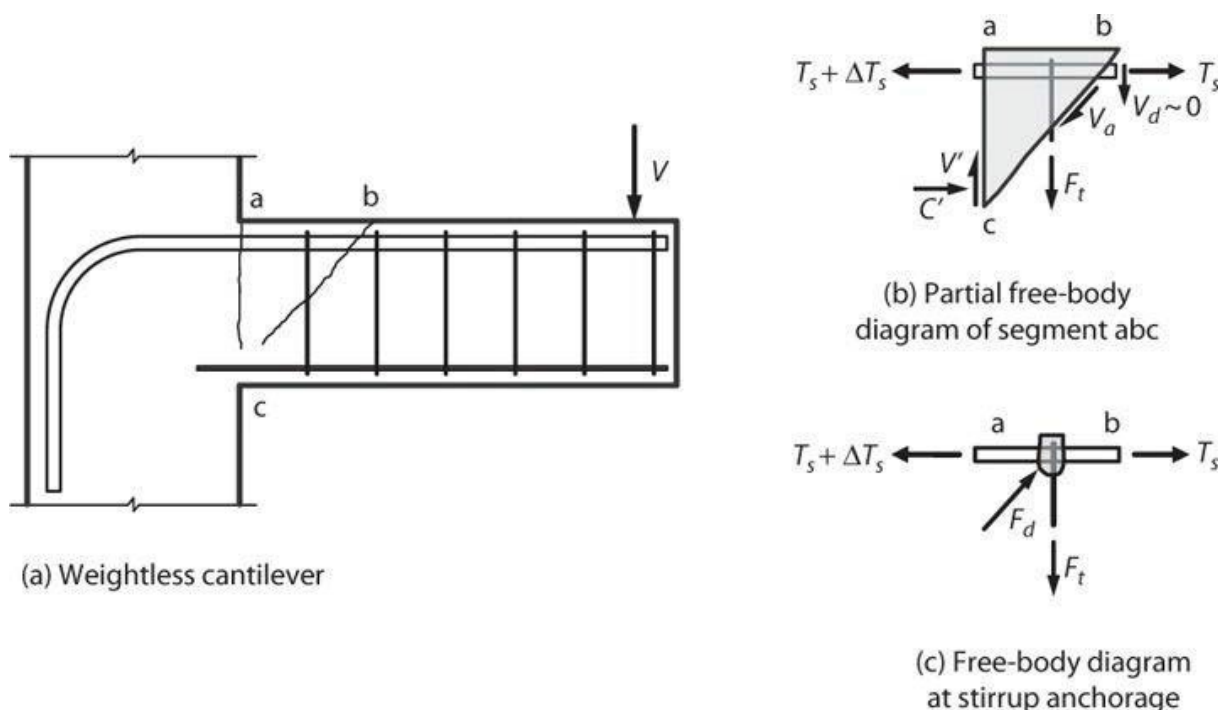


Figure 9 - Internal forces in member with transverse reinforcement [Moe14].

Now consider the free-body diagram of Figure 9c, in which longitudinal and transverse reinforcement have been cut from the surrounding concrete, leaving a small concrete "node" at their intersection. The transverse reinforcement, being anchored around the longitudinal reinforcement, creates a downward reaction on the longitudinal reinforcement. Similarly, as a simplification, it is supposed that horizontal force ΔT_s is anchored entirely at the intersection of the longitudinal and transverse reinforcement. Consequently, a diagonal compression force F_d is required in the concrete to equilibrate the node.

The diagonal compression force F_d identified in Figure 9c is similar to the diagonal compression force F_d identified in Figure 8b. The concept of reinforcement acting as tension ties, concrete acting as struts, and their intersections acting as nodes is a powerful tool for analysis of reinforced concrete members. Section 2.2.3 further pursues this concept.

2.2.3 Truss Model

Since the late 1800s many researchers were interested in the resistant mechanisms of reinforced concrete elements with transverse reinforcement. Ritter and Morsh are the two most representative (Figure 10). Through many experimental tests they postulated that for loads close to the collapse RC beams behave as a truss with elements in tension and in compression. In the truss can be identified an upper and a lower chord (one in tension and one in compression) that are linked through a drape of inclined struts of concrete and vertical steel ties (Figure 11).

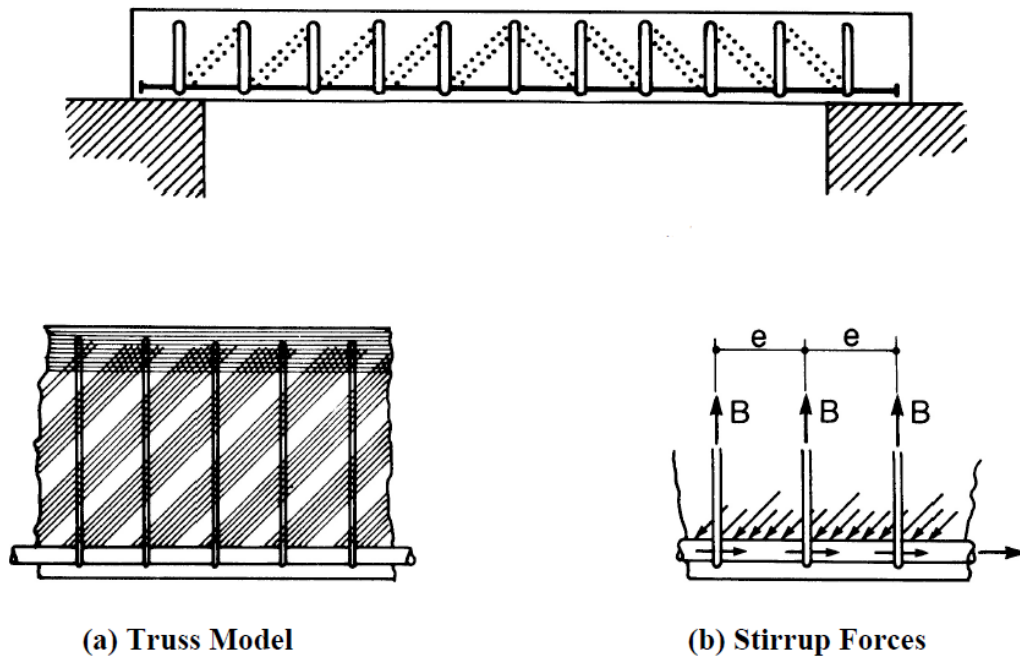


Figure 10 – Ritter's original drawing of the truss analogy (a) and shear forces (b) [CM97].

Using just equilibrium, the structural problem of Figure 11 cannot be solved unless the angle θ is already picked. In fact the first studies used $\theta=45^\circ$, during the years the inclination of the struts was made variable ($\theta<45^\circ$) basically because the theoretical results were conservative compared with the experimental one.

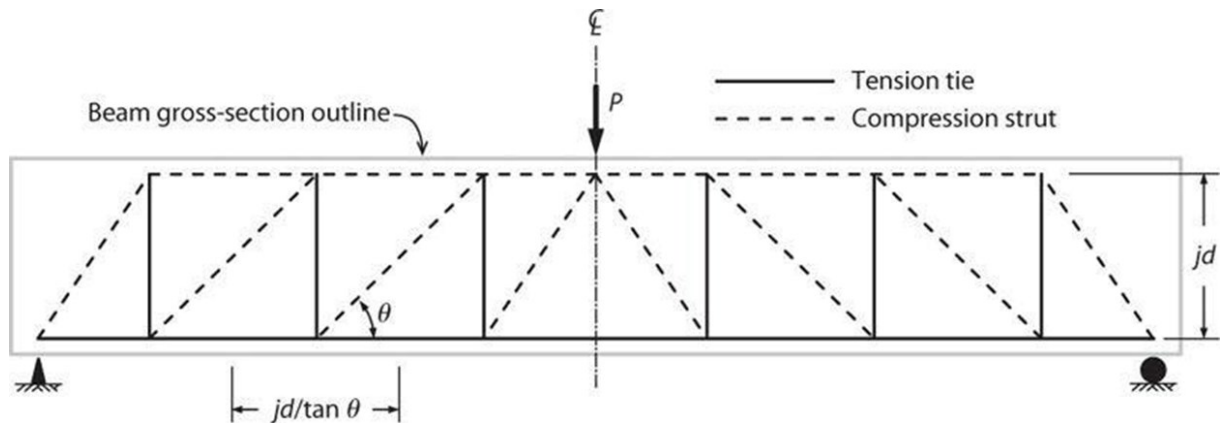


Figure 11 – Truss model for simple supported beam [Moe14].

2.2.4 Empirical Approach for Shear Strength of Beams and Columns

Advances in strut-and-tie models, especially since the 1980s, have greatly improved understanding of design requirements for shear, especially for D-regions where internal forces can be highly non uniform. Prior to this development, designs were based largely on empirical expressions and ad hoc procedures. For B-regions, empirical expressions still provide an efficient and effective approach for design, and are used widely. Next section presents test results demonstrating strength trends, followed by some of the empirical expressions and design requirements of ACI 318 for beam and column design.

2.2.5 Strength of Members without Transverse Reinforcement

Shear strength of beams without transverse reinforcement has been studied through hundreds of laboratory tests all over the world. From these tests were understood the primary variables affecting shear strength and the mechanisms of shear resistance. A series of beam tests reported by Leonhardt (1962) are shown in Figure 12. The beams were simply supported and subjected to two point loads (Figure 12).

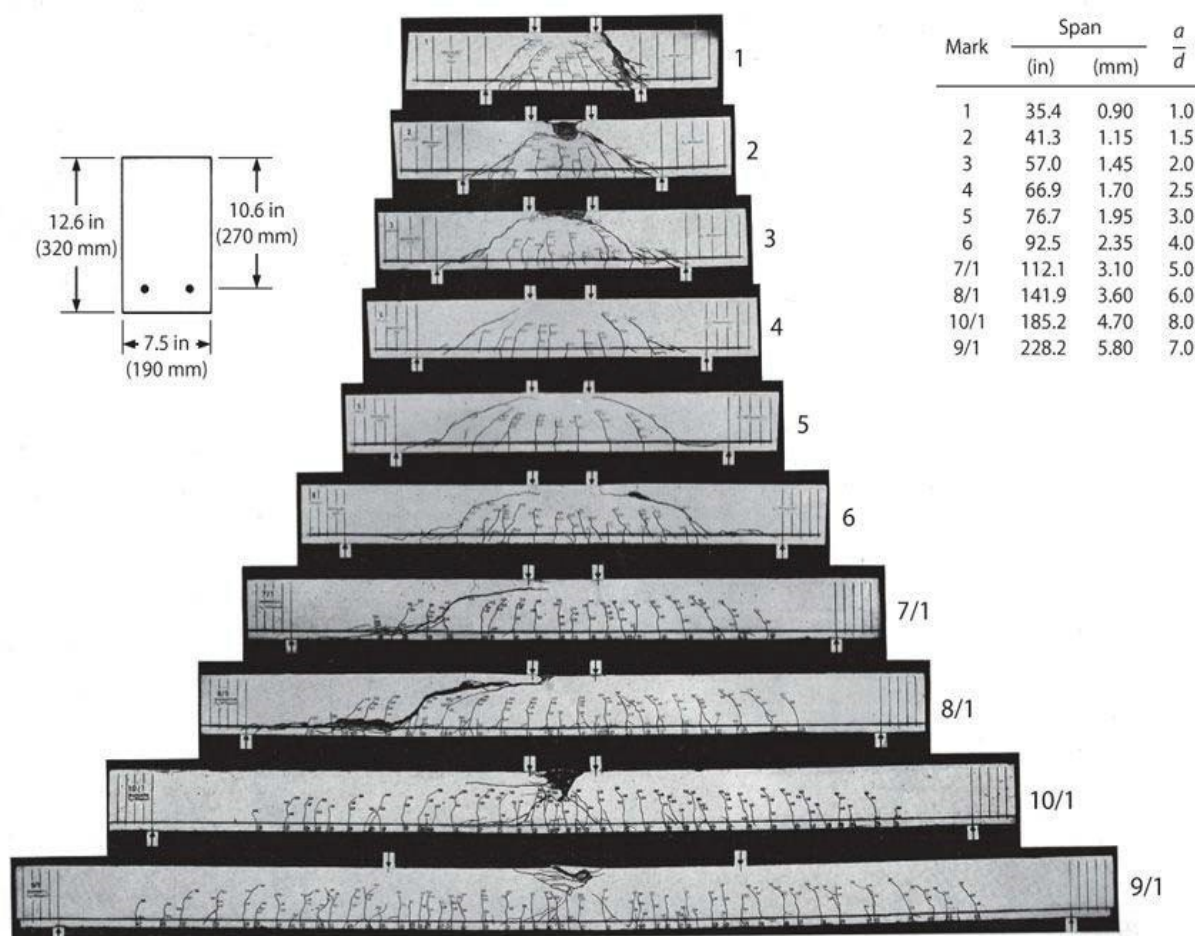


Figure 12 - Damage at failure in series of tests on beams without transverse reinforcement. (After Leonhardt, 1962.)

In the Leonhardt tests, the behavior was strongly influenced by shear span ratio a/d , where a is span from point load to reaction and d is beam effective depth.

- Beams with largest a/d had shear strength exceeding the shear corresponding to flexural yielding (beams 10/1 and 9/1). They developed cracks mainly perpendicular to the beam longitudinal axis, with slight crack inclination due to shear. Failure was by crushing of the flexural compression zone, without shear failure.
- Beams with $2.5 < a/d < 6$ sustained shear failures associated with steeply inclined cracks (beams 8/1, 7/1, 6, 5, and 4). Initially, the beams were stable owing primarily to transfer shear through aggregate interlock across inclined cracks. Further loading increased crack opening, reducing aggregate interlock, and leading to diagonal tension failure. Failure is characterized by steeply inclined cracks extending along the bottom longitudinal bars, which are sheared off the bottom of the beam. Such failures can be especially brittle and coupled with bond failure. The primary inclined cracks also may penetrate the flexural compression zone, leading to compression zone failure.
- Beams with $a/d < 2.5$ developed a diagonal compression strut that supported the concentrated loads through arch action (beams 1, 2, and 3). Failure can be by splitting of

the diagonal compression strut, as occurs in a split cylinder test, or by failure of the compression chord at the top of the beam.

The different force-resisting mechanisms in beams with different aspect ratios result in different beam strengths. Figure 13 plots measured shear strength as function of aspect ratio a/d for the beams shown in Figure 12. Beams with aspect ratio $a/d = 7$ and 8 developed flexural strength prior to shear failure. For smaller a/d , the shear force corresponding to flexural failure increases (broken curve in Figure 13), such that shear failure occurred before flexural strength was reached. Shear strength was nearly constant for a/d to around 3, but increased rapidly for smaller a/d . Apparently, the arch mechanism that develops for $a/d < 2.5$ results in shear strength significantly exceeding the strength observed for larger values of a/d .

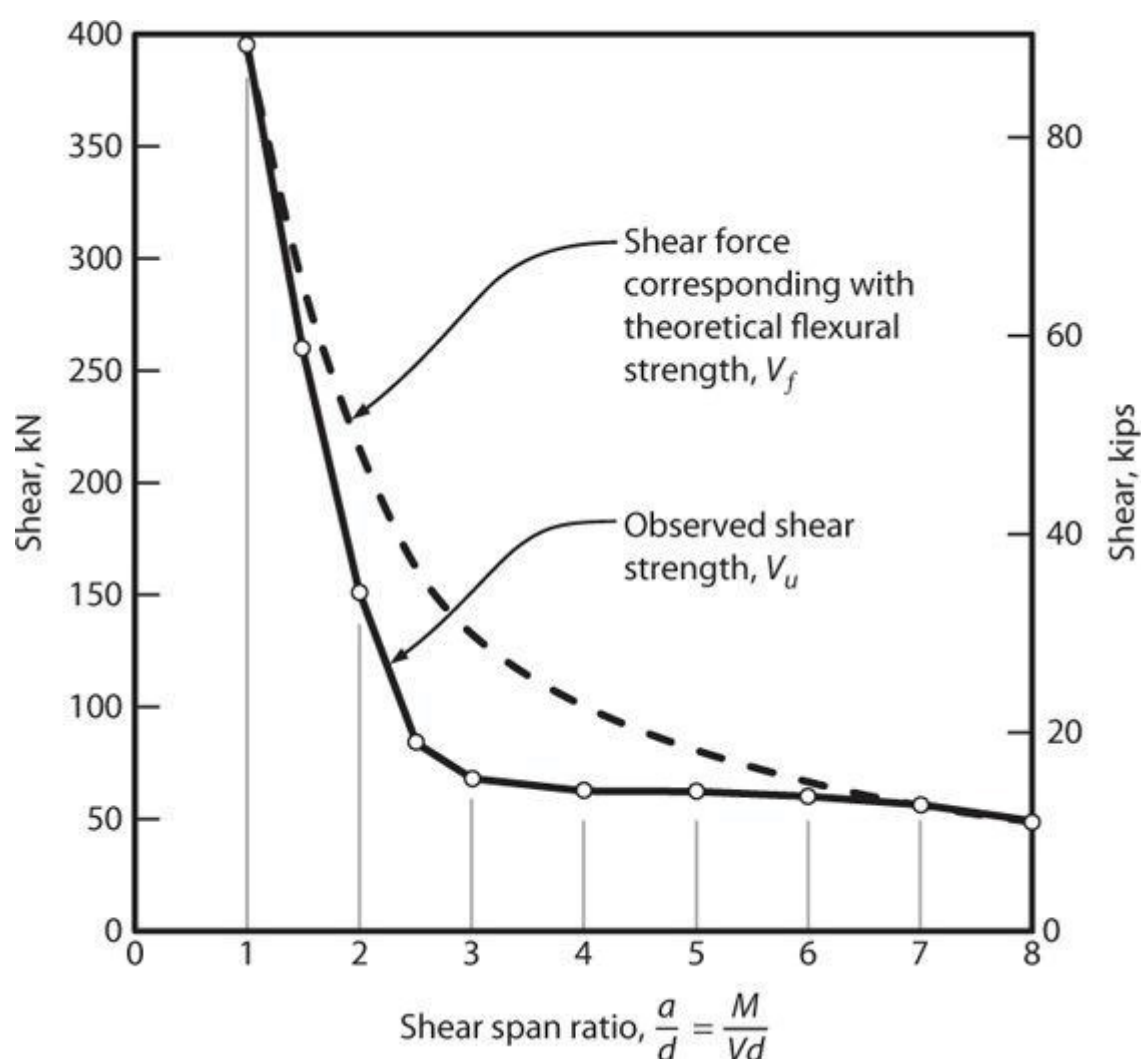


Figure 13 - Shear at failure as function of aspect ratio for beams without transverse reinforcement [PP75].

For a cracked reinforced concrete flexural member, flexural stresses and, hence, shear flow act over section depth extending from the extreme flexural compression fiber to the flexural tension reinforcement at depth d . Thus, it is conventional to define average nominal shear stress as, $v =$

$V/b_w d$, in which b_w is section width (or web width for flanged members) and d is the effective depth to centroid of flexural tension reinforcement.

Studies show that nominal shear strength of beams increases with increasing concrete compressive strength f'_c , increasing longitudinal reinforcement ratio ρ_w , and decreasing a/d . The term a/d is applicable only to simply supported beams subjected to concentrated loads. To be applicable to more general loading cases, the term M/Vd must be substituted for a/d . Figure 14 plots nominal shear strength of beams without transverse reinforcement using a functional form presented by ACI-ASCE 326 (1962) as follows:

$$v_c = 0.16\sqrt{f'_c} + 17\rho_w \frac{Vd}{M} \leq 0.29\sqrt{f'_c}, \text{ MPa} \quad (2.7)$$

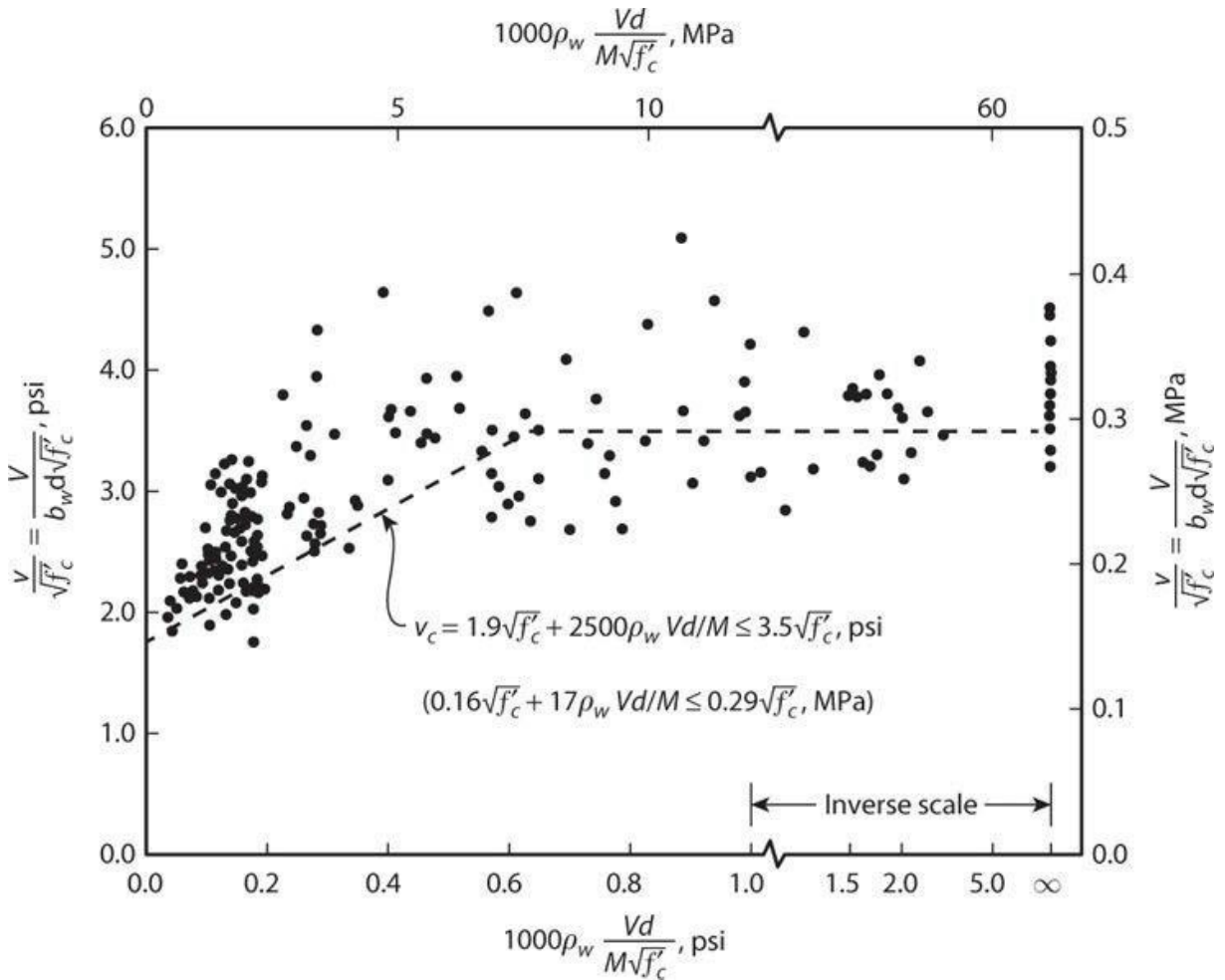


Figure 14 - Nominal shear strength of beams without transverse reinforcement (After ACI-ASCE 326, 1962).

Axial stress also affects shear strength in fact in many codes is a variable that must be considered. For example in EC2, the shear strength for members without transversal reinforcement is equal to

$$V_{Rd,c} = [C_{Rdc} k (100 \rho_l f_{ck})^{1/3} + k_1 \sigma_{cp}] b_w d, \text{ MPa} \quad (2.8)$$

Where C_{Rdc} represents the mean shear stress, it is modified by $k = 1 + \sqrt{200/d} \leq 2$ (d in mm) that considers the aggregate interlock decreasing when d increases.

ρ_l is the longitudinal reinforcement ratio,

f_{ck} is the compressive strength,

$\sigma_{cp} = \frac{N_{Ed}}{A_c}$ represents the beneficial effect of compressive axial load (eventually coming from post tensioning) because it postpones the cracks opening,

$k_1 = 0.15$ is a fixed parameter.

2.2.6 Members with Transverse Reinforcement

Early truss models assumed compression diagonals inclined at 45° with respect to the beam longitudinal axis. With this assumption, and the approximation that $jd \sim d$, can be proven that

$$V_s = \sum A_v f_{yt} = \frac{A_v f_{yt}}{s} d \quad (2.9)$$

in which shear resisted by the transverse reinforcement is now denoted by V_s . Tests confirmed that eq. (2.9) was conservative compared with test results.

Given the conservatism of eq. (2.9), and the observation that concrete beams resist shear without transverse reinforcement, a common approach has been to express shear strength as the sum of concrete and transverse reinforcement components, as in

$$V_n = V_c + V_s \quad (2.10)$$

in which $V_c = v_c b_w d$, with v_c defined by eq. (2.7) and V_s is defined by eq. (2.9). Figure 15 compares results of eq. (2.10) with test data.

In Figure 15, $v_s = V_s / b_w d$.

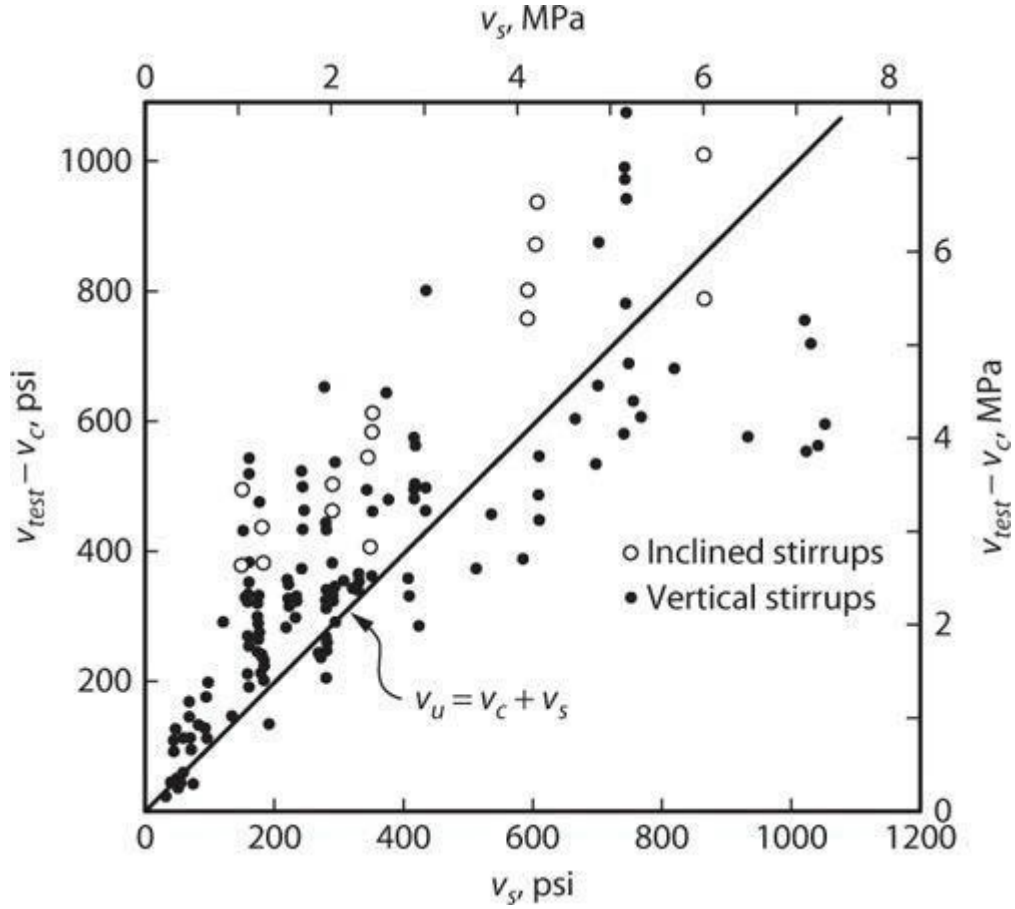


Figure 15 - Comparison of measured and calculated strengths as function of v_s provided (After ACI-ASCE 326, 1962).

The EC2 does not allow the sum between V_c and V_s in fact the design equations are:

$$V_{Rd,max} = \alpha_{cw} b_w j d (v_1 f_{cd}) / (\cot\theta + \tan\theta) \quad (2.11)$$

$$V_{Rd,s} = \frac{A_v f_{yt}}{s} j d \cot\theta$$

$\alpha_{cw} \geq 1$ is a parameter that consider the compressive axial load,

$$v_1 = 0.6; \text{ with } f_{ck} < 60 \text{ MPa}$$

$$v_1 = 0.9 - \frac{f_{ck}}{200} > 0.5; \text{ with } f_{ck} > 60 \text{ MPa}$$

v_1 considers the more demanding biaxial stress state of the concrete in the web region. The limit of 60 MPa is due to shear cracking, in fact when the concrete strength f_{ck} increases the crack can occur through the aggregates and so dropping the interlock.

2.2.7 Effects of Inelastic Cyclic Loading

Plastic strains in slender flexural members lead to degradation of the shear-resisting mechanisms, and can lead to eventual shear failure. For this reason, it is usually good design practice to maintain a margin against shear failure in slender flexural members. Consider a cantilever beam idealized using truss models (Figure 16). Note that two different truss models are required, one for loading in the downward direction and another for loading upward. If the member is designed with insufficient transverse reinforcement, that reinforcement will yield in tension for loading in each direction. Consequently, plastic tensile strains in transverse reinforcement will accumulate with each loading cycle, leading to dilation of the member with continued cycling (Figure 16d). This is in contrast with flexural behaviour at reversing plastic hinges where the longitudinal reinforcement is subjected to alternating tensile and compressive forces due to flexure.

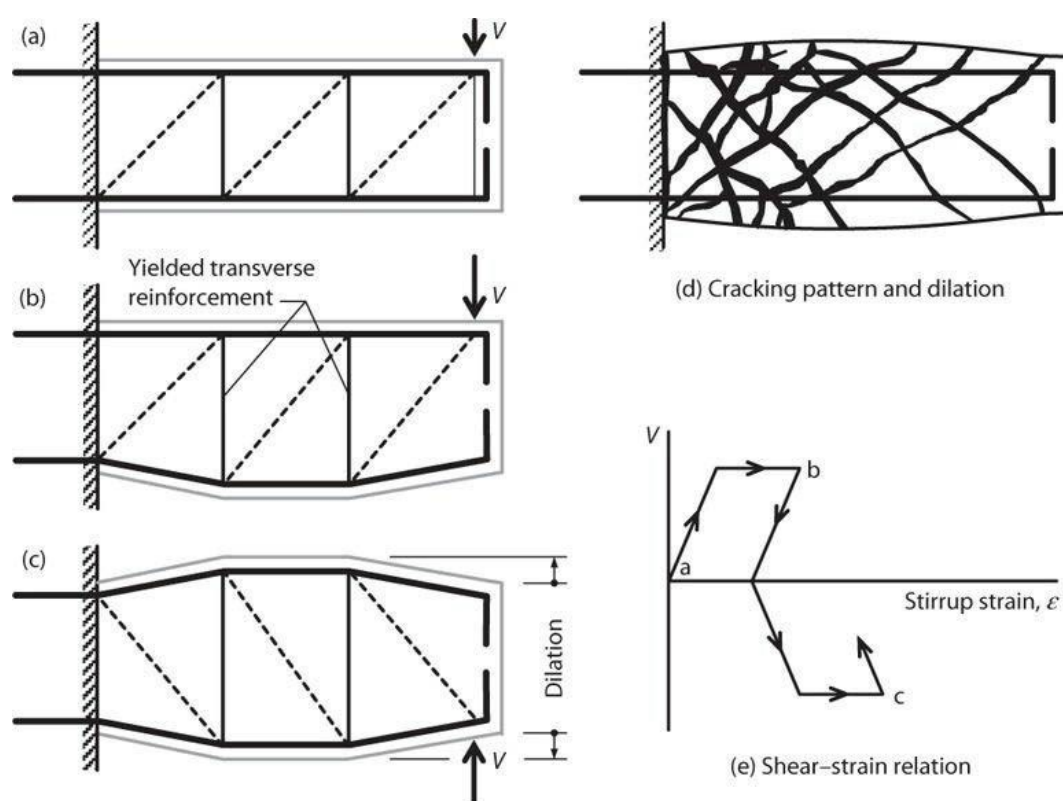


Figure 16 - Idealized behaviour for yielding transverse reinforcement [Moe14].

In cases where shear-yielding dominates, reversed cyclic loading will produce a set of crisscrossed diagonal cracks that effectively subdivide the member into a series of concrete segments separated by inclined fissures called shear-flexure cracks (Figure 16d and Figure 17). For shear applied in one direction, corresponding diagonal compression struts must form, closing any cracks that cross the struts. Shear force reversal requires that diagonal compression struts develop in the opposing direction. This requires the segments to shift orientation, a process that usually occurs with limited shear resistance. Significant lateral force resistance can be achieved only after the segments have shifted to a position that enables formation of diagonal compression struts effective for the loading direction. In a member with well-developed set of diagonal cracks,

considerable lateral displacement may be required to open and close the opposing cracks. This can result in "pinched" hysteresis loops in shear-damaged members.

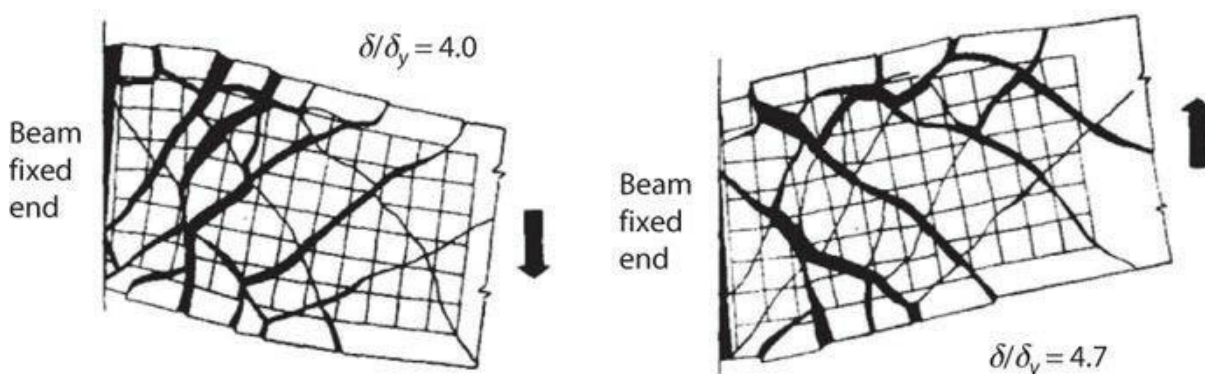


Figure 17 - Surface deformations and cracks of beam in advanced stages of cyclic loading. Crack widths and deformations are amplified by factor 5.0 (After Popov, 1984).

Figure 18 illustrates force-displacement relations measured in laboratory tests of two fixed-ended columns. Figure 18a shows flexure dominated response. For this condition, shear-displacement loops are relatively full without strength degradation to large displacements. Figure 18b shows results for a nearly identical column proportioned so that shear failure occurs shortly following flexural yielding. Rapid strength loss associated with shear failure is clear. Additionally, the shear-displacement loops are "pinched" for reasons described below.

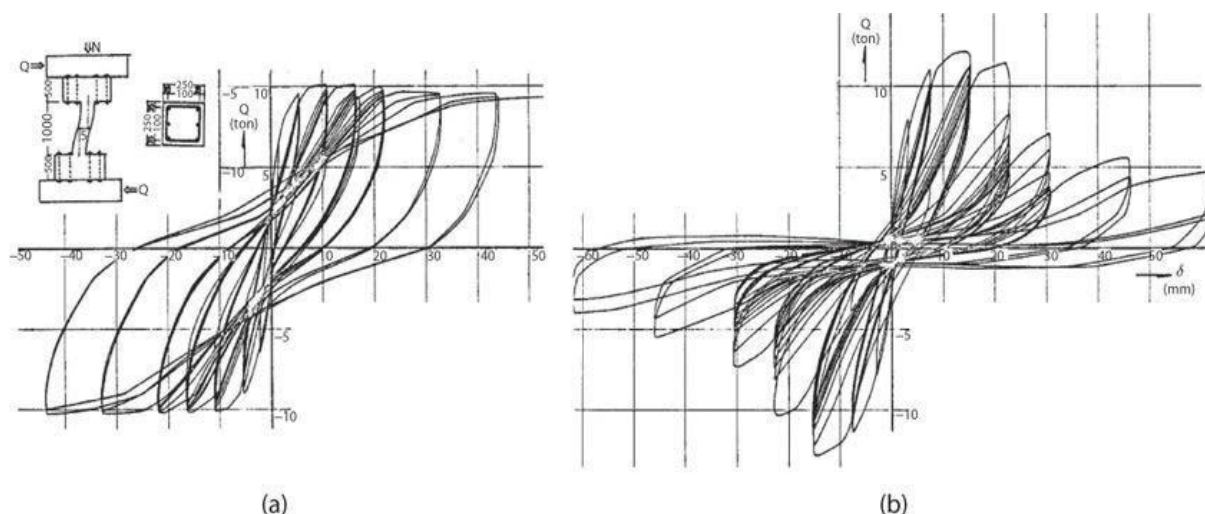


Figure 18 - Shear-displacement relations for (a) flexure-controlled column and (b) shear-controlled column. (After Higashi and Hirose, 1974.)

Even if classical design methods treat shear and flexure as independent mechanisms, and control the resistance in a separated way, truss models suggest instead that they are coupled.

Many of these do not take into account the interaction between flexural ductility and shear resistance in the zone where plastic hinge occurs. In others, the influence of the axial load or the pretension is not explicitly considered in the reinforced concrete member.

Members with low axial loads gradually elongate as a result of accumulated plastic strain in longitudinal reinforcement (Figure 19a). This elongation leads to rotation of inclined compression struts, which reduces shear resistance mechanisms. Longitudinal strain also may reduce strength of diagonal compression struts further contributing to shear strength degradation. Lee and Watanabe [LW03] have presented empirical models that show good correlation between inelastic flexure, axial elongation, and shear strength degradation (Figure 19b). Degradation effects may be less pronounced for members with moderate axial loads because axial elongation is suppressed in such members. Effects of axial force above the balanced point are not extensively studied, though it seems likely that crushing of the flexural compression zone would reduce diagonal compression strength and, hence, result in a faster shear failure. This effect was evident in tests reported by Sezen and Moehle [SM06].

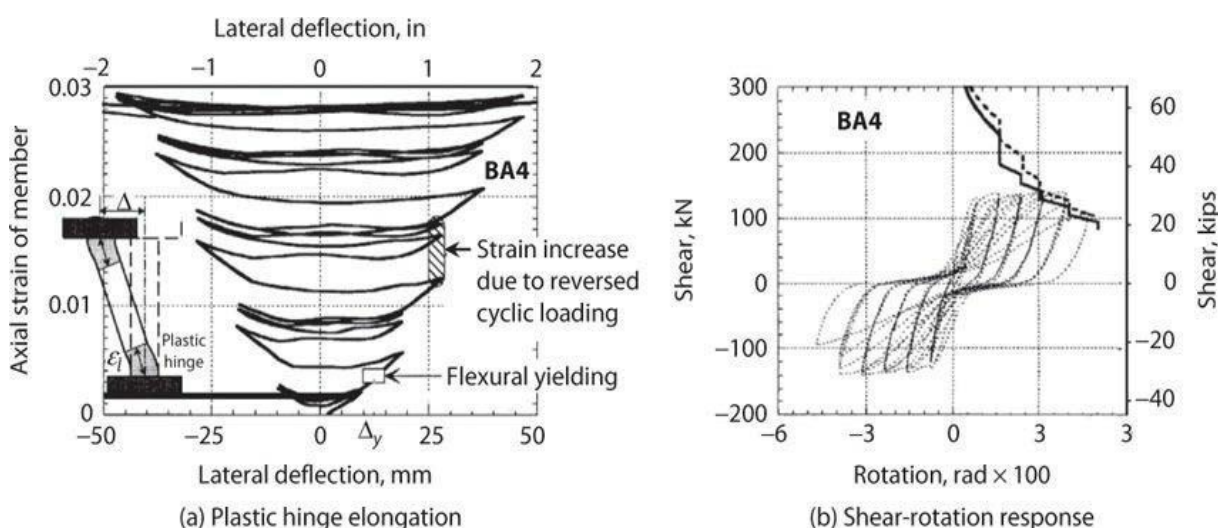


Figure 19 - Elongation of flexural plastic hinge with cycling [LW03].

Several empirical models for shear strength degradation of flexural members have been developed. Most models express shear strength as $V_n = V_c + V_s$ or $V_n = V_c + V_p + V_s$, in which V_c represents contribution of concrete, V_p represents contribution of axial force, and V_s represents contribution of transverse reinforcement. In most of these models, based on an interpretation that concrete diagonal compressive strength and aggregate interlock are degrading, only the concrete contribution V_c degrades with increasing flexural deformation demand (ATC 12, 1983; Ang et al., 1989; Aschheim and Moehle, 1992; Ichinose, 1992; Priestley et al., 1994 and 2000; Lee and Watanabe, 2003; Biskinis et al., 2004).

The first model that will be examined is the “Modified UCSD model” formulated by Priestley et al. [PCK07]. In this model, the shear resistance is sum of three terms in which V_c represents contribution of concrete, V_p represents contribution of axial force, and V_s represents contribution of transverse reinforcement.

The concrete term is defined as

$$V_c = k \sqrt{f'_c} A_e = \alpha \beta \gamma \sqrt{f'_c} 0.8 A_g, \text{ MPa} \cdot \text{mm}^2$$

$$1 \leq \alpha = 3 - \frac{M}{VD} \leq 1.5 \quad (2.12)$$

$$\beta = 0.5 + 20\rho_l \leq 1$$

The parameter γ , is expressed in MPa, and has a trend illustrated in Figure 20. As can be seen, it depends mainly on the flexural ductility, if the bending moment is uniaxial or biaxial and on the nature of the analysis (design Figure 20a or assessment Figure 20b).

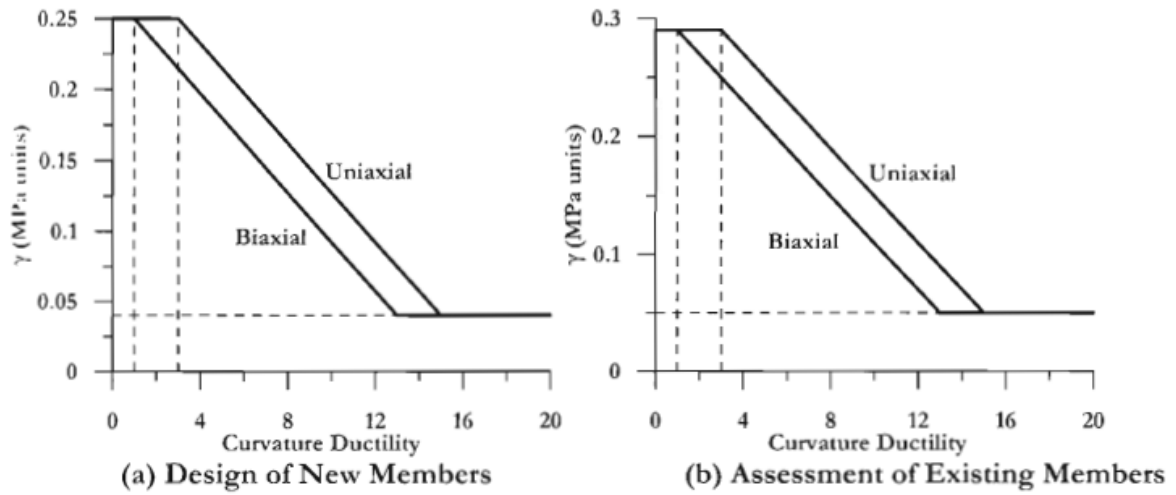


Figure 20 – γ parameter for V_c [PCK07].

The term V_p in many design codes is incorporated in the previously indicated V_c resistance. This would mean that the increasing in the concrete shear resistance V_c due to axial load should be reduced with increasing the curvature, but this is not supported by experimental evidence. In this model, the resistance due to the axial load V_p is independent from V_c . For example in case of columns, V_p is reached according to a mechanism with diagonal strut as shown in Figure 21.

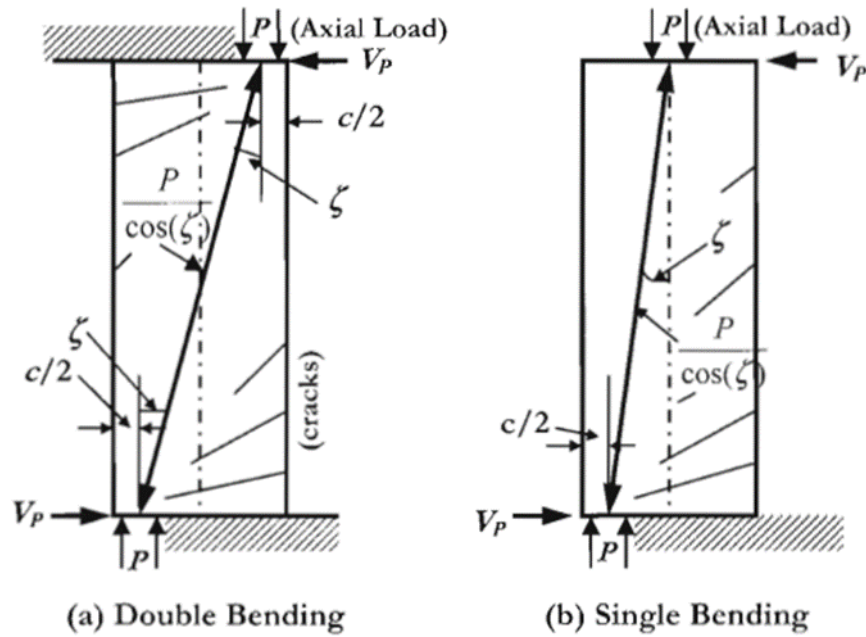


Figure 21 – V_p contribution [PCK07].

$$\begin{aligned} V_p &= 0.85 P \tan \zeta \\ V_p &= P \tan \zeta \end{aligned} \quad (2.13)$$

In eq. (2.13) ζ is the angle that the strut forms with the vertical axis of the element, P is the axial load in case of design V_p is reduced of the 15% as shown in eq. (2.13).

The term V_s is defined as in eq. (2.9).

Other models degrade both V_c and V_s , based on an interpretation that the overall shear-resisting mechanism is degrading (Biskinis et al., 2004; Sezen and Moehle, 2004). This can be explained thinking that also the stirrups loss effectiveness for high value of ductility demand because the surrounding concrete is cracked or no more participating. ASCE 41 for seismic rehabilitation of buildings adopts the model by Sezen and Moehle (2004).

According to this model, column shear strength is defined by

$$V_n = k(V_c + V_s) \quad (2.14)$$

in which V_s is defined by eq. (2.9) and V_c is defined by

$$V_c = \left(\frac{0.5\lambda\sqrt{f'_c}}{M/Vd} \sqrt{1 + \frac{N_u}{6\sqrt{f'_c}A_g}} \right) 0.8A_g, MPa \quad (2.15)$$

in which $\lambda = 0.75$ for lightweight aggregate concrete and 1.0 for normal weight aggregate concrete; N_u is the axial compressive force, taken equal to 0 for axial tension; M/Vd is the largest ratio of moment to shear times effective depth under design loadings for the column but not less than 2, nor greater than 4; and it is permitted to take $d = 0.8h$.

In eq. (2.14), k is a parameter to represent shear strength degradation, defined by Figure 22a. Figure 22b compares test and calculated shear strengths according to eq. (2.14), with an emphasis on older-type columns with relatively wide hoop spacing.

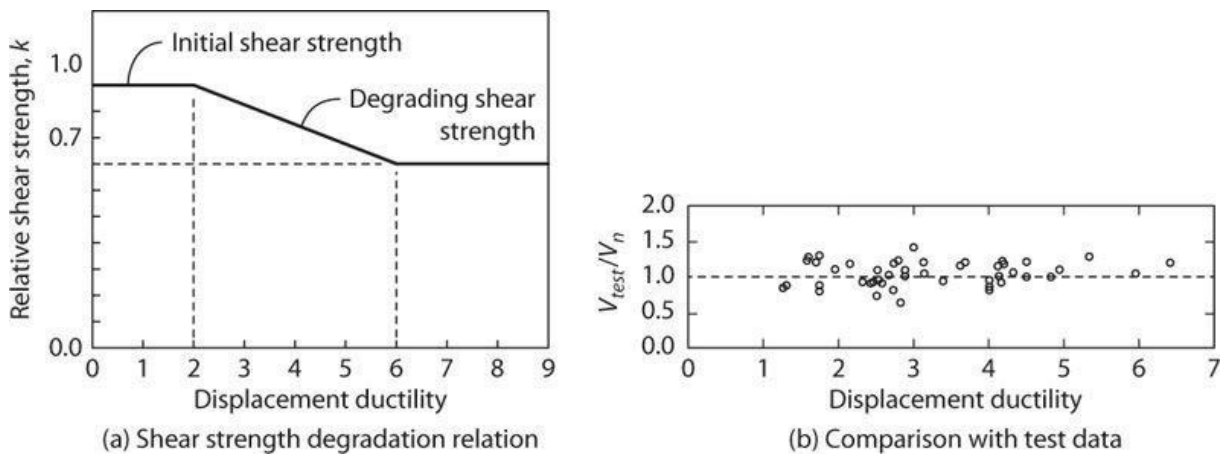


Figure 22 - Shear strength degradation model [SM04].

3 FINITE ELEMENT FORMULATIONS

3.1 Introduction

In this chapter an extensive description of the most used finite element formulations for framed structures is performed. Particular emphasis is given to the development of the formulations from the beginning to the most complex and recent.

A proper session is devoted to the use of the distribution theory to formulate finite element capable to solve complex structural problems.

Moreover, some final considerations on the nature of the numerical solutions obtained with the different models are made.

Seismic vulnerability analysis adopt numerical models with extensive use of inelastic frame elements to reproduce the behaviour of framed buildings. The inelasticity can be assigned according to a lumped approach (concentrated) or distributed type (Figure 23); there is also a third approach that is an evolution of the first one called spread plasticity type.

In the lumped approach the positions (usually the extremal sections corresponding with the nodes) in which the plasticity can occur are predetermined and the element zones remain of constant length during the analysis. The nonlinearities are considered by means of a moment-rotation/curvature relationship for the flexural components and force-displacement relationship for the axial component. In other words, the constitutive laws are expressed in terms of generalized quantity as moment-curvature/rotation without knowing which the state of any particular point in the element cross section is. A crucial aspect is the calibration of the P-M interaction in order to calculate accurately the moment-curvature/rotation behaviour.

In the distributed type, the element can experience plastic deformation at any point and the nonlinearities can diffuse across the entire length.

The nonlinear behaviour is introduced by means of nonlinear constitutive laws that can be expressed at sectional level in terms of generalized forces ($N(x)$, $M(x)$, $V(x)$) and deformation ($\varepsilon_0(x)$, $\chi(x)$, $\gamma(x)$) according to the classical theory of plasticity, or explicitly computed according to a fiber section discretization. In the latter case to each fiber a nonlinear uniaxial constitutive stress-strain relation is assigned. The main advantage of this type of discretization is that the P-M interaction is self calculated at each step and so the moment-curvature/rotation behaviour.

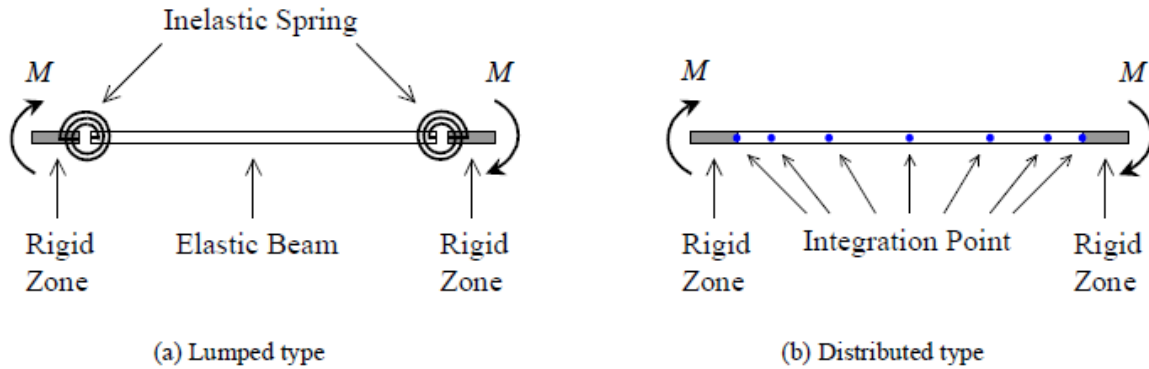


Figure 23– Inelastic beam element, (a) lumped, (b) distributed [MID15].

As shown in Figure 24 the distribution of bending moment of elements subject to lateral forces is linear; the presence of gravity load modify the distribution and in the case that the latter are dominant is necessary to increase the number of finite elements to capture this variation. When the member experiences inelastic deformations, plastic deformations tend to spread from the joint interface resulting in curvature distribution as shown in Figure 24. Section along the element will also exhibit different flexibility characteristics, depending on the degree of inelasticity observed. This concept means that the curvature variation is very far from be linear in all the plastic regions.

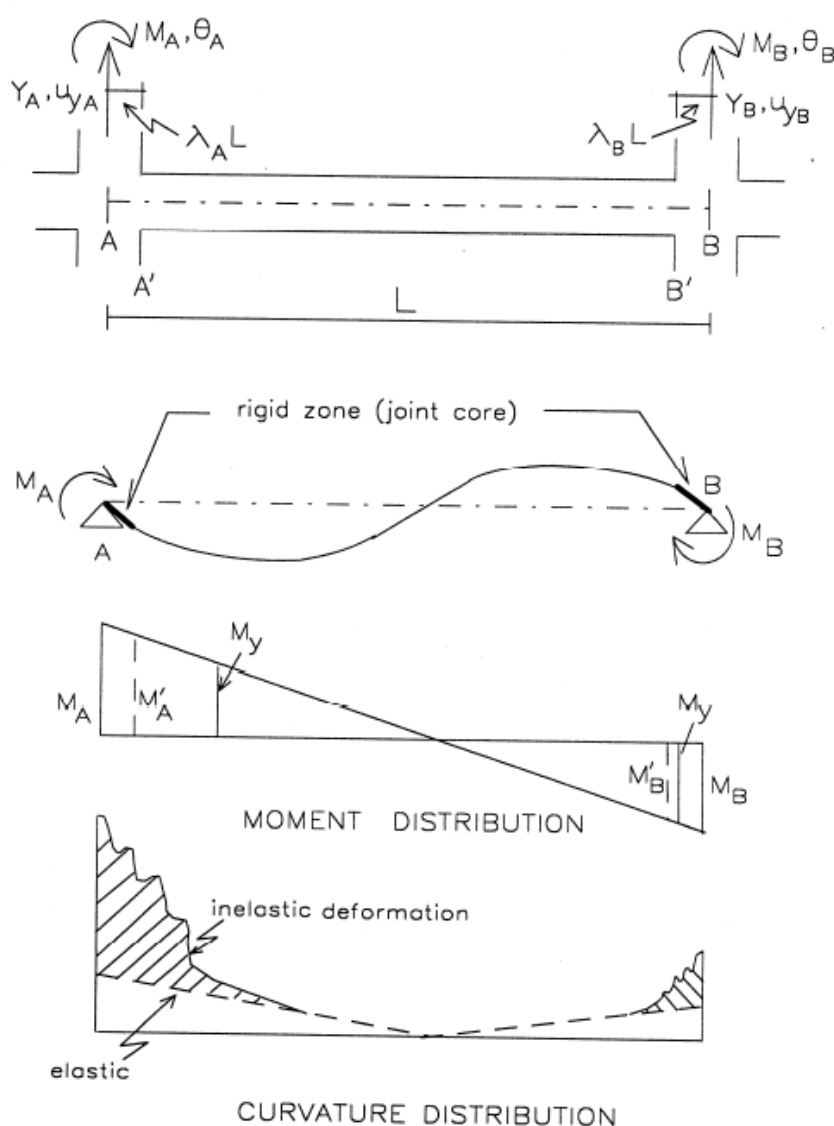


Figure 24 – Curvature distribution along the element [IDA96].

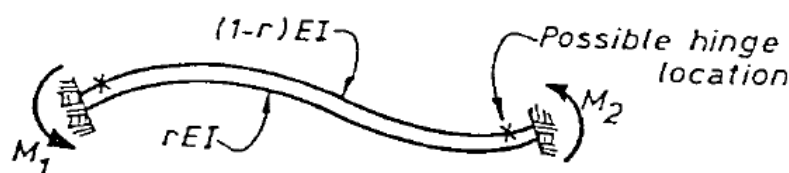
In order to capture this scattered flexibility distribution, meeting the needs of computational efficiency, the spread type approach was formulated.

Also in this case the nonlinearities are considered by means of a moment-rotation/curvature relationship for the flexural components and of a force-displacement relationship for the axial component. In other words, the constitutive laws are expressed in terms of generalized quantity as moment-curvature/rotation without knowing which the state of any particular point in the element cross section is. A crucial aspect is the calibration of the P-M interaction in order to calculate accurately the moment-curvature/rotation behaviour.

In the next sections, a description of the tree approaches is performed.

3.1.1 Lumped plasticity

Clough and Johnston [CJ65] formulated the first lumped plasticity element that was called "two component beam model"; it consists in a linear beam element in parallel with a perfectly elasto-plastic element (Figure 25). The elastic element reproduces the armature strain hardening, while the elasto-plastic element reproduces the yield strength. As it was formulated only a bilinear behavior moment-rotation was allowable.



If member end is elastic both members carry moment at that end.

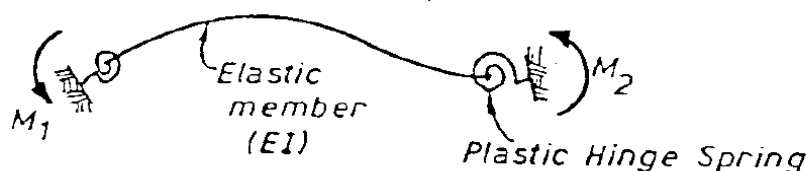
If yield moment is exceeded a perfect hinge is introduced at that end in the $(1-r)EI$ component.

EI = Elastic Properties

r = Bi-linear factor

Figure 25 - Two component beam model.

To overcome this restriction Giberson [Gib67] formulated a different one that was called "one component beam model"; it consists in an elastic element with two inelastic springs at the ends (Figure 26).



Spring Stiffness for elastic member is infinite (i.e. rigid)

For Plastic Member Stiffness K_s

$$K_s = f \cdot \frac{4EI}{L}$$

where $f = \frac{L}{4H} \left(\frac{r}{1-r} \right)$

EI = Elastic Properties

L = Member length

H = Plastic Hinge length

r = Bi-linear factor

Figure 26 – Giberson one component beam model.

This configuration allows to assign the rotational springs with any moment-rotation hysteretic laws. Subsequently Al-Haddad and Wight [AW86] and Kunnath and Reinhorn [KR89] have added to the one component element two rigid end zones to take into account the high rigidity of the connection panels where converge beams and columns (Figure 27).

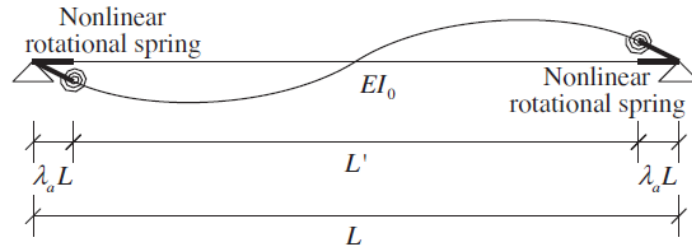


Figure 27 – One component element with rigid end zones.

Advanced models have taken into account the interaction between the axial force and the bending moment in the study of plane frames called “P-M interaction”; as well as the interaction between the axial force and biaxial bending moments. Furthermore, there were introduced rotational springs of finite length.

3.1.2 Distributed plasticity

This type of approach is constituted by a stiffness matrix using the shape functions for the discretization of the displacement field. The element displacements field $u(x)$ of eq. (3.1) depends on the values of the nodal displacements (Figure 28).

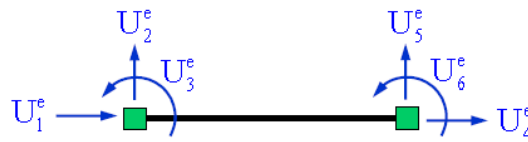


Figure 28 – Finite element degree of freedom.

$$u(x) = \begin{bmatrix} u(x) \\ v(x) \end{bmatrix} \cong N_U(x) U_e \quad (3.1)$$

On the displacement field a differential operator is applied in order to define the generalized strains, in the case of in plane Euler Bernoulli beam they are as in eq. (3.2):

$$e^s(x) = \begin{bmatrix} \varepsilon_0(x) \\ \chi(x) \end{bmatrix} = \begin{bmatrix} u'(x) \\ v''(x) \end{bmatrix} \cong \begin{bmatrix} \frac{d}{dx} & 0 \\ 0 & \frac{d^2}{dx^2} \end{bmatrix} N_U(x) U_e = B(x) U_e \quad (3.2)$$

Where $\varepsilon_0(x)$ is the centroid strain and $\chi(x)$ is the curvature, these two quantity form the generalized strains vector $e^s(x)$.

At this point the Principle of virtual work in the virtual displacement form is applied in order to obtain the stiffness matrix equation, eq. (3.3):

$$K_T^e = \int_0^L B^T(x) k_T^s(x) B(x) dx \quad (3.3)$$

In eq. (3.3) the section stiffness matrix $k^s(x)$ contains the mechanical nonlinearities and so it represents the link between generalized strains and stresses. For the linear case the sectional constitutive law is expressed as in eq. (3.4):

$$s^s(x) = \begin{bmatrix} N(x) \\ M(x) \end{bmatrix} = \begin{bmatrix} EA & 0 \\ 0 & EI \end{bmatrix} \begin{bmatrix} \varepsilon_0(x) \\ \chi(x) \end{bmatrix} = k^s(x) e^s(x) \quad (3.4)$$

For the nonlinear behavior case it is necessary to think in incremental terms and therefore for any increase in the generalized deformations corresponds an increase of generalized stresses, see eq. (3.5):

$$ds^s(x) = k_T^s(x) de^s(x) \quad (3.5)$$

At least from a theoretical point of view, if the quantity inside the integral of eq. (3.3) was known exactly the inelastic stiffness matrix K_T^e could be determined exactly. This is not feasible because the matrices $B(x)$ and $k^s(x)$ are only approximate representations of the real behavior of the structural element. In fact, the shape functions for the EB beam element are the Hermite polynomials, from what follows that the generalized deformation field $e^s(x)$ may describe at most constant axial deformation and linear curvatures which, as mentioned, are insufficient to describe the real inelastic behavior (see for example Figure 24). The sectional stiffness matrix, considering also the bending moment along the y direction, can be written as in eq. (3.6):

$$k_T^s(x) = \int_A \alpha^T(x) E(x, y, z) \alpha(x) dA = \int_A \begin{bmatrix} 1 & z & -y \end{bmatrix} E(x, y, z) \begin{bmatrix} 1 \\ z \\ -y \end{bmatrix} dA \quad (3.6)$$

As can be seen from eq. (3.6) the sectional stiffness matrix is function of the Young modulus $E(x, y, z)$ of which is composed the element; if inelastic deformations occur, the elastic modulus on that point is changed according to the constitutive law chosen and this affects the integrals inside $k_T^s(x)$. The nonlinear behaviour is introduced by means of nonlinear constitutive laws

that can be expressed at sectional level in terms of generalized forces ($N(x)$, $M(x)$, $V(x)$) and deformation ($\varepsilon_0(x)$, $\chi(x)$, $\gamma(x)$) according to the classical theory of plasticity, or explicitly computed according to a fiber section discretization.

The latter consists in dividing into fibers (Figure 29) the element cross section; each fiber follows precise cyclic uniaxial constitutive laws. From the strain state of all the fibers is possible to define the current tangent modules so as to integrate the sectional stiffness matrix in a discrete way.

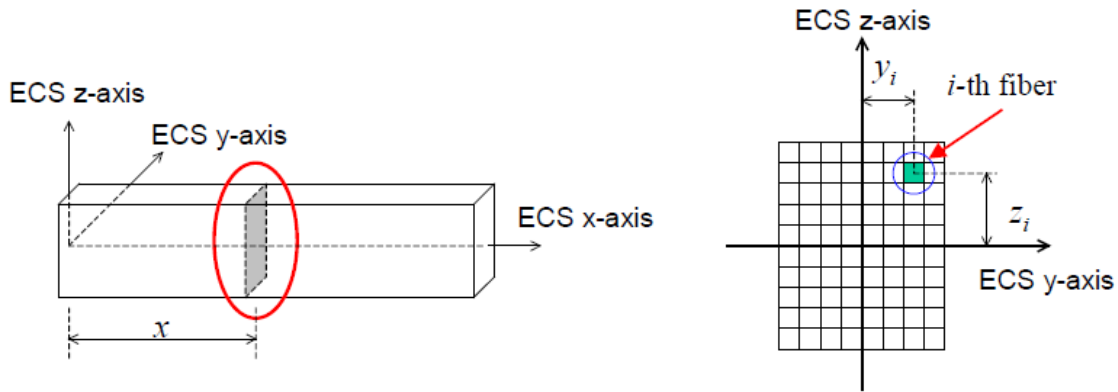


Figure 29 – Fibers discretization of the element cross section [MID15].

Therefore, the strain of each fiber is defined by the hypothesis that the cross sections, of the deformed element, remain plane and orthogonal to the longitudinal axis line (typical of Euler Bernoulli beam). This implies that the configuration in the cross section is univocally defined by three parameters which are the two curvatures, and the centroid fiber deformation. It means that the i -th strain fiber can be defined according to eq. (3.7):

$$\varepsilon_i = [1 \quad z_i \quad -y_i] \begin{bmatrix} \varepsilon_0(x) \\ \chi_y(x) \\ \chi_z(x) \end{bmatrix} \quad (3.7)$$

Where,

x is the coordinate that identify the section,

χ_y is the curvature in y ,

χ_z is the curvature in z ,

ε_0 the centroid fiber deformation,

y_i is the y coordinate of the i -th fiber,

z_i is the z coordinate of the i -th fiber.

More over, the integral along x in eq (3.3) is not solved analytically but through a numerical integration that approximate the integral with a summation. Such summation samples the function inside the integral in proper points called Gauss points. The values of the function at these points are multiplied by the weights which substantially describe the "importance" that that point has for the summation.

The versatile aspect of this approach is that it is possible to assign to each fiber a different constitutive law; for a reinforced concrete section, this is of considerable importance because it is possible to separate the behavior of unconfined concrete from the confined one and explicitly describe the role of the longitudinal bars (Figure 30).

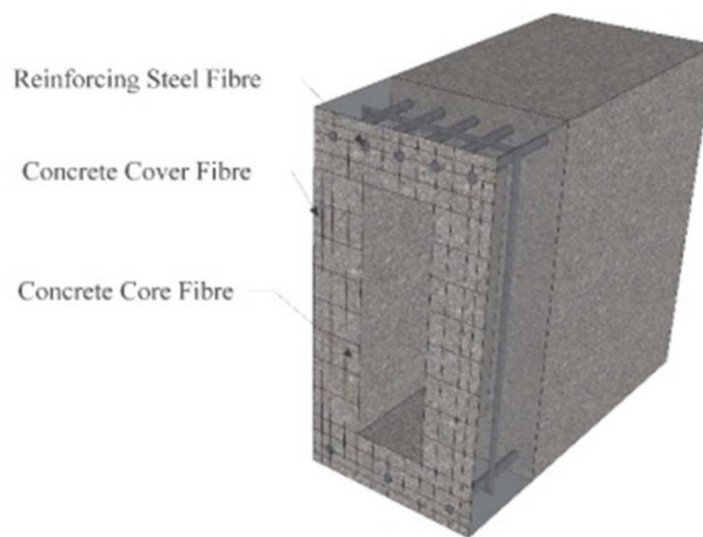


Figure 30 – Discretized rc cross section.

One of the first distributed approach was the one of prof. Taylor that expresses the prototype of what now mean fiber beam element (Figure 31). The use of this approach became more popular with the advent of more powerful and faster computers, because the time required for the assembling of the stiffness matrix was no longer a problem.

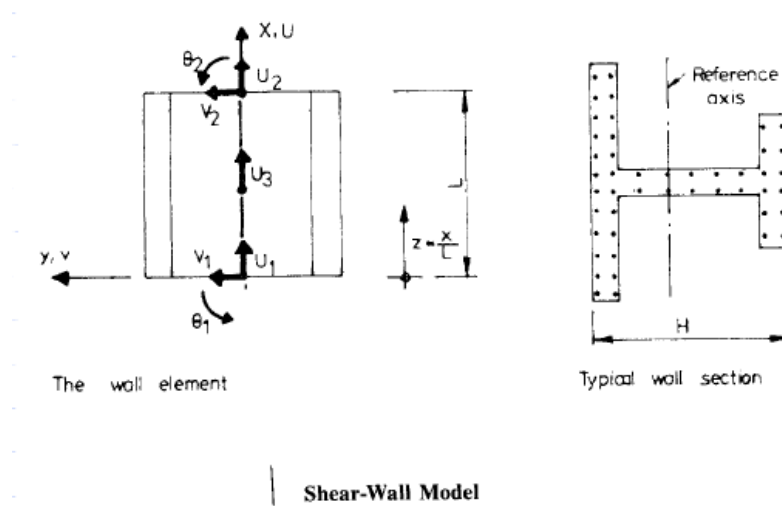


Figure 31 – Filament model (Taylor 1976).

A less dated example was the one of Malerba and Bontempi [MB89] who published a work on the formulation of a distributed finite element for the study of reinforced concrete structures capable of considering both the mechanical and geometric nonlinearity. One of the interesting aspects of this work is the integration scheme of the stiffness matrix, in fact the numerical integration according to Gauss-Legendre is used not only along the x coordinate, but also in the y - z (on the cross section domain). In particular, it was used a scheme to three Gauss points along the longitudinal coordinate, Figure 32 (a), while the cross section was divided into quadrilaterals subdomains with four sampling points by means of an isoparametric transformation as shown in Figure 32 (b).

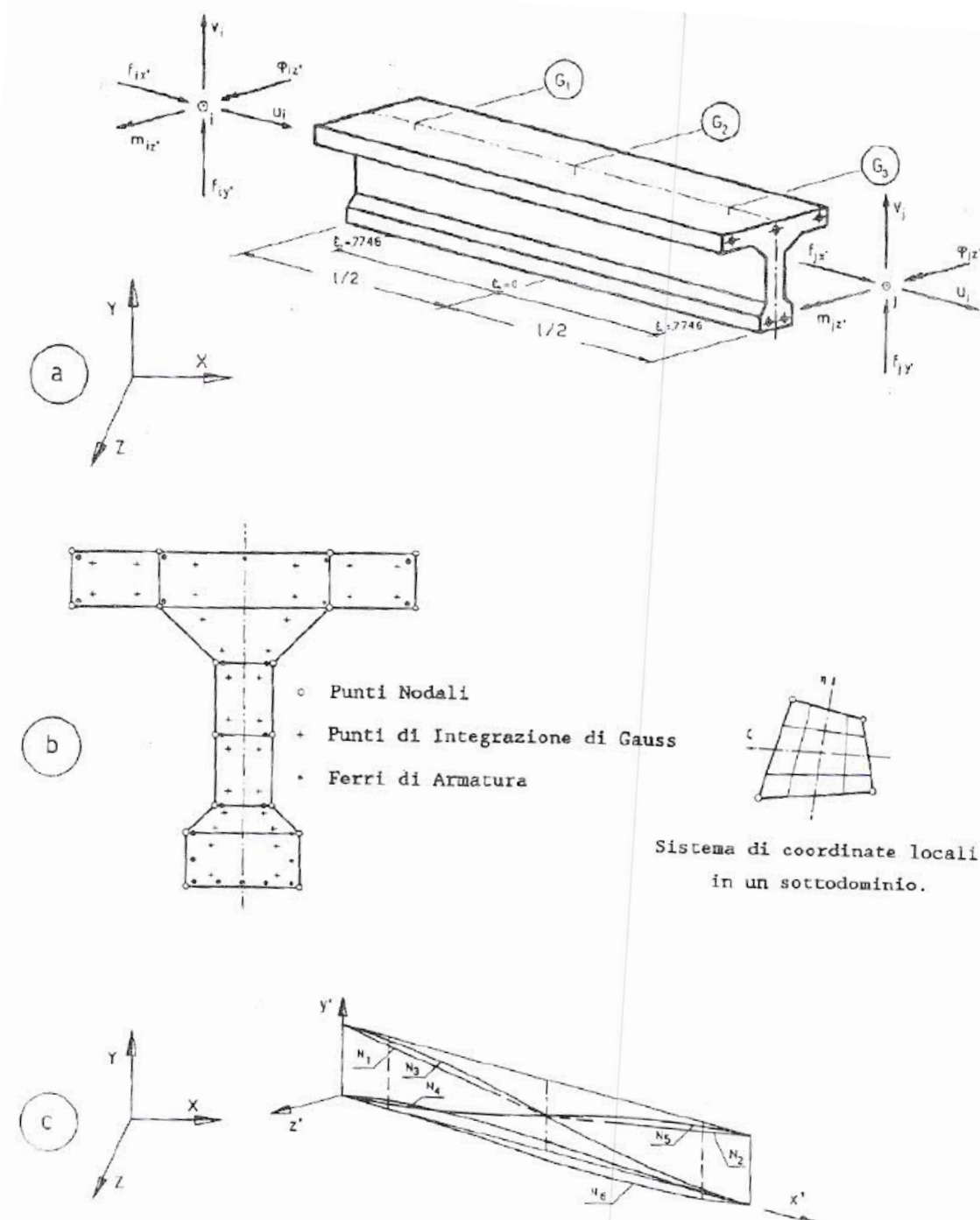


Fig. 1. L'elemento trave in C.A. :

- Sistema di coordinate locali (x', y', z') ; Forze $(f_{ix'}, f_{iy'}, f_{iz'}, m_{ix'}, m_{iy'}, m_{iz'}, \dots)$ e Spostamenti Nodali $(u_i, v_i, \phi_i, \dots)$; Sezioni campione per l'integrazione (G_1, G_2, G_3, \dots) a 3 punti di Gauss).
- Suddivisione della sezione G_k in sottodomini quadrilateri.
- Funzioni di forma N_1, N_2, \dots, N_6 .

Figure 32 – Malerba-Bontempi's finite element; (a) coordinate system, nodal forces, nodal displacements, Gauss points; (b) section quadrilateral subdomain; (c) Shape functions [MB89].

Another widely used model is the one of Spacone et al. [SFT96] where instead of the usual formulation based on the displacement he used a force approach (Figure 33).

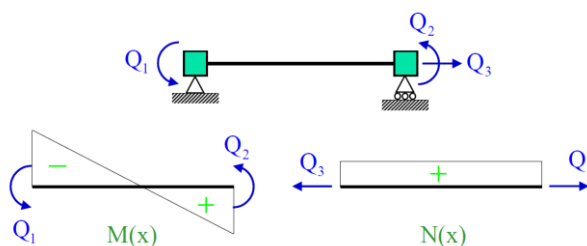


Figure 33 Shape function of the element [SFT96].

This choice is based on the consideration that, whatever the degree of non-linearity of the element is, the linear description of the force field remains exact (if there are not distributed loads). Moreover, this formulation is also consistent in the elastic case if the element is not prismatic.

3.1.3 Spread plasticity

In order to solve problems related to the stiffness distribution variability along the member, the discrete element models and the spread plasticity models were introduced (Figure 24).

The discrete element models consist in subdividing the member into short line segments along the length of the member, with an assigned nonlinear hysteretic characteristic for each short segment. The nonlinear stiffness can be assigned within a segment, or at the connection of two adjacent segments.

Wen and Janssen [WJ65] presented a method for nonlinear analysis of plane framed structures consisting of elasto-plastic member divisions. Powell [Po75] suggested a degrading stiffness hysteresis model for rigid inelastic connecting springs (Figure 34a). Shorter segments were recommended in a region of high moment, and longer segments in a low-moment region.

Takayanagi and Schnobrich [TS76] proposed to divide a member into short segments, each segment with a piecewise constant flexural stiffness that varies with a stress history of the segment as shown in Figure 34b. This model marks the direction for the spread plasticity formulation; in fact in a discrete sense it can be seen as a spread plasticity element.

These first two models, shown in Figure 34, require a extensive computational effort compared with other lumped plasticity models and may therefore be considered appealing only when very accurate results are required.

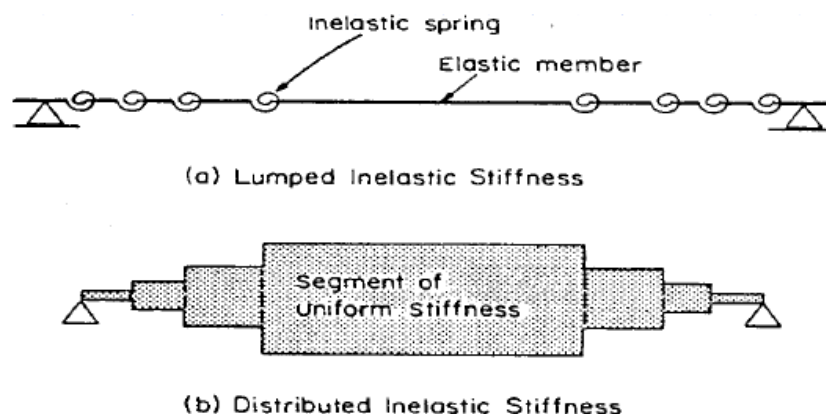


Figure 34 – Discrete Element models (a) [Po75] and (b) [TS76] from [OTA80].

The spread plasticity models provide a more general methodology to nonlinear structural analysis, in fact the nonlinearities develop anywhere along the structural member. The spread approach does not use shape functions and numerical integration rules to calculate the element stiffness matrix, in fact, it is computed with a direct approach.

The latter property permits the formulation not to be affected by the shear locking problem, in fact this is a numerical issue due to the shape functions adopted that in such models are not used.

Instead of dividing the member into shorter segments as shown for [TS76], Takizawa [TAK73] developed a model that assumes a prescribed flexural stiffness distribution along the length of the member. A parabolic distribution, with an elastic value of the flexibility at the inflection point shown in Figure 35. The flexural flexibility at the member ends is given by a hysteretic model dependent on the stress history.

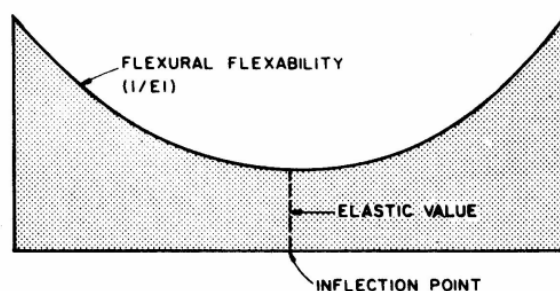


Figure 35 – Takizawa's model [TAK73] from [OTA80].

Another spread or distributed model considering a linear distribution of the flexibility was proposed by Park et al. [PRK87] and implemented in the original version of IDARC2D [IDA96]. The distribution is linear from the ends of the member to the inflection point as shown in Figure 36.

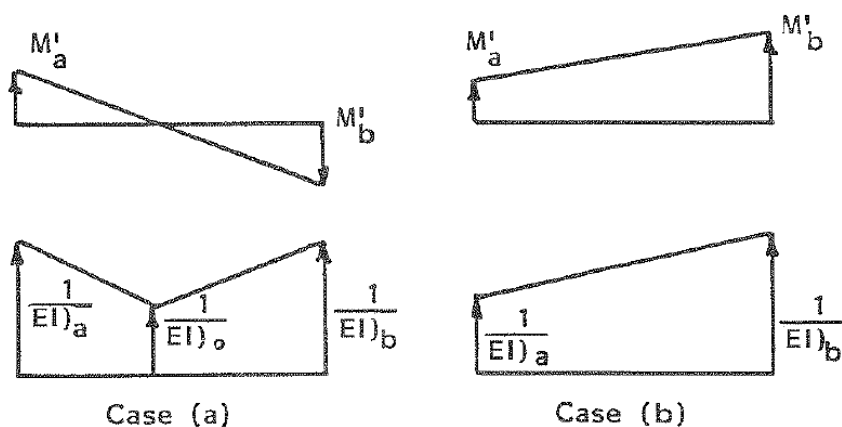


Figure 36 – Park et al. model from [PRK87].

In order to overcome numerical problems of solution stability a linear spread plasticity model and a uniform spread plasticity model, presented in Figure 37, were proposed in [KR89].

This is due to the fact that during time history analysis the inflection point shifts quickly inside the member length and so it determines a continuum updating of the element stiffness matrix causing numerical instabilities.

In [KR89] the flexibility varies only in the inelastic zones while the rest of the member is elastic with a constant flexibility.

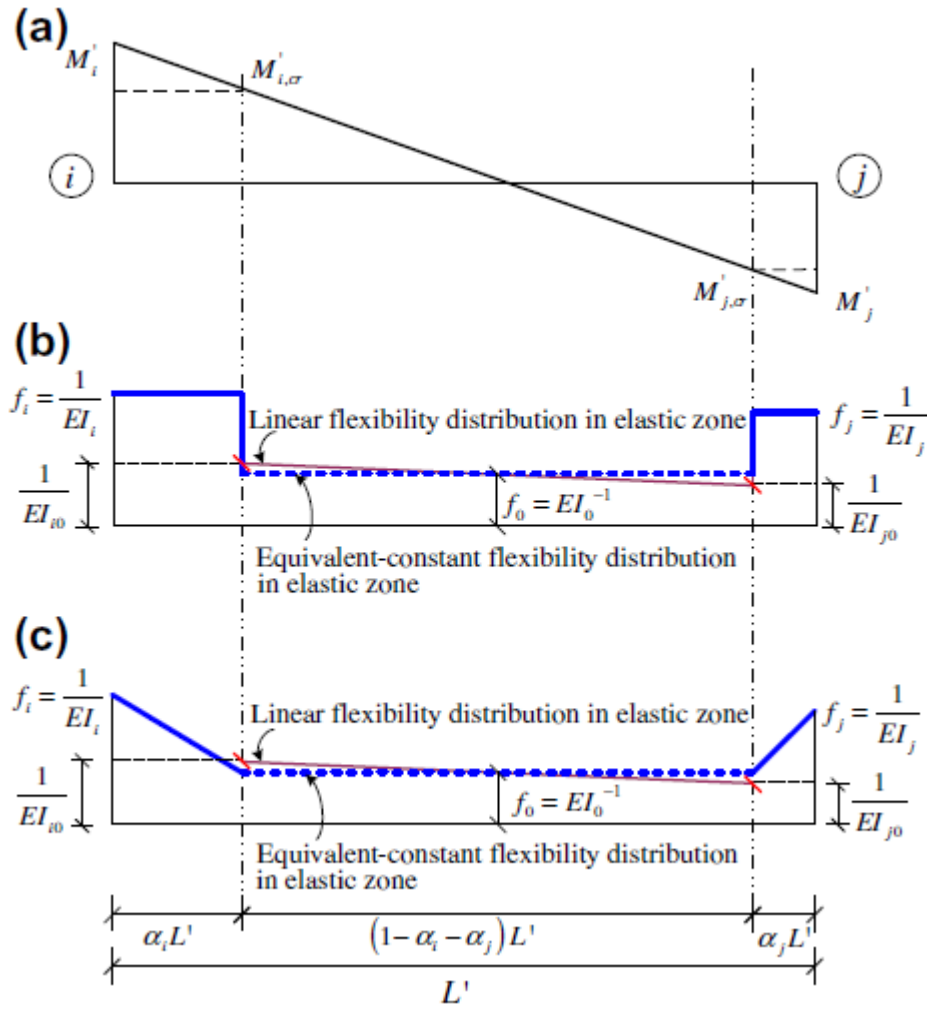


Figure 37 – Spread models with constant (b) and linear (c) flexibility [RRL12].

The spread plasticity model uses nonlinear constitutive laws that are expressed at sectional level in terms of generalized forces ($M(x)$, $V(x)$) and deformation ($\chi(x)$, $\gamma(x)$) according to the classical theory of plasticity.

In subsequent the interaction between the axial force and the bending moment was taken into account; as well as the interaction between the axial force and the biaxial bending moments P- M_x - M_y interaction using a fiber method.

In order to have a refined knowledge on spread model approaches, let us pass through the classical formulation.

The flexibility distribution is assumed to follow the trends of Figure 37 for the two alternative case (constant and linear spread plasticity models); EI_i and EI_j are the current flexural stiffnesses of the sections at ends ‘i’ and ‘j’, respectively. EI_0 is the “mean” flexural stiffness in the elastic segment of the element, i.e. where $M' < M'_{cr}$. The shear stiffness GA_0 is considered constant throughout the length of the member. The plastic zones, i.e. the segments where $M' > M'_{cr}$ are defined by the dimensionless parameters called yield penetration coefficients α_i and

α_j , while L' is the length of the element without rigid zones. The flexural stiffnesses EI_i and EI_j are determined from the hysteretic models, based on the moment–curvature envelope evaluated, for example, with a fiber approach. The equivalent stiffness EI_0 and the yield penetration coefficients α_i and α_j are calculated with the moment distribution and the previous yield penetration history. In fact it is assumed that the current α_i and α_j cannot be less than the previous one.

The rotation at each ends can be expressed using the flexibility matrix, this is given by eq. (3.8):

$$\begin{bmatrix} \theta'_i \\ \theta'_j \end{bmatrix} = \begin{bmatrix} f_{ii} & f_{ij} \\ f_{ji} & f_{jj} \end{bmatrix} \begin{bmatrix} M'_i \\ M'_j \end{bmatrix} \quad (3.8)$$

where f_{ij} are the flexibility coefficients, θ'_i and θ'_j are the rotations at the ends of the element, while M'_i and M'_j are the corresponding moments. The flexibility coefficients are obtained from the principle of virtual work as written in eq. (3.9).

$$f_{ij} = \int_0^{L'} \frac{m_i(x)m_j(x)}{EI(x)} dx + \int_0^{L'} \frac{v_i(x)v_j(x)}{GA(x)} dx \quad (3.9)$$

where $m_i(x)$ and $m_j(x)$ are the moment distributions due to a virtual unit moment at end “i” and “j”, respectively; $v_i(x)$ and $v_j(x)$ are the corresponding shear distributions ($1/L'$). Such distributions are shown in Figure 38.

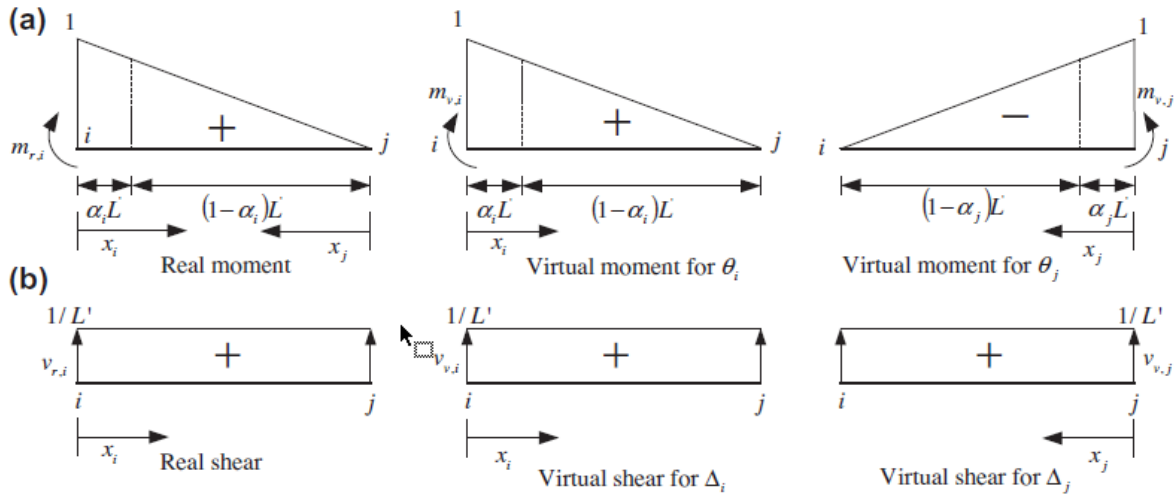


Figure 38 – Unit virtual force: (a) moments and (b) corresponding shears at the ends i and j [RRL12].

The flexibility coefficients for the constant spread plasticity distribution is given in eq. (3.10):

$$\begin{aligned}
 f_{ii} &= L' \left[\left(\frac{1}{EI_0} + \frac{1}{EI_i} \right) - \frac{1}{EI_0} \alpha_i (3 - 3\alpha_i - \alpha_i^2) + \left(\frac{1}{EI_j} - \frac{1}{EI_0} \right) \alpha_j^3 \right] + \frac{1}{GA_0 L'} \\
 f_{ij} &= -\frac{L'}{6} \left[\frac{1}{EI_0} + \left(\frac{1}{EI_i} - \frac{1}{EI_0} \right) \alpha_i^2 (3 - 2\alpha_i) + \left(\frac{1}{EI_j} - \frac{1}{EI_0} \right) \alpha_i^2 (3 - 2\alpha_i) \right] \\
 &\quad + \frac{1}{GA_0 L'} \\
 f_{ji} &= f_{ij}
 \end{aligned} \tag{3.10}$$

$$f_{jj} = -\frac{L'}{3} \left[\frac{4}{EI_0} + \left(\frac{1}{EI_j} - \frac{1}{EI_0} \right) \alpha_i (3 - 3\alpha_i - \alpha_i^2) + \left(\frac{1}{EI_i} - \frac{1}{EI_0} \right) \alpha_i^3 \right] + \frac{1}{GA_0 L'}$$

where GA_0 is the “mean” shear stiffness that is considered constant throughout the length of the member. In the case of a linear variation of shear flexibility, GA_0 is defined as $2GA_{i0}GA_{j0}/(GA_{i0} + GA_{j0})$. GA_{i0} and GA_{j0} are the elastic shear stiffnesses of the sections at the ends of the element. The stiffness EI_0 is an equivalent constant flexural stiffness of the elastic portion of the member and is defined as $2EI_{i0}EI_{j0}/(EI_{i0} + EI_{j0})$, where EI_{i0} and EI_{j0} are the elastic stiffnesses of the sections at the ends of the element.

Analogously, for the case of linear spread plasticity distribution, the flexibility matrix terms are written in eq. (3.11).

$$\begin{aligned}
 f_{ii} &= \frac{L'}{12} \left[\frac{4}{EI_0} + \left(\frac{1}{EI_i} - \frac{1}{EI_0} \right) (6\alpha_i - 4\alpha_i^2 + \alpha_i^3) + \left(\frac{1}{EI_j} - \frac{1}{EI_0} \right) \alpha_j^3 \right] + \frac{1}{GA_0 L'} \\
 f_{ij} &= \frac{L'}{12} \left[\frac{-2}{EI_0} - \left(\frac{1}{EI_i} - \frac{1}{EI_0} \right) (2\alpha_i^2 - \alpha_i^3) - \left(\frac{1}{EI_j} - \frac{1}{EI_0} \right) (2\alpha_j^2 - \alpha_j^3) \right] + \frac{1}{GA_0 L'} \\
 f_{ji} &= f_{ij}
 \end{aligned} \tag{3.11}$$

$$f_{jj} = \frac{L'}{12} \left[\frac{4}{EI_0} + \left(\frac{1}{EI_j} - \frac{1}{EI_0} \right) (6\alpha_j - 4\alpha_j^2 + \alpha_j^3) + \left(\frac{1}{EI_i} - \frac{1}{EI_0} \right) \alpha_i^3 \right] + \frac{1}{GA_0 L'}$$

The yield penetration parameters, α_i and α_j , multiplied by L' gives the length of the element where the acting moment is greater than the section cracking moment, $M_{i,cr}$ or $M_{j,cr}$. These parameters are first calculated from the current moment distribution, and then checked with the

previous maximum penetration lengths $\alpha_{i,\max}$ and $\alpha_{j,\max}$, equation (3.12). The yield penetration parameters cannot be smaller than the previous maximum values regardless of the current moment distribution.

$$\alpha_i = \frac{M'_i - M'_{i,cr}}{M'_i - M'_j} \leq 1 \quad \text{for } |M'_i| < |M'_{i,cr}|$$

$$\alpha_j = \frac{M'_j - M'_{j,cr}}{M'_j - M'_i} \leq 1 \quad \text{for } |M'_j| < |M'_{j,cr}|$$
(3.12)

Recently Roh, Reinhorn and Lee [RRL12] proposed a general power form to account for different flexibility distributions of the member as written in eq. (3.13). The power n represents the variation of flexural flexibility from the ends of the element to the boundary of the plastic strain zone and the subscripts i and j represent the sections at the ends of the element. For section i , the flexural flexibility distribution is defined in eq. (3.13) and it is shown in Figure 39:

$$f^m(x_i) = (f_i^m - f_0^m) \left(1 - \frac{x_i}{\alpha_i L'}\right)^{n_i} + f_0^m \quad \text{for } 0 \leq x_i \leq \alpha_i L' \quad (3.13)$$

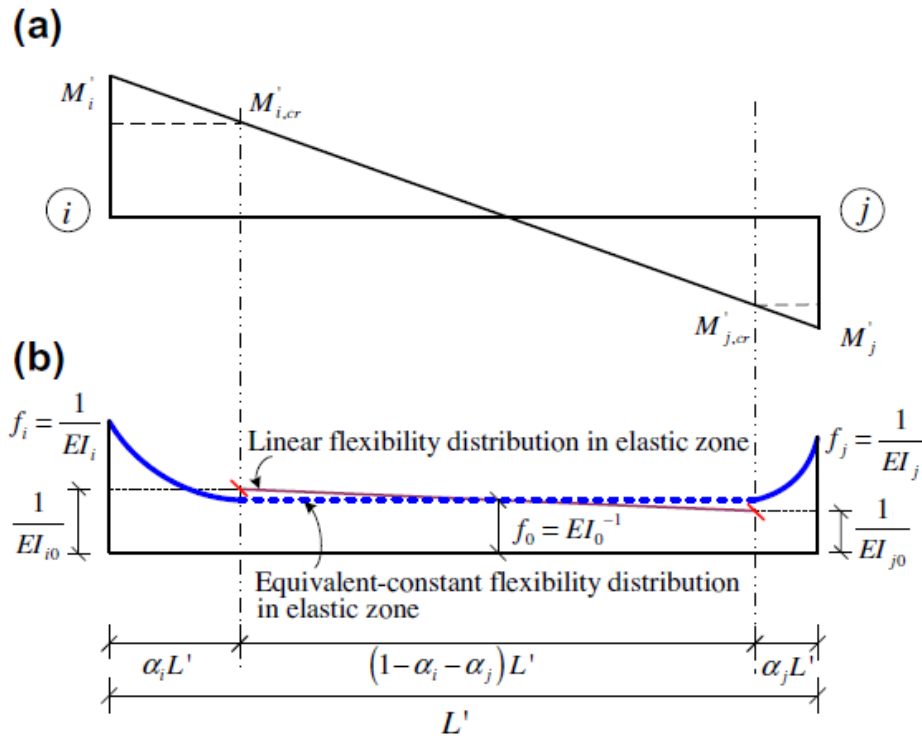


Figure 39 - Distribution of: (a) moment and (b) flexibility [RRL12].

With the increasing of the parameter n , it is possible to reach different flexibility distributions based on the plastic gradient of the analysis (Figure 40).

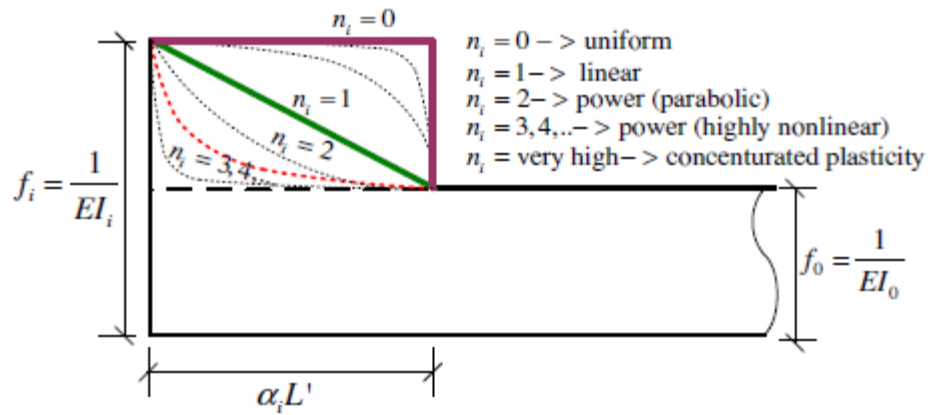


Figure 40– Type of distributions for different values of the power n at section i [RRL12].

In [RRL12] also for this case the flexibility matrix terms are calculated the details are omitted because it goes beyond the purpose of this work.

3.2 Final considerations

The spread plasticity approach is a great evolution of the concentrated plasticity models, and as such helps to improve results especially in cyclic non-linear analysis. The fact that the length of the plastic zone can evolve during the analysis, leads to a greater correspondence with the physical reality of the problem, in fact, the choice of the plastic hinge length (which is not necessarily equal to the plastic zone length) for the concentrated plasticity models will greatly influence the results.

4 BEAM MODELS WITH MULTIPLE SINGULARITIES

4.1 Introduction

The study of differential equations to model the elasto-static behaviour of beams is interesting in many fields. For example in tapered structural elements or in case of abrupt changing in the material composition. Another example is the back analysis to find the position and the intensity of a damage in a structural element. In both of them, the differential equation solution can be found by making use of the distribution theory such as unit step and Dirac's delta functions.

4.2 Euler–Bernoulli beams with multiple singularities

Biondi and Caddemi in 2005 [BC05] reconsidered the theory of distributions to propose an integration procedure of Euler–Bernoulli (EB) beams with a single discontinuity over a unique integration domain without enforcement of continuity conditions at the discontinuities. According to the latter procedure, discontinuities of the curvature or of the slope function are treated as singularities of the flexural stiffness modelled by means of unit step functions or Dirac's deltas, respectively. Later the same authors generalized the procedure to the multiple singularities case [BC07].

The integration procedure leads to closed form expressions of the response functions requiring the evaluation of integration constants, only, by means of the boundary conditions.

In case of multiple singularities, the distribution of flexural stiffness along the domain can be expressed as in eq. (4.1):

$$E(x)I(x) = E_0I_0 \left[1 - \sum_{i=1}^n \alpha_i D(x - x_{0,i}) \right] \quad (4.1)$$

The latter equation describes a reference flexural stiffness $E_0 I_0$ with n variations of intensity α_i at abscissa $x_{0,i}$, modelled by means of n distributions here indicated as $D(x-x_{0,i})$. In what follows two cases of distributions, able to reproduce physical conditions for the Euler–Bernoulli beam, are considered. Two types of distributions, such as n unit step distributions $U(x-x_{0,i})$ and m Dirac's deltas $\delta(x-x_{0,i})$, are considered leading to two different models as follows in eq. (4.2) and Figure 40 and Figure 41:

$$\begin{aligned} E(x)I(x) &= E_0 I_0 \left[1 - \sum_{i=1}^n \gamma_i U(x - x_{\gamma,i}) \right], \\ E(x)I(x) &= E_0 I_0 \left[1 - \sum_{j=1}^m \beta_j \delta(x - x_{\beta,j}) \right], \end{aligned} \quad (4.2)$$

Where $E_0 I_0$ is the reference rigidity, γ and β are parameters that reproduce the intensity of the discontinuity while $x_{\gamma,i}$ and $x_{\beta,j}$ the position.

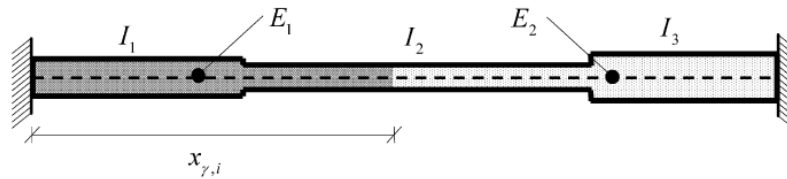


Figure 41 –Beam with discontinuities in the Young modulus $E(x)$ and in the inertia moment $I(x)$ [BC07].

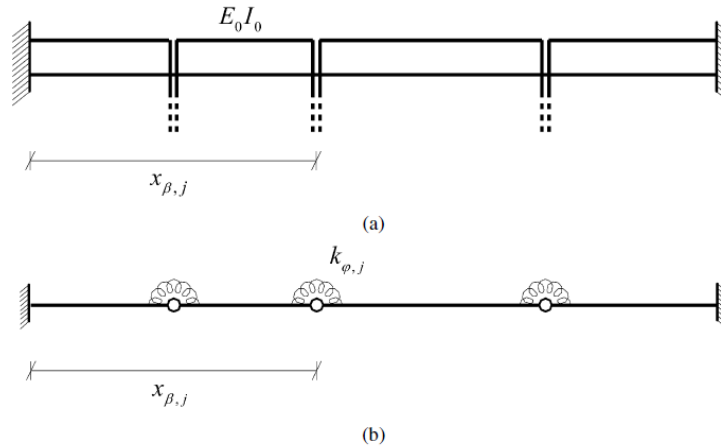


Figure 42–A beam with Dirac's delta singularities in the flexural stiffness, correspondent to (b) a beam with internal hinges and rotational springs with stiffnesses $k_{\phi,i}$. [BC07].

Only the case of multiple jump discontinuities in the flexural stiffness, will be treated because of more interest. Such case has been treated in the literature, without major difficulty, both for single [YSM00] & [YSR01] and double jumps [YS01]. In particular, in those procedures enforcement of continuity conditions, at the sections where jumps appear, is required. Aim of the integration procedure followed in [BC07] is avoiding enforcement of the continuity

conditions and providing closed form solutions for any number and position of the discontinuities (coincident with those provided in the literature for single and double discontinuities). In the case of flexural stiffness composed by n unit step distributions, the governing equation assumes the form written in eq. (4.3):

$$\left[E_0 I_0 \left(1 - \sum_{i=1}^n \gamma_i U(x - x_{\gamma,i}) \right) u''(x) \right]'' = q(x). \quad (4.3)$$

Where $q(x)$ is a generic load distribution, $u(x)$ is the vertical displacement, while the symbol $()'$ denotes differentiation with respect to the spatial coordinate x spanning from 0 to the length l of the beam.

A double integration leads to:

$$u''(x) = \frac{b_1 + b_2 x + q^{[2]}(x)}{E_0 I_0 (1 - \sum_{i=1}^n \gamma_i U(x - x_{\gamma,i}))} \quad (4.4)$$

where b_1 and b_2 are integration constants and $q^{[k]}(x)$ indicates a primitive of order k of the external load function $q(x)$. After simple algebra and making use of the unit step function properties, is possible to rewrite eq. (4.4) in eq. (4.5):

$$\chi(x) = -u''(x) = - \left(2c_3 + 6c_4 x + \frac{q^{[2]}(x)}{E_0 I_0} \right) \left(1 + \sum_{i=1}^n \gamma_i \mu_i \mu_{i+1} U(x - x_{\gamma,i}) \right) \quad (4.5)$$

Where the following position have been accounted for:

$$c_3 = \frac{b_1}{2E_0 I_0}; c_4 = \frac{b_2}{6E_0 I_0}; \mu_i = \frac{1}{1 - \sum_{k=1}^{i-1} \gamma_k} \quad (4.6 \text{ a-c})$$

With further integrations, it is possible to obtain the rotation function $\varphi(x)$ and the deflection $u(x)$:

$$\begin{aligned} \varphi(x) = -u'(x) = & -c_2 - 2c_3 \left[x + \sum_{i=1}^n \gamma_i \mu_i \mu_{i+1} (x - x_{\gamma,i}) U(x - x_{\gamma,i}) \right] \\ & - 3c_4 \left[x^2 + \sum_{i=1}^n \gamma_i \mu_i \mu_{i+1} (x^2 - x_{\gamma,i}^2) U(x - x_{\gamma,i}) \right] \\ & - \frac{q^{[3]}(x)}{E_0 I_0} - \sum_{i=1}^n \gamma_i \mu_i \mu_{i+1} \frac{q^{[3]}(x) - q^{[3]}(x_{\gamma,i})}{E_0 I_0} U(x - x_{\gamma,i}) \end{aligned} \quad (4.7)$$

$$\begin{aligned} u(x) = & c_1 - c_2 x - 2c_3 \left[x^2 + \sum_{i=1}^n \gamma_i \mu_i \mu_{i+1} (x - x_{\gamma,i})^2 U(x - x_{\gamma,i}) \right] \\ & + c_4 \left[x^3 + \sum_{i=1}^n \gamma_i \mu_i \mu_{i+1} (x^3 - 3x_{\gamma,i}^2 x + 2x_{\gamma,i}^3) U(x - x_{\gamma,i}) \right] \\ & + \frac{q^{[4]}(x)}{E_0 I_0} + \sum_{i=1}^n \gamma_i \mu_i \mu_{i+1} \frac{q^{[4]}(x) - q^{[4]}(x_{\gamma,i}) - q^{[3]}(x_{\gamma,i})(x - x_{\gamma,i})}{E_0 I_0} U(x - x_{\gamma,i}) \end{aligned} \quad (4.8)$$

The bending moment function is obtained by multiplying the curvature function by the flexural stiffness as written in eq. (4.9):

$$M(x) = E(x)I(x)\chi(x) = -E_0 I_0 \left(2c_3 + 6c_4 x + \frac{q^{[2]}(x)}{E_0 I_0} \right) \quad (4.9)$$

The shear force function in eq. (4.10) is obtained by means of differentiation of eq. (4.9):

$$V(x) = M'(x) = -E_0 I_0 \left(6c_4 + \frac{q^{[1]}(x)}{E_0 I_0} \right) \quad (4.10)$$

It has to be remarked that the discontinuity intensities γ_i and positions $x_{\gamma,i}$ will appear explicitly in the integration constants c_3, c_4 for statically indeterminate beams only.

4.3 Final considerations

The spread plasticity model is based on the principle of virtual work in order to determine the element flexibility matrix, this is equivalent to imposing equilibrium in the nodes. As in every finite element method the outputs that are obtained are nodal quantities and it is not always possible to know what happens within the nodes. The stress recovery phase is in fact quite complex and also knowing the kinematic quantities within the finite element beyond the elastic limit is not in general obtainable. However, there are alternatives methods that are not using the principle of virtual work to determine the general solution and the element flexibility matrix, one of these makes use of the theory of distributions to solve the differential equations that directly govern the structural problem.

In other words, using a standard spread plasticity model, the only way to know what happens within the nodes is to refine the mesh because is based on the principle of virtual work and it has the control only in the nodes (weak formulation). Instead, using the model presented in this chapter and in section 6.1.1, adopting Heaviside's distributions function to model abrupt, both flexural and shear, stiffness discontinuities of the beam, it is possible to lead to the exact closed-form solution because it is based on the differential equation associated (strong formulation). This alternative approach was exposed because it is the base of the proposed finite element.

5 RC FRAME STRUCTURES ELEMENTS WITH SHEAR MODELLING

5.1 Introduction

This chapter is dedicated to the review of the main existing beam-column elements formulation with shear modelling, underling their characteristics.

5.2 Main approaches

5.2.1 Martinelli's model

Martinelli has developed a fiber frame element based on the Timoshenko beam theory to model the cyclical response of the critical areas at the ends of the bridge piers feature a medium-low shear strain [MA98]. The author has proposed a finite element based on the model of Garstka et al. [GKS93], coupling a 3D fiber model for bending and axial deformation with a hyperstatic inelastic truss model composed by transverse reinforcement and concrete compression diagonals in tension and compression. The element is formulated with an displacement approach with the tree nodes; the intermediate node has a reduced number of degrees of freedom with respect to external nodes: only rotations and axial displacements. The element does not suffer of shear-locking phenomenon having a constant average shear strain along the element and a linear variation of curvature. Bending and axial contributions are calculated as volume integrals split in area integrals, approximated by summation over cross-section's fibers, and line integrals computed using a five point Gauss-Lobatto scheme. Shear contribution is computed by integration along the element of the shear force acting at the cross-sections. The displacement vector $u(x)$ in eq. (3.1) has the components shown in Figure 43, with five (3-D

beam) or three degrees (2-D beam) of freedom per node (torsion not accounted for):

$$u(x) = \{u(x), v(x), w(x), \theta_y(x), \theta_z(x)\}^T \quad (5.1)$$

The shear resultant for the cross section is derived from different resistance mechanisms: arch mechanism, the truss mechanism, the compressed concrete above the neutral axis, and the aggregate interlock, each of which is studied independently, as described in the following.

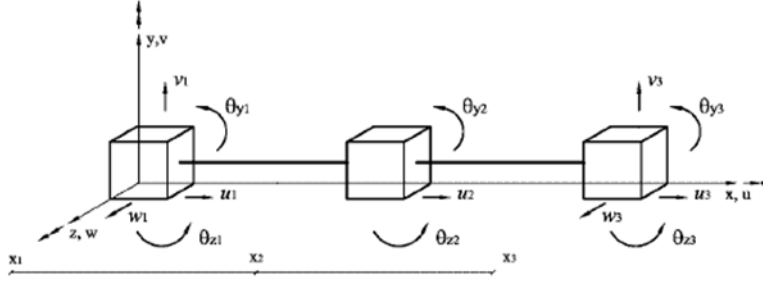


Figure 43– Nodal degrees of freedom of Martinelli's Fiber element [MAR98].

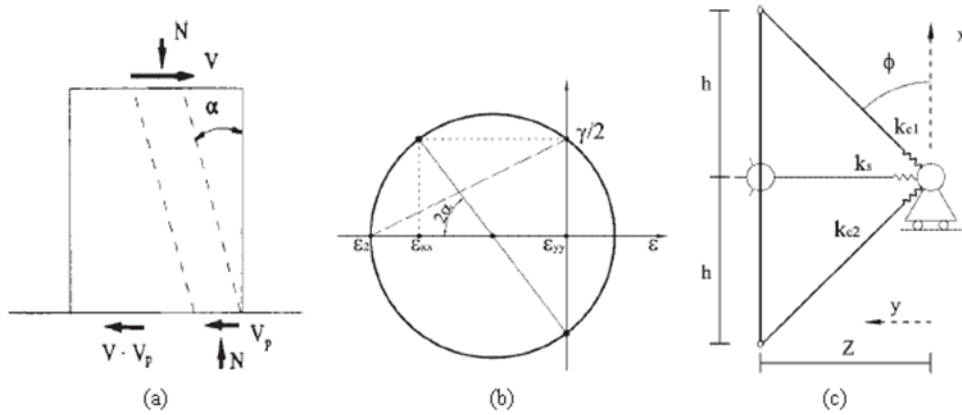


Figure 44 – (a) Inclined strut, (b) Mohr's circle used in arch action mechanism, and (c) assemblage used to model truss mechanism [MAR98].

The arch effect is schematically represented in Figure 44 (a), where it is observed that the inclined strut transfers a shear force proportional to the axial force: $V_p = N \cdot \tan \alpha$. The fibers are aligned with the strut, and the inclination is calculated by knowing the nodal moments (M_{zi} , M_{yi} , M_{zf} , M_{yf}), as well as the resultant of the compressive stresses. As a function of α , ϵ_{xx} and assuming $\epsilon_{yy} = 0$, it is derived the principal stress σ_2 of compression and shear deformation by $\gamma_{xy} / 2$ starting from Mohr circle Figure 44 (b). The constitutive laws used in conjunction with the strut mechanism are uniaxial and ϵ_2 is used to calculate the principal compression stress σ_2 , with the assumption $\sigma_1 = 0$, that is the principal tensile stress. From σ_2 , the normal and shear stresses, σ_{xx} , and τ_{xy} , are calculated through the Mohr circle. The resulting forces are derived

from an integration of the stresses on the gross section area A and the compressed concrete area A_{cc} as shown in eq. (5.2):

$$\begin{aligned} N &= \int \sigma_{xx} dA, V_{pxy} = \int \tau_{xy} dA, V_{pxz} = \int \tau_{xz} dA, \\ M_y &= \int \sigma_{xx} z dA, M_z = - \int \sigma_{xx} y dA, \end{aligned} \quad (5.2)$$

An iterative process is required to calculate α , even if the author notes that in the step by step dynamic analysis, α can be assumed, in a simplified way, as the value at the end of the previous step. The truss mechanism in the xy plane is based on the assembly of Figure 44 (c); it is composed by the transverse reinforcement (the horizontal element of Figure 44 (c), where Z is the lever arm) and the diagonal of concrete in compression and tension (respectively with subscripts 1 and 2 in Figure 44 (c)). The slope of the diagonal ϕ is a model parameter and is assumed to be equal to the inclination of the concrete cracks. The truss deformation is obtained by the shear strain calculated using the kinematics of the Timoshenko beam (ϵ_{xx} and γ_{xy} that are known quantities), while ϵ_{yy} is assumed to be equal to the transverse steel strain. Using the Mohr's circle the principal deformation are directly calculated. The transverse strain is obtained imposing the equilibrium along the y direction of the truss model ($\sigma_{yy} = 0$). The shear stress τ_{xy} acting in the cross section is derived by knowing the inclination of both diagonals in compression and tension and the corresponding principal stresses. The shear transferred by the truss action is calculated by integrating the shear stress on the concrete surface in tension of the cross-section: $V_t = \tau_{xy} A_t$. The shear stiffness contribution to the section stiffness matrix, K_{shear_xy} , due to the stiffness of the transverse reinforcement and of concrete fibers of the two diagonals, K_s , K_{C1} , K_{C2} , Figure 44, is calculated with eq. (5.3):

$$K_{shear_xy} = \left\{ \frac{1}{(\tan\phi)^2} (E_1 \alpha_{y,c1}^4 + E_2 \alpha_{y,c2}^4) \left[1 - \frac{E_1 \alpha_{y,c1}^4 + E_2 \alpha_{y,c2}^4}{E_1 \alpha_{y,c1}^4 + E_2 \alpha_{y,c2}^4 + \rho_s E_s} \right] \right\} A_t \quad (5.3)$$

where E_1 , E_2 , E_s are the tangent moduli of the fibers for concrete and steel, respectively; A_t is the area of the concrete in tension, $\alpha_{i,j}$ is the cosine of the angle between the i and j axes; ρ_s is the geometric transverse reinforcement ratio. The K_{shear_xz} contribution is calculated using a similar assembly to that used for modeling the mechanism of the truss in the xy plane and then, with reference to eq. (5.3), the subscript y must be replaced by z . To model the aggregate interlock, it is assumed that a set of diagonal cracks of constant spacing s (parameter of the model), inclined at a constant angle ϕ with respect to the beam axis, characterizes the concrete in traction. The τ_{xyIN} tangential component on the cross section is calculated from the normal and shear stresses arising from relative movements to the faces of the crack and calculated by ϵ_{xx} deformations, γ_{xy} and $\epsilon_{yy} = \epsilon_s$ derived from the truss model. The shear force due to the

aggregate interlock mechanism is derived from the integration of shear stresses τ_{xyIN} on the area of loaded concrete: $V_{IN} = \tau_{xyIN} A_t$. The shear resistance is provided by the sum of contributions V_p , V_t and V_{IN} .

The section stiffness matrix is provided by eq.(5.4):

$$\mathbf{K}_s = \begin{bmatrix} \int_A E & 0 & 0 & -\int_A yE & \int_A zE \\ 0 & K_{shear_xy} & 0 & 0 & 0 \\ 0 & 0 & K_{shear_xz} & 0 & 0 \\ -\int_A yE & 0 & 0 & \int_A y^2 E & -\int_A yzE \\ \int_A zE & 0 & 0 & -\int_A yzE & \int_A z^2 E \end{bmatrix} \quad (5.4)$$

where E is the elastic tangent modulus, and the two shear stiffness coefficients K_{shear_xy} and K_{shear_xz} are due to the truss contributions, eq. (5.3).

5.2.2 Ranzo and Petrangeli's model

With the aim of developing a beam element that models the shear behavior of the section to perform the seismic analysis of RC structures, Ranzo and Petrangeli [RP98] have proposed a 2D fiber element following a flexibility approach. The axial-flexural behavior is a function of axial deformation ϵ_x and curvature χ_y of the section, as in the traditional fiber model, while the shear behavior is a function of the section distortion $\gamma(x)$ equivalent to a non-linear truss model. The two mechanisms are then coupled by a damage criterion at the sectional level, following the model of Priestley et al. [PVX94], and it is integrated along the element.

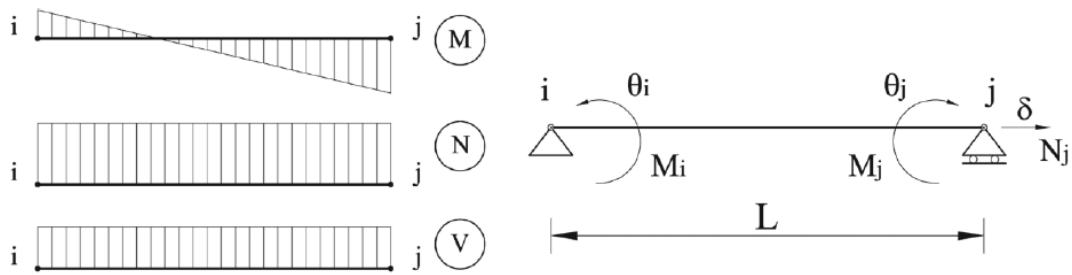


Figure 45– Stress shape functions and element forces and deformations [RP98].

In the element formulation, the shape functions of the forces field are introduced in the 2 nodes element (see Figure 45), in such a way that the axial forces, bending moment and shear can be expressed by eq. (5.5):

$$N(x) = N_j, M(x) = -(1 - x/L)M_i + (x/L)M_j, V(x) = (M_i + M_j)/L \quad (5.5)$$

where N_j is the axial load supposed constant, M_i and M_j are the moments at the ends. These forces are associated with the deformation of the ends, the axial elongation δ and the two rotations θ_i and θ_j . The vector of the section generalized forces $p(x)=[N(x), V(x), M(x)]^T$ and the vector of the generalized deformation $q(x)=[\epsilon_0(x), \gamma(x), \chi(x)]^T$ are connected through the section stiffness matrix in eq. (5.6):

$$K_{sec} = \begin{bmatrix} \sum_{i=1}^{nfib} E_i A_i & 0 & \sum_{i=1}^{nfib} E_i y_i A_i \\ 0 & \frac{\partial V(\gamma, \epsilon_{max})}{\partial \gamma} & 0 \\ \sum_{i=1}^{nfib} E_i y_i A_i & 0 & \sum_{i=1}^{nfib} E_i y_i^2 A_i \end{bmatrix} \quad (5.6)$$

Consequently, the axial and flexural stiffnesses are calculated in the usual way, by using the one-dimensional cyclic constitutive laws of the materials, while the shear stiffness is derived from the shear constitutive relation (including the backbone curve, unloading and reloading branches, shown in Figure 46) $V(\gamma, \varepsilon_{\max})$ as a function of the distortion γ and of the discrete variable ε_{\max} (equal to the maximum value of axial tensile strain recorded during the loading cyclic), as described below. It is worth noting that, no explicit bending-shear coupling is introduced in the definition of the section stiffness matrix in equation (5.6), implementation of this constitutive law in a force-based element couples bending and shear forces at the element level through equilibrium.

Since the element is forces based but has been implemented in the context of a finite element code based on the displacements, in the element state determination, the vector of generalized displacements is not known in advance and it is necessary to implement an iterative procedure.

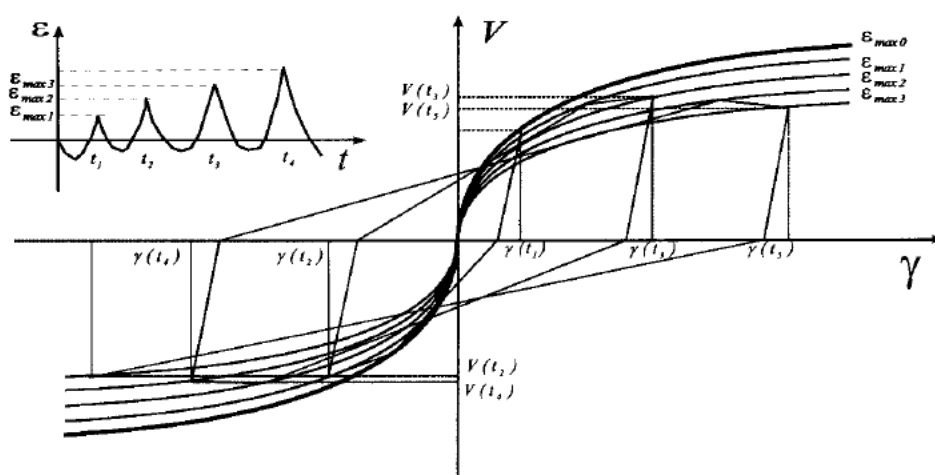


Figure 46— Section shear hysteretic model — skeleton and degraded curves [RP98].

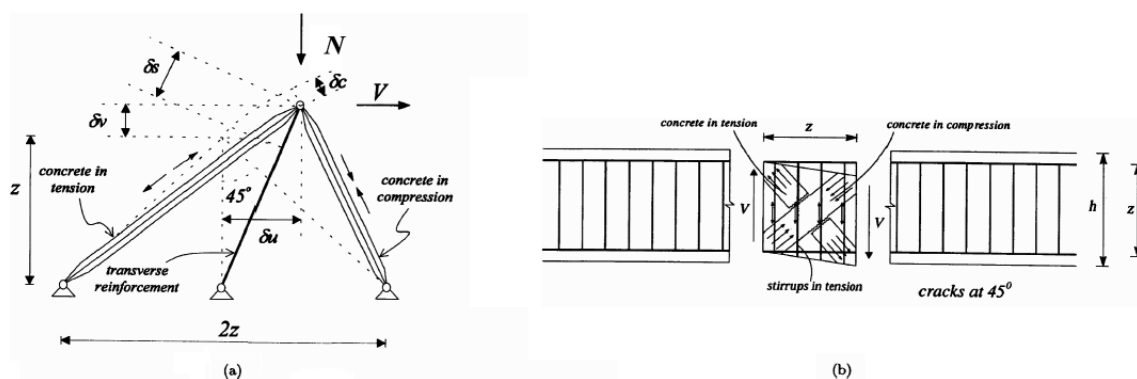


Figure 47 – Beam segment truss idealization [RP98].

The V - γ curve is determined by solving the truss model in Figure 47(a), having defined a constant mean value ϕ of inclination function of the axial load N , the shear reinforcement and behavior of the concrete diagonals in compression. The V - γ curve is obtained by applying the force V in small increments $\Delta V(i)$ up to collapse, with the distortion γ defined as $\delta u/(z + \delta v) \approx \delta u/z$ and using analytic functions to interpolate these discrete points, $V(i)=f(\gamma(i))$, to obtain a continuous curve. This procedure leads to the cracking determination, the yielding point and ultimate values of the shear strength and the distortion. To take into account the dependency of shear resistance by the ductility level, the skeleton branch of the hysteresis curve incorporates a degrading criterion in which the primary curve is a function of the maximum axial ε_{\max} , chosen as the damage indicator (Figure 46). The structural configuration shown in Figure 47(a) is a detailed representation of the beam segment illustrated in Figure 47(b), and displays the deformation of the concrete strut δ_c and steel δ_s . The strut of concrete in compression / tension is a single element of the truss whose area is a percentage of the gross surface area (depending on the neutral axis depth after cracking in bending). The segment of the shear reinforcement, however, is equivalent to a chord whose cross-section is equal to the sum of the crossing bars along the length of the segment plus a percentage of the longitudinal bars (assumed to be 0.3% of the gross section).

It is worth noting that the equivalent truss approach here used for the back bone curve is than scaled with the parameter ε_{\max} function of the ductility demand of the section. It means that some calibration is needed to find the best fit using a similar experimental test output.

5.2.3 Petrangeli, Pinto and Ciampi's model

Petrangeli et al. [PPC99] have developed a flexibility fiber element to model the shear behavior and its interaction with the axial force and the bending moment for beams and columns. This formulation leads to a 2D element with two nodes. The generalized variables are:

$$\begin{aligned} \mathbf{p}(\xi) &= [N(\xi) \ V(\xi) \ M(\xi)]^T \\ \mathbf{q}(\xi) &= [\varepsilon_0(\xi) \ \gamma(\xi) \ \chi(\xi)]^T \end{aligned} \quad (5.7)$$

where $\xi=x/L$ is the dimensionless coordinate.

The components of $\mathbf{p}(\xi)$ are expressed as already written in eq. (5.5) and shown in Figure 45. Also in this model an iterative procedure is used in order to calculate the vector $\mathbf{q}(\xi)$.

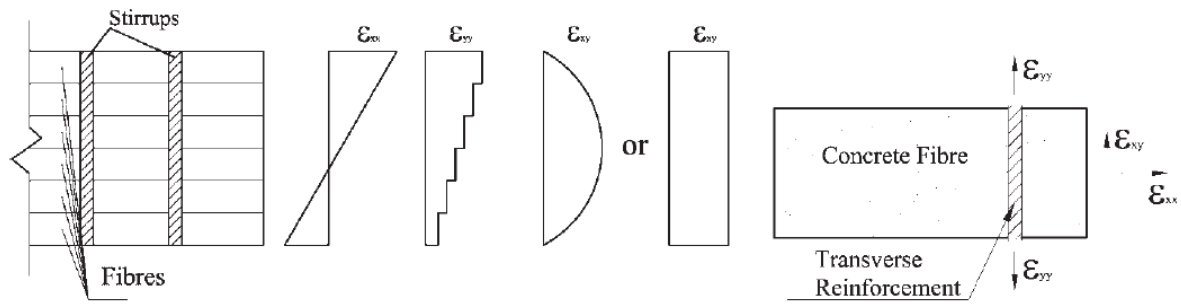


Figure 48– Section and fiber mechanics [PPC99].

The plane section hypothesis was adopted for the determination of the longitudinal strain field, $\varepsilon_{xx}(y)$. For the distortion, the authors used several predefined shear functions: the classic hypothesis of Timoshenko with a constant shear strain along the section, and a parabolic distribution (Figure 48), stating that both the shape functions have been tested with equally acceptable results. In order to find the strain in the transverse direction, ε_{yy} , equilibrium has been imposed in the vertical direction between concrete and steel for each fiber. Therefore, a complete strain vector $[\varepsilon_{xx}, \varepsilon_{yy}, \varepsilon_{xy}]^T$, is derived iteratively in every fiber.

Knowing the strain vector in every fiber, to describe the concrete behavior, a biaxial constitutive model should be introduced. For the i -th concrete fiber, eq. (5.8) in an incremental relation derived from the static condensation of the degree of freedom in the transverse direction y :

$$\begin{bmatrix} d\sigma_{xx}^i \\ d\sigma_{xy}^i \end{bmatrix} = \begin{bmatrix} K_a^i & K_{as}^i \\ K_{sa}^i & K_s^i \end{bmatrix} \begin{bmatrix} d\varepsilon_{xx}^i \\ d\varepsilon_{xy}^i \end{bmatrix} \quad (5.8)$$

where the fiber stiffness coefficients for axial force K_a^i and for shear K_s^i , as well as those that make coupling K_{as}^i and K_{sa}^i are written in eq. (5.9):

$$\begin{aligned} K_a^i &= (D_{11}^i - D_{12}^i D_{21}^i \alpha^i) \\ K_{as}^i &= (D_{13}^i - D_{12}^i D_{23}^i \alpha^i) \\ K_{sa}^i &= (D_{31}^i - D_{32}^i D_{21}^i \alpha^i) \\ K_s^i &= (D_{33}^i - D_{23}^i D_{32}^i \alpha^i) \end{aligned} \tag{5.9}$$

As biaxial constitutive relationships for concrete, the author selected a modified microplane model, which links together the microplane approach [BO85] and an equivalent uniaxial rotating concept. This model has the great feature to be one of the first with a biaxial constitutive law capable to reproduce monotonic and cycling loading, without a superimposed model for the shear behaviour. In fact, the sectional stiffness matrix in equation (5.8) is fully populated reflecting the coupling at sectional level.

On the other hand, the iterative procedure described has to be performed for each fiber at each load step, and so the effectiveness of the model is jeopardized.

5.2.4 Vecchio and Collins' model

Vecchio and Collins have presented the “dual-section analysis method” to predict the response of RC beams subject to shear and flexure; the authors have developed only a sectional model, without introducing the finite element formulation. The cross section is discretized in layers as shown in Figure 49. It is assumed that the cross-sections of the element remains plane. The analysis is called "dual" because the τ_{xy} tangential stresses calculation, equation (5.10), it is provided by the finite difference of the normal stresses distribution on each side of a layer of finite length (Figure 50):

$$\tau_{xy}(x) = -\frac{1}{b(y)} \int_{A'}^{B'} \frac{\partial \sigma_{xx}}{\partial x} b(y) dy \quad \text{dove} \quad \frac{\partial \sigma_{xx}}{\partial x} \cong \frac{\sigma_{xx}(x_2) - \sigma_{xx}(x_1)}{S} \quad (5.10)$$

where $b(y)$ is the section's width, y_b is the coordinate of the bottom layer, $\sigma_{xx}(x_2)$ e $\sigma_{xx}(x_1)$ are the normal stresses of the layer in the two analyzed sections, at distance S ($= H/6$, with H being the beam's depth).

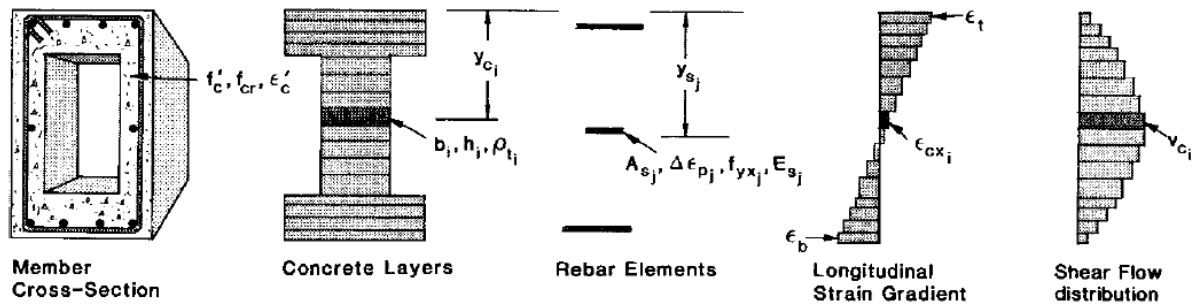


Figure 49 - Beam section discretization. Estimates of longitudinal strain gradient and shear flow distribution are required across section [VC88].

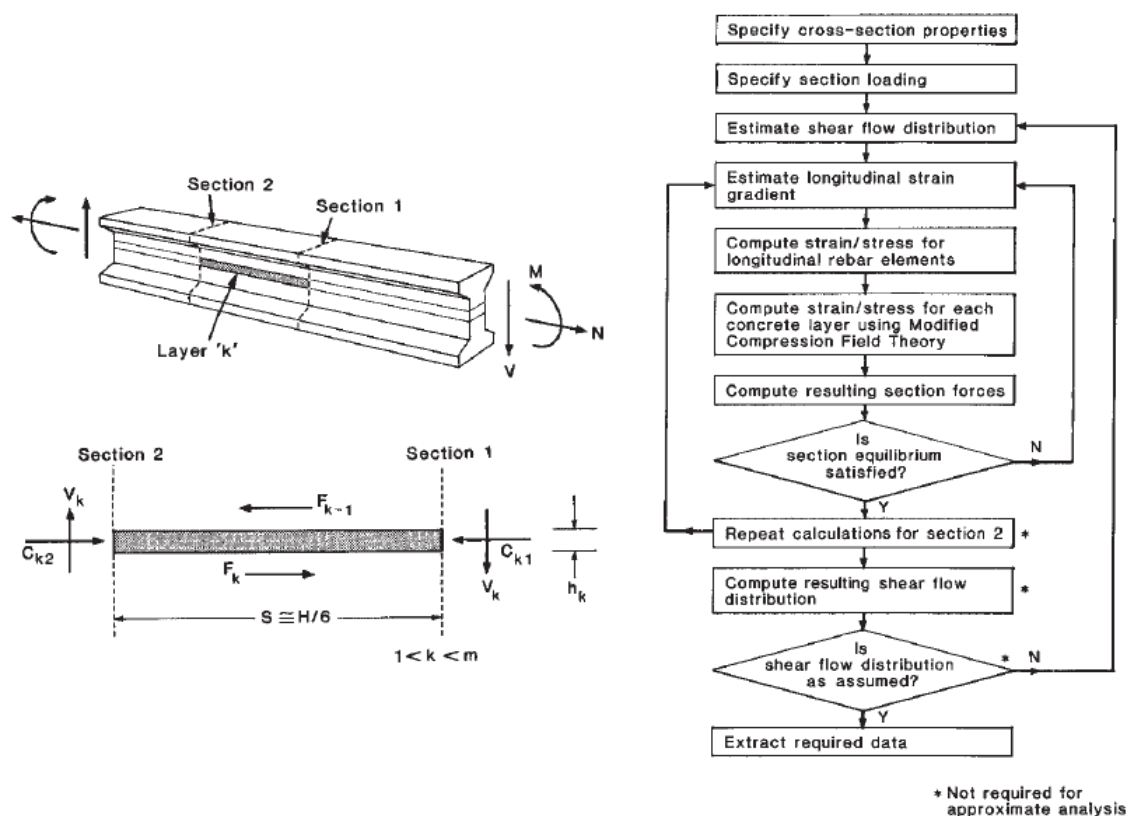


Figure 50– Dual section analysis: (a) scheme and free-body diagram for concrete layer k , and (b) solution procedure for beam analysis model [VC88].

The solution procedure for the sectional model is given in Figure 50 by mean of a flowchart. Since this analytical model requires a considerable computational effort, Vecchio and Collins have proposed two alternatives and approximate solutions assuming a priori a constant shear stresses distribution or a parabolic shear strain distribution. The assumption of one of these two approximations leads to the iterations elimination on the estimation of the tangential stresses distribution along the cross section (indicated with an asterisk in Figure 50) of the flow chart. As found by the authors, the approximate procedures lead to results, in terms of the global behavior of the beam, which are very close to those obtained using the most rigorous "dual section analysis". However, the constant shear flow assumption overestimates the shear stresses in the tension region (conservative results), while the parabolic shear strain assumption overestimates the shear stresses in the compression region of the section (unconservative predictions).

5.2.5 Marini and Spacone's model

Marini and Spacone, [MS06], have proposed a simplified approach using a phenomenological relation $V-\gamma$ for shear and distortion. Potentially the element has the enormous advantage of having a computational cost very low compared to other formulations of literature, for example, [PPC99], however, its effectiveness depends on the accuracy of the $V-\gamma$ constitutive law on which the model is based and it is necessary to provide new formulations.

In detail it has been formulated a 2D Timoshenko finite element with the forces approach that follows the formulation described in [SFT96]. Forces and nodal displacements are shown in Figure 51.

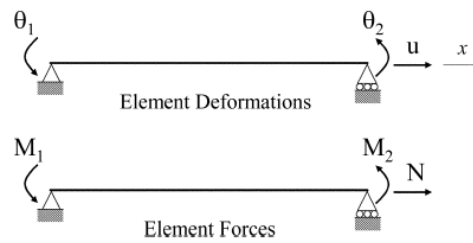


Figure 51 – Frame element forces and deformations [MS06].

Figure 52 shows section deformations, section forces and strain distribution along the height.

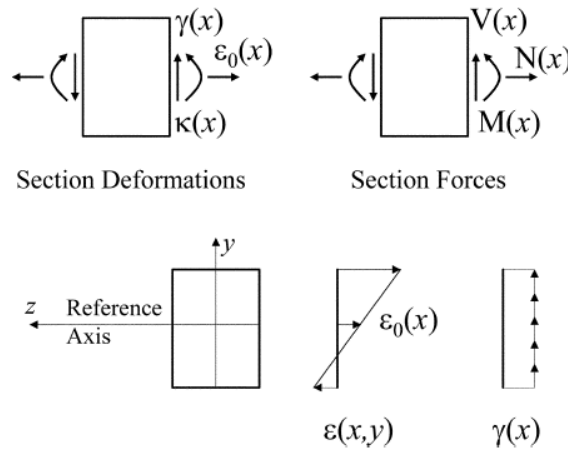


Figure 52– Timoshenko element: section forces, deformations, and strain distributions [MS06].

As shown in Figure 52, the element is formulated without rigid body modes, nodal forces and displacements are collected as in eq. (5.11).

$$\begin{aligned} P &= [M_1 M_2 N]^T \\ U &= [\theta_1 \theta_2 u]^T \end{aligned} \quad (5.11)$$

The generalized forces $s(x)$ and deformations $\varepsilon(x)$ are collected as in eq. (5.12).

$$\begin{aligned} s(x) &= [M(x) \quad N(x) \quad V(x)]^T \\ \varepsilon(x) &= [\chi(x) \quad \varepsilon_0(x) \quad \gamma(x)]^T \end{aligned} \quad (5.12)$$

At this point the Principle of virtual work in the virtual forces form is applied in order to obtain the eq. (5.13):

$$\delta P^T U = \int_0^L \delta s^T(x) \varepsilon(x) dx \quad (5.13)$$

Using equilibrium, the section forces $s(x)$ are written as functions of the end forces P through the force interpolation function $N_P(x)$ as in eq. (5.14)

$$s(x) = N_P(x)P \quad (5.14)$$

where

$$N_P(x) = \begin{bmatrix} \frac{x}{L} - 1 & \frac{x}{L} & 0 \\ 0 & 0 & 1 \\ -\frac{1}{L} & \frac{1}{L} & 0 \end{bmatrix} \quad (5.15)$$

Introducing the constitutive law to relate forces and deformation, it is possible to write eq. (5.16)

$$\varepsilon(x) = f(x)s(x) \quad (5.16)$$

where $f(x)$ is the section flexibility matrix and depends on the section model used for the element.

After substitution of eq. (5.14) and (5.16) in eq. (5.13), and after elimination of δP^T based on the arbitrariness argument, the element matrix compatibility equation is written as in eq. (5.17):

$$U = FP \quad (5.17)$$

where F is the element flexibility matrix without rigid body modes.

The sectional constitutive model is described in eq. (5.18) and eq. (5.19). As can be seen, at sectional level the shear strain is decoupled with respect the longitudinal deformation.

$$s(x) = \left\{ \begin{array}{l} \sum_{i=1}^{nfib} \sigma_i y_i A_i \\ \sum_{i=1}^{nfib} \sigma_i A_i \\ V = V(\gamma) \end{array} \right\} \quad (5.18)$$

$$k(x) = \left[\begin{array}{ccc} \sum_{i=1}^{nfib} E_i y_i^2 A_i & - \sum_{i=1}^{nfib} E_i y_i A_i & 0 \\ - \sum_{i=1}^{nfib} E_i y_i A_i & \sum_{i=1}^{nfib} E_i A_i & 0 \\ 0 & 0 & \frac{dV}{d\gamma} \end{array} \right] \quad (5.19)$$

It is worth noting that, while bending and shear forces are not related at the section level, implementation of this constitutive law in a force-based element couples bending and shear forces at the element level through equilibrium.

Equation (5.14) and (5.15) enforce equilibrium between internal and nodal forces. Therefore, if shear failure at the section level occurs before bending failure, the element bending moments are bound by the element shear forces. This is the main advantage of using a force-based element for a nonlinear Timoshenko beam. Even though the shear and bending responses are not coupled at the constitutive law level, they must be in equilibrium and thus failure in either bending or shear affects the force in either shear or bending.

The shear response is modeled using a nonlinear V - γ law. Different envelope curves are shown in Figure 53 and Figure 54 for the cyclic case. In Figure 53 the shear law has an initial parabolic branch and peaks at V_{Rd} , γ_y , which represents the section shear capacity. A linear branch follows, whose initial and final points are V_{Rd} , γ_y and V_u , γ_u , respectively. The last point represents the residual shear capacity.

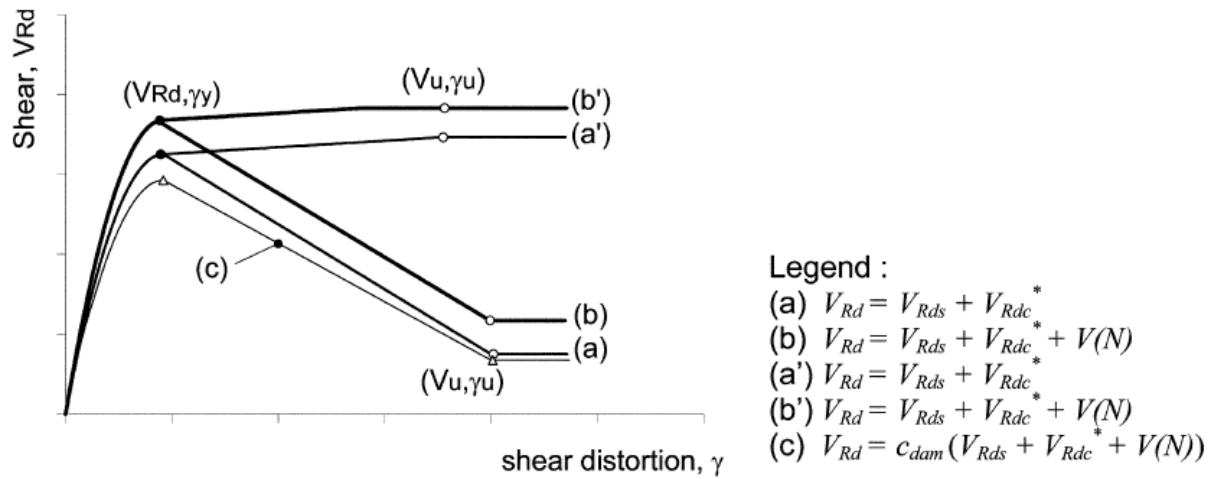


Figure 53 – Section shear law: possible envelope curves [MS06].

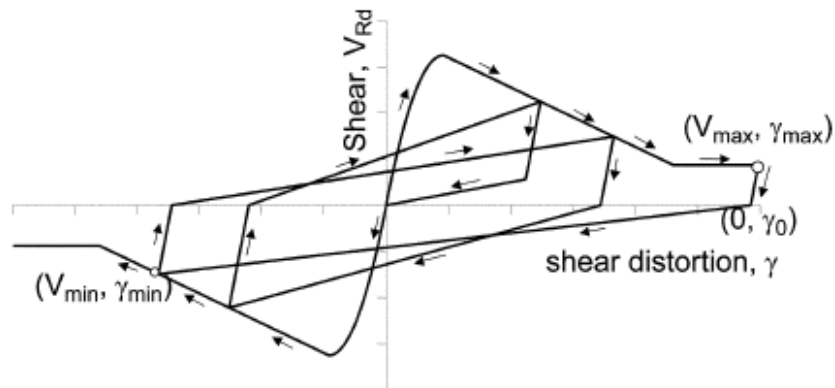


Figure 54– Section shear law: hysteretic rules [MS06].

The shear section resistance V_{Rd} is evaluated in accordance with a trinomial equation such as in [PP75]. Depending on the ductility that is found in the section due to the stirrups confining the concrete, it is possible to adopt the curves a' and b' or a and b in Figure 53.

It is also possible to degrade the shear strength, by the curve (c), through a coefficient C_{adm} , see [PP75]) that depends on the maximum longitudinal steel strain ε according to eq. (5.20):

$$\begin{aligned} C_{adm} &= 1 \text{ for } \varepsilon \leq \varepsilon_1 \\ C_{adm} &= 1 - \frac{\varepsilon - \varepsilon_1}{\varepsilon_2 - \varepsilon_1} \text{ for } \varepsilon_1 \leq \varepsilon \leq \varepsilon_2 \\ C_{adm} &= C_{adm,res} \text{ for } \varepsilon \geq \varepsilon_2 \end{aligned} \tag{5.20}$$

ε_1 and ε_2 are two limit strain values. Damage occurs as the shear distortion exceeds the lower limit ε_1 , whose value can be set to the yield strain of the longitudinal reinforcing bars (thus $\varepsilon_1 = \varepsilon_y$). No further damage occurs when the tensile strain exceeds the limit value ε_2 , and the damage coefficient is set to a constant value $C_{adm,res}$.

5.2.6 Ceresa et al. model

In the work of Ceresa et al. [CPPS09], a displacement based fiber element is formulated with a constitutive model that belongs to the smeared crack approach. The latter consists in treating cracked RC as an orthotropic material where cracks are smeared and allowed to rotate. Principal strain–stress directions are those corresponding to the average elastic compressive and tensile strains (crack directions). The Modified Compression Field Theory (MCFT) developed in 1986 by Vecchio and Collins [VC86], and one of its refinements, represented by the Disturbed Stress Field Model (DSFM) [VEC99] are used by the authors because it seems to be capable of accurately predict the shear strength of both reinforced and prestressed concrete members subjected to shear, flexure and axial loads. The MCFT was not formulated for cyclic loads but only for the monotonic case, to overcome this, Vecchio enlarged the formulation introducing a plastic offset capable to model cyclic loads [VEC00].

The element formulation is the simplest possible for a Timoshenko frame element, in fact the displacement field is interpolated by means of linear functions. This is because no internal nodes are inserted in the element length and so for each displacement component just two parameters can be used (there are two nodes).

In order to overcome the shear-locking problem, to the linear shape functions have been introduced an additional term, a linked term defined bubble function $N_b(x)$, for the transversal displacement field, following the formulation proposed by Auricchio [AU03]:

$$\begin{aligned} u(x) &= N_u(x)U \\ v(x) &= N_v(x)V + N_b(x)l(b\theta) \\ \theta(x) &= N_\theta(x)\theta \end{aligned} \quad (5.21)$$

Where $[U; V; \theta]$ are the nodal displacements, l is the element length, $N_u(x) = N_v(x) = N_\theta(x) = \left[1 - \frac{x}{l}, \frac{x}{l}\right]$ are the linear shape functions, $b = [1, -1]$ and $N_b(x) = \frac{1}{2}\left(1 - \frac{x}{l}\right)\frac{x}{l}$ is the special bubble function.

The kinematic assumption of the Timoshenko beam theory is that in the deformed element, the cross sections are still plane but no more orthogonal to the longitudinal axis line, it means that

$$v'(x) \neq \theta(x) \rightarrow \gamma_{xy} \neq 0$$

The sectional formulation involves the implementation of the proposed flexure–shear model, based on the MCFT, into a fiber beam–column finite element. It means that for each fiber i , a constitutive stiffness matrix of the composite material in the x-y system is evaluated (Figure 55).

$$\begin{bmatrix} \sigma_{xx} \\ \sigma_{yy} \\ \tau_{xy} \end{bmatrix}_i = \begin{bmatrix} D_{11} & D_{12} & D_{13} \\ D_{21} & D_{22} & D_{23} \\ D_{31} & D_{32} & D_{33} \end{bmatrix}_i \begin{bmatrix} \varepsilon_{xx} \\ \varepsilon_{yy} \\ \gamma_{xy} \end{bmatrix}_i - \begin{bmatrix} \sigma_{0xx} \\ \sigma_{0yy} \\ \tau_{0xy} \end{bmatrix}_i \quad (5.22)$$

The matrix $[D]_i$ is the stiffness matrix of the composite material in the x-y system, evaluated for each fiber i as in [VC86]. The vector $\begin{bmatrix} \sigma_{0xx} \\ \sigma_{0yy} \\ \tau_{0xy} \end{bmatrix}_i$ contains the plastic offset for cyclic loads [VEC00].

The $[D]_i$ can be divided in the sum of three terms:

$$[D]_i = [D_c]_i + [D_{sx}]_i + [D_{sy}]_i \quad (5.23)$$

where $[D_c]_i$ is the concrete material stiffness matrix, $[D_{sx}]_i$ and $[D_{sy}]_i$ are the reinforcement material stiffness matrices in the x- and y-directions. It means that longitudinal and transvers steel reinforcements can be explicitly taken into account in a smeared way.

As shown in Figure 55, in order to determine all the strains in eq.(5.22), equilibrium in the lateral direction between concrete and steel is imposed for each fiber, following the formulation proposed by [PPC99]. Therefore, a complete strain vector is derived iteratively for each fiber:

$$\sigma_{yy} = 0 \rightarrow \varepsilon_{yy} = \frac{\varepsilon_{xx}D_{21} + \gamma_{xy}D_{23}}{D_{22}} - \frac{\sigma_{0yy}}{D_{22}} \quad (5.24)$$

Once the equilibrium in the transverse direction is achieved within a specific tolerance error for each fiber, the static condensation of eq.(5.27) leads to the determination of the axial and shear stresses for each fiber:

$$\begin{bmatrix} \sigma_{xx} \\ \tau_{xy} \end{bmatrix}_i = \begin{bmatrix} \tilde{D}_{11} & \tilde{D}_{12} \\ \tilde{D}_{21} & \tilde{D}_{22} \end{bmatrix}_i \begin{bmatrix} \varepsilon_{xx} \\ \gamma_{xy} \end{bmatrix}_i + \begin{bmatrix} \sigma_{0xx} - \sigma_{0yy}\alpha_{12} \\ \tau_{0xy} - \sigma_{0yy}\alpha_{32} \end{bmatrix}_i \begin{bmatrix} \sigma_{0xx} \\ \sigma_{0yy} \\ \tau_{0xy} \end{bmatrix}_i \quad (5.25)$$

Where $\tilde{D}_{11}, \tilde{D}_{21}, \tilde{D}_{12}, \tilde{D}_{22}$ are the coefficients of the condensed composite material matrix and $\alpha_{12}=D_{12}/D_{22}$ and $\alpha_{32}=D_{32}/D_{22}$. This condensed matrix establishes a direct coupling between the axial and the shear strains, and therefore between axial and shear stresses at sectional level. In the flow chart of Figure 55 the procedure to determine the element stiffness matrix and the internal forces is described.

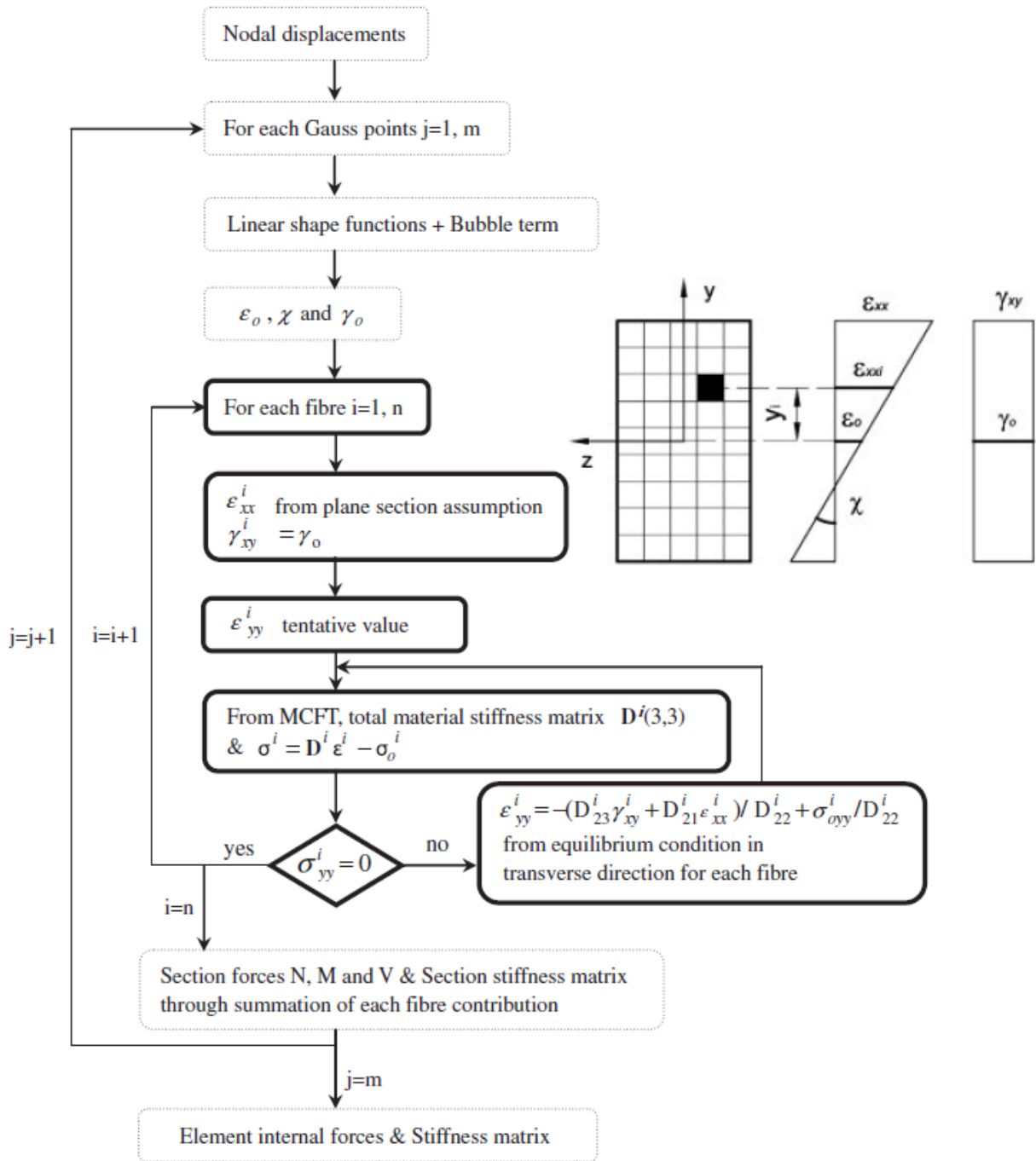


Figure 55 - Element state determination of the developed Timoshenko fiber beam element from [CPPS09].

The implemented uniaxial cyclic models are shown in Figure 56 according to [VEC00].

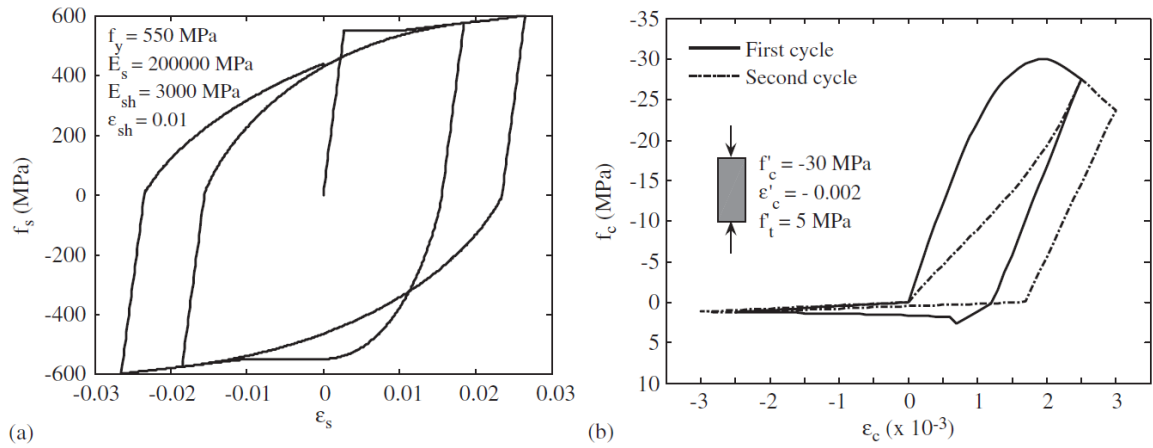


Figure 56 – Uniaxial laws for reinforcement (a) and concrete (b) from [CPPS09].

Also for this finite element, the iterative procedure described have to be performed for each fiber at each load step, and so the effectiveness of the model is jeopardized.

5.2.7 Mergos and Kappos's model

Mergos, Kappos and Beyer [MK08], [MB13], [MK12] have formulated a finite element model accounts for shear strength degradation with inelastic curvature demand, as well as coupling between inelastic flexural and shear deformations after flexural yielding, observed in many experimental studies. An empirical relationship is proposed for evaluating the average shear distortion of R/C columns at the onset of stirrup yielding based on the UCSD model of Priestley [PSC96].

This finite element consists of two sub-elements with spread flexibility, representing inelastic flexural and shear responses. The two sub-elements are connected by equilibrium and interact throughout the analysis to capture the shear–flexure interaction effect. The flexibility matrix of the finite element is calculated as the sum of the flexibilities of its sub-elements and can be inverted to produce the stiffness matrix.

The flexural sub-element is used for modelling the flexural behaviour of an RC member subjected to cyclic loading and it is capable to consider the yielded longitudinal reinforcement. It is formed by a hysteretic moment–curvature (M – ϕ) behaviour applied at the member end sections and the flexural stiffness distribution along the entire member is modelled with a spread plasticity approach.

The M – ϕ relationship at each end section of the member is formed by the backbone curve and the rules determining its cyclic behaviour. The primary M – ϕ relationship is derived using the standard section analysis, with proper constitutive laws for concrete and steel.

The multi-linear, ‘yield-oriented’ with slip, hysteretic model of Sivaselvan and Reinhorn [SR99] is adopted for describing M – ϕ behaviour. This model is an evolution of the Park et al. [PRK87] model; it accounts for stiffness degradation, strength deterioration, pinching effect, and nonsymmetric response. The work [SR99] is appropriately modified by the authors in order to be compatible with a bilinear skeleton curve because it was formulated for a trilinear curve model.

The stiffness distributions along the member have the profile of Figure 57, where L is the length of the member; EI_A and EI_B are the current flexural rigidities of the sections at the member ends A and B, respectively; EI_0 is the reference stiffness (normally taken equal to the secant value at yield M_y/ϕ_y); and α_A and α_B are the “yield penetration” coefficients.

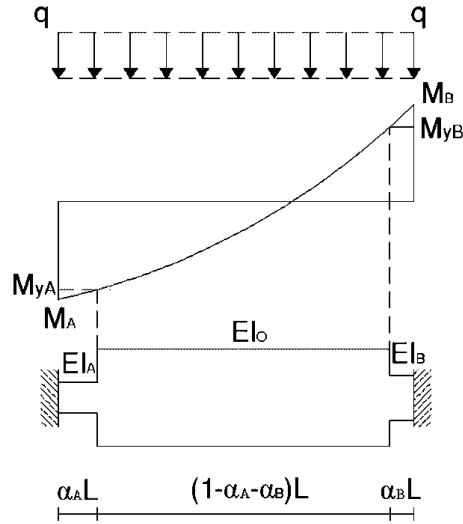


Figure 57- Flexural sub-element [MK08].

The flexural stiffness EI_A and EI_B are determined from the $M-\phi$ hysteretic relationship of the corresponding end sections. In this study, it was assumed that the state (loading, unloading, reloading) and the stiffness of the spread plastic zone is controlled by the state and the section stiffness at the end of the member; in other words the control sections coincide with the element nodes.

Once the stiffness values for each segment are known, the coefficients of the flexibility matrix of the flexural sub-element can be derived from eq. (5.26). The flexibility matrix is obtained using the Principle of virtual work on the member with the variable stiffness distribution of Figure 57.

$$\begin{aligned}
 f_{11}^{flex} &= \frac{(4EI_A EI_B + 4(EI_0 EI_B - EI_A EI_B)(3\alpha_A - 3\alpha_A^2 + \alpha_A^3) + 4(EI_0 EI_A - EI_A EI_B)\alpha_B^3)L}{12EI_0 EI_A EI_B} \\
 f_{12}^{flex} &= \frac{(-2EI_A EI_B - 2(EI_0 EI_B - EI_A EI_B)(3\alpha_A^2 - 2\alpha_A^3) - 2(EI_0 EI_A - EI_A EI_B)(3\alpha_B^2 - 2\alpha_B^3))L}{12EI_0 EI_A EI_B} \\
 f_{22}^{flex} &= \frac{(4EI_A EI_B + 4(EI_0 EI_B - EI_A EI_B)(3\alpha_B - 3\alpha_B^2 + \alpha_B^3) + 4(EI_0 EI_B - EI_A EI_B)\alpha_A^3)L}{12EI_0 EI_A EI_B}
 \end{aligned} \tag{5.26}$$

The shear sub-element is used for modelling the shear behaviour of an RC member subjected to cyclic loading and it is capable to consider the cracked state due to shear.

It is formed by a hysteretic shear force vs shear strain ($V-\gamma$) behaviour applied at the member end sections. The shear stiffness distribution along the entire member is modelled with a spread

plasticity approach. The shear strain γ , is defined as the average shear deformation along the discrete regions (cracked or uncracked) of the shear sub-element.

Initially, the backbone curve is calculated without including shear–flexure interaction effects (initial backbone). Then, shear–flexure interaction effects are modelled by using an appropriate analytical procedure.

The V – γ backbone curve is shown in Figure 58. The first branch connects the origin and the shear cracking point, which is defined as the point where the nominal principal tensile stress exceeds the mean tensile strength of concrete.

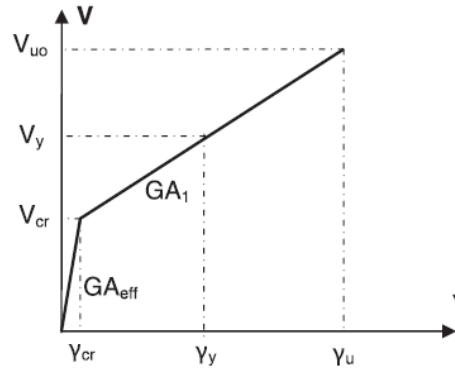


Figure 58 - Primary curve without degradation for shear force vs shear deformation [MK08].

The shear force at cracking is calculated using the procedure suggested by Sezen and Moehle [SM04], where the value is obtained with eq. (5.27):

$$V_c = \frac{f_{ctm}}{L_s/h} \sqrt{1 + \frac{N}{f_{ctm} A_g}} 0.8 A_g \quad (5.27)$$

where f_{ctm} is the mean concrete tensile strength, N is the compressive axial load, L_s/h is the shear span ratio, and A_g is the gross area of the concrete section. In eq. (5.27) is assumed an effective cross section area equal to the 80% of the gross area section.

The second branch of the initial primary curve connect the cracking point to the “failure” point (V_{uo}, γ_u) , this approach does not include the post peak branch of the response. The second and third branches are separated at the point corresponding to flexural yielding (V_y, γ_y) . This approach was adopted in order to distinguish hysteretic shear behaviour before and after flexural yielding [OS89].

The mean shear distortion at the onset of transverse reinforcement yielding, γ_y , is estimated using the truss analogy approach proposed by Park and Paulay [PP75] and Kowalsky and

Priestley [KP95]. In this method, in a cracked member, the shear deformation will arise from the extension of transverse reinforcement and the compression of the diagonal compression struts; the resulting shear distortion, γ_s , after shear cracking is provided by eq. (5.28)

$$\gamma_s = \frac{V_{cr}}{G A_{eff}} + \frac{V_s}{d - d'} \left(\frac{s}{E_s A_w \cot \theta^2} + \frac{1}{E_c b \sin \theta^3 \cos \theta \cot \theta} \right) \quad (5.28)$$

where A_w is the area of transverse reinforcement oriented parallel to the shear force; $d-d'$ is the distance measured parallel to the applied shear between the centers of longitudinal reinforcement; s is the spacing of transverse reinforcement; b is the width of the cross section; E_c is the elastic modulus of concrete, and E_s the elastic modulus of steel; V_s is the shear force resisted by the transverse reinforcement, and θ is the angle defined by the column axis and the direction of the diagonal compression struts. Then, γ_u is calculated using the eq. (5.28) by setting V_s equal to the shear strength contributed by the transverse reinforcement, V_y .

Regarding the shear strength, V_u , the approach proposed by Priestley et al. [PSC96] is invoked, which has been developed for both circular and rectangular columns. According to this approach, V_u is given by eq. (5.29):

$$V_u = k \sqrt{f_c} 0.8 A_g + N \tan \alpha + \frac{A_w f_{yw} (d - d') \cot \theta}{s} \quad (5.29)$$

where k is a parameter depending on the curvature ductility demand as shown in Figure 59, and α is the angle between the column axis and the line joining the centers of the flexural compression zones at the top and bottom of the column.

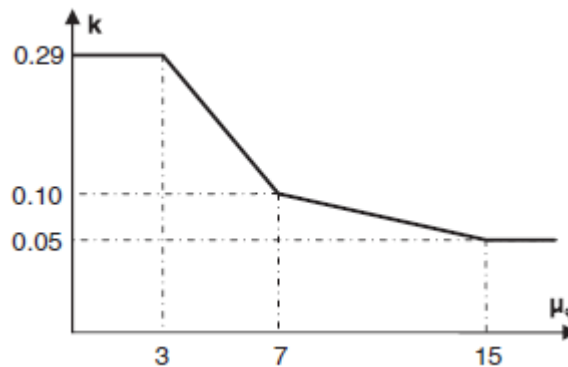


Figure 59 - Relationship between curvature ductility demand and strength of concrete shear resisting mechanisms [PSC96].

As implied by eq. (5.29), the shear strength decreases as the curvature ductility demand increases. So far, in the vast majority of nonlinear analyses of RC structures, this effect was taken into account by using, conservatively, the lower bound of shear strength. However, this approach has proven to be excessively conservative in many cases [PSC96]. In the work of [MK08] the shear strength degrades according to the current maximum curvature ductility demand. This is achieved using the following procedure.

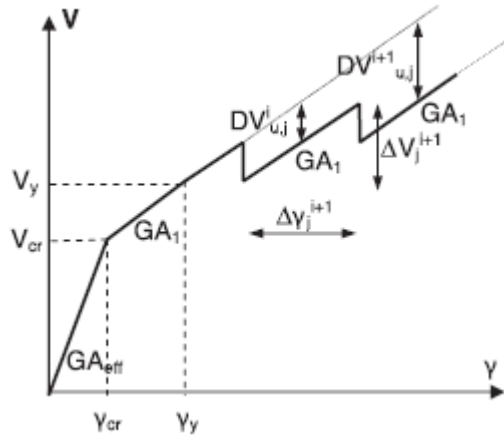


Figure 60 - Shear-flexure interaction procedure [MK08].

First, at each time step i of the analysis, the maximum curvature ductility demand of the critical cross section j ($j = A, B$), $\mu_{\phi j, max}^i$, of the critical cross section of the flexural sub-element is defined. Then, the corresponding k_j^i factor is determined from Figure 59 and this factor is used to calculate the current shear strength, $V_{u,j}^i$; hence, the shear strength degradation is

$$DV_{u,j}^i = V_{u0,j} - V_{u,j}^i \quad (5.30)$$

This shear strength degradation is then modelled by reducing the ordinate of the backbone curve of the respective end section of the shear sub-element, as shown schematically in Figure 60. In order to reset equilibrium, the shear force increment at the next time step $i+1$, ΔV_j^{i+1} , is calculated by the total moment distribution at this time step minus the respective shear force of the previous time step, V_j^i . Assuming uniform gravity load distribution, it is equal to

$$\Delta V_A^{i+1} = -\frac{qL}{2} + \frac{M_A^{i+1} - M_B^{i+1}}{L} - V_A^i \quad (5.31)$$

$$\Delta V_B^{i+1} = \frac{qL}{2} + \frac{M_A^{i+1} - M_B^{i+1}}{L} - V_B^i$$

Assuming that the end section of the shear sub-element still remains in the loading phase, the shear force increments calculated using the above equilibrium equations give rise to the respective shear strain increments, $\Delta\gamma_j^{i+1}$, defined by eq.(5.32) and shown schematically in Figure 61.

$$\Delta\gamma_j^{i+1} = \frac{\Delta V_j^{i+1}}{GA_1} \quad (5.32)$$

Combining the analytical procedure shown in Figure 60 and the relationship between curvature ductility demand and the RC shear strength resisting mechanisms presented in Figure 59, it yields to the modified shear primary curve shown in Figure 61. Furthermore, it is assumed that the curvature ductility capacity of the critical cross section exceeds the value of 15 (which is often not the case in old-type members) and that the element fails in shear after yielding in flexure.

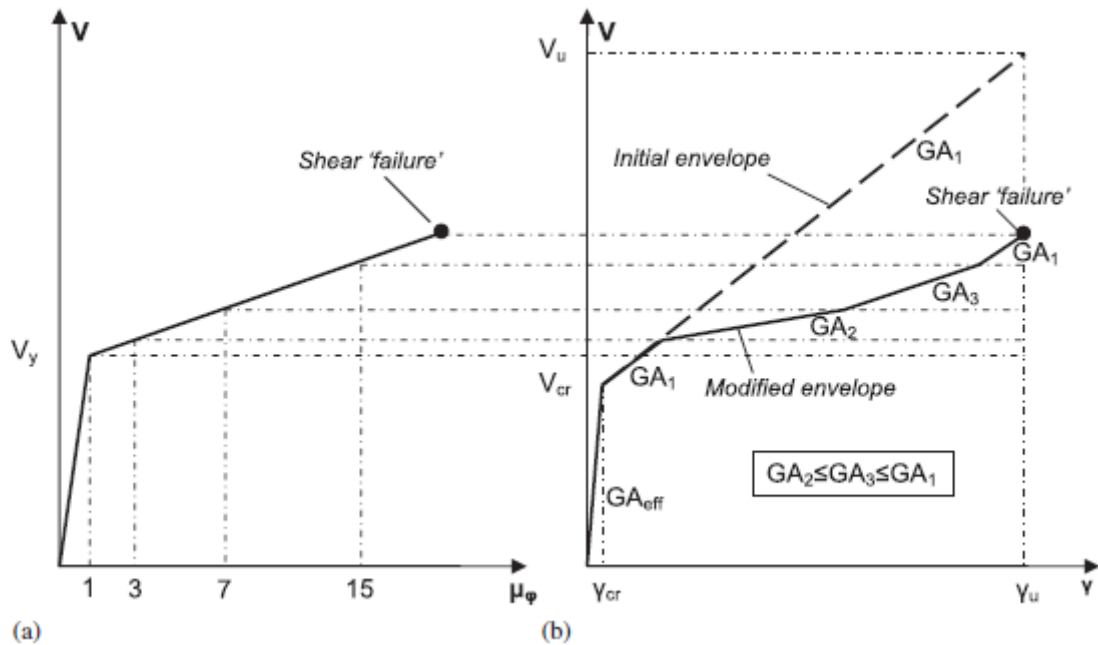


Figure 61 - Derivation of shear primary curve after modelling shear-flexure interaction effect: (a) flexural primary curve in terms of member shear force and curvature ductility demand of the critical cross section and (b) shear ($V-\gamma$) primary curve after modelling shear-flexure interaction [MK08].

The shear rigidity distribution along the member is assumed to have the form shown in Figure 62, where GA_A and GA_B are the current shear rigidities of the regions at the ends A and B,

respectively; GA_0 is the shear stiffness at the intermediate part of the element; and α_{As} and α_{Bs} are the shear cracking penetration coefficients, which specify the proportion of the element where the acting shear is greater than the shear cracking force of the end section.

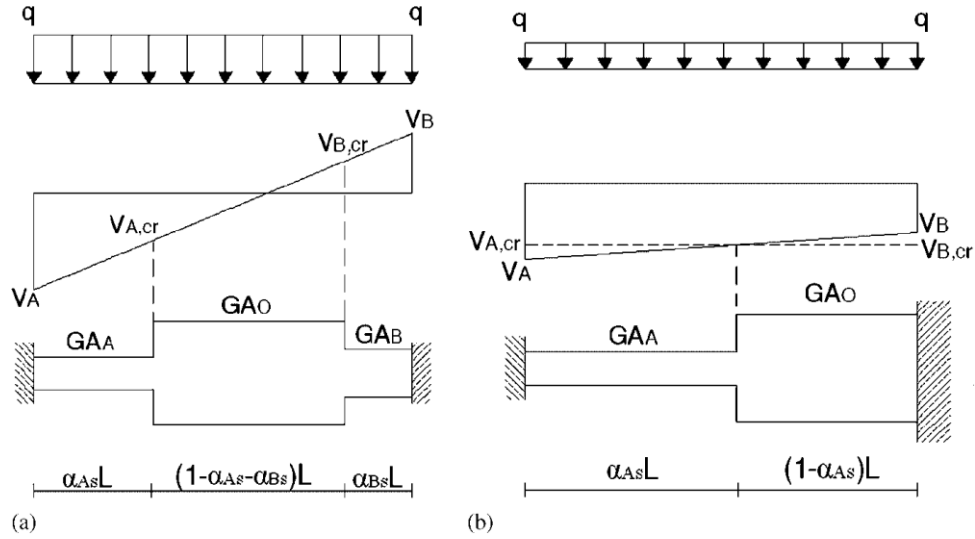


Figure 62 - Shear sub-element: (a) dominant gravity loading and (b) dominant seismic loading.

These coefficients are calculated using eqs (5.33) and (5.34):

When acting shear force at end A is greater than cracking shear ($|V_A| > |V_{A,cr}|$), α_{As} is given by

$$\alpha_{As} = \frac{V_A - V_{A,cr}}{V_A - V_B} \leq 1 \quad (5.33)$$

Similarly, when $|V_B| > |V_{B,cr}|$, α_{Bs} is given by

$$\alpha_{Bs} = \frac{V_B - V_{B,cr}}{V_B - V_A} \leq 1 \quad (5.34)$$

Otherwise, these coefficients are taken equal to zero. When shear forces at both ends are of the same sign ($V_A \cdot V_B > 0$) and they are greater than the respective cracking shears (this is the typical case for column elements after shear cracking), it is assumed that $\alpha_{As} = \alpha_{Bs} = 0.5$.

The shear cracking penetration lengths are first calculated for the current shear distribution, then compared with the previous maximum penetration lengths, and cannot be smaller than the latter ('model with memory'). After determining the distribution of GA along the RC member at each step of the analysis, the coefficients of the flexibility matrix of the shear sub-element are given by eq. (5.35):

$$f_{ij}^{shear} = \frac{\alpha_{As}}{GA_A L} + \frac{1 - \alpha_{As} - \alpha_{Bs}}{GA_0 L} + \frac{\alpha_{Bs}}{GA_B L} \quad (5.35)$$

where i, j=1, 2

6 THE PROPOSED FINITE ELEMENT

6.1 Introduction

The proposed model relies on the adoption of Heaviside's and Dirac's delta distributions to model abrupt and concentrated, both flexural and shear, stiffness discontinuities of the beam that lead to exact closed-form solutions of the elastic response in presence of static loads. Based on the latter solutions, a novel frame element for the analysis of framed structures with an arbitrary distribution of singularities is proposed. In particular, the presented closed-form solutions were exploited to formulate the relevant explicit form of the stiffness matrix using a direct approach. The first step of this thesis work was to reproduce the flexibility matrix presented in the work of Mergos and Kappos [MK08] presented in session 5.2.7. As it would be proven the latter leads to the same flexibility matrix. The second step was to formulate a novel finite element (session 6.2) inspired by the work of [MK08]. The third step is to test the proposed model through elastic and inelastic analysis presented in chapter 7.

6.1.1 Timoshenko beams with multiple singularities

Analogously of what have been presented for the case of the EB beams in section 4.2, the case of Timoshenko beam can be treated following the papers [CCCR13] and [CCC13]. The Timoshenko beam model subjected to external transversal loads $q(x)$ and moment loads $m(x)$, and accounting for a spatial variable flexural stiffness $E(x)I(x)$ and shear stiffness $G(x)A(x)$, is governed by the coupled differential equations:

$$\begin{aligned} \frac{d}{dx} \left[E(x)I(x) \frac{d}{dx} \varphi(x) \right] &= G(x)A(x) \left[\frac{d}{dx} v(x) + \varphi(x) \right] - \bar{m}(x) \\ \frac{d}{dx} \left[G(x)A(x) \left[\frac{d}{dx} v(x) + \varphi(x) \right] \right] &= -\bar{q}(x) \end{aligned} \quad (6.1)$$

where $v(x)$ e $\varphi(x)$ are the deflection and the rotation functions, respectively.

Singularities of different types in the response functions can be obtained by means of the adoption of appropriate distributions, in the expressions of both the flexural and the shear stiffness, as follows:

$$\begin{aligned} E(x)I(x) &= E_0 I_0 \left[1 - \sum_{j=1}^{n_\beta} (\bar{\beta}_j - \bar{\beta}_{j-1}) U(x - x_{\beta_j}) \right] \left[1 - \sum_{i=1}^{n_\gamma} \bar{\gamma}_i \delta(x - x_{\gamma_i}) \right] \\ G(x)A(x) &= G_0 A_0 \left[1 - \sum_{j=1}^{n_\beta} (\bar{\beta}'_j - \bar{\beta}'_{j-1}) U(x - x_{\beta_j}) \right] \left[1 - \sum_{i=1}^{n_\gamma} \bar{\gamma}'_i \delta(x - x_{\gamma_i}) \right] \end{aligned} \quad (6.2)$$

where U is the Heaviside (unit step) function and δ is the Dirac's delta function. The models presented can be adopted for the case of n_β , n_γ singularities of different types contemporarily present along the beam span at abscissae $x_{\beta,j}$ e $x_{\gamma,i}$, respectively. In particular, the terms containing the Heaviside function represent abrupt variations of the cross-section or of the material at abscissae $x_{\beta,j}$, while the presence of the Dirac's deltas both in the flexural stiffness and in the shear stiffness represents slope discontinuities and transversal deflection discontinuities at abscissae $x_{\gamma,i}$. The parameters γ_i , γ'_i , β_j e β'_j are associated with the intensity of the flexural and shear stiffness jumps, respectively, ruling the correspondent discontinuities of the response. Slope discontinuities modeled as Dirac's delta distribution appearing in the flexural stiffness function are usually obtained by means of an internal hinge.

A physical example which requires the Dirac's delta function is shown in Figure 63.

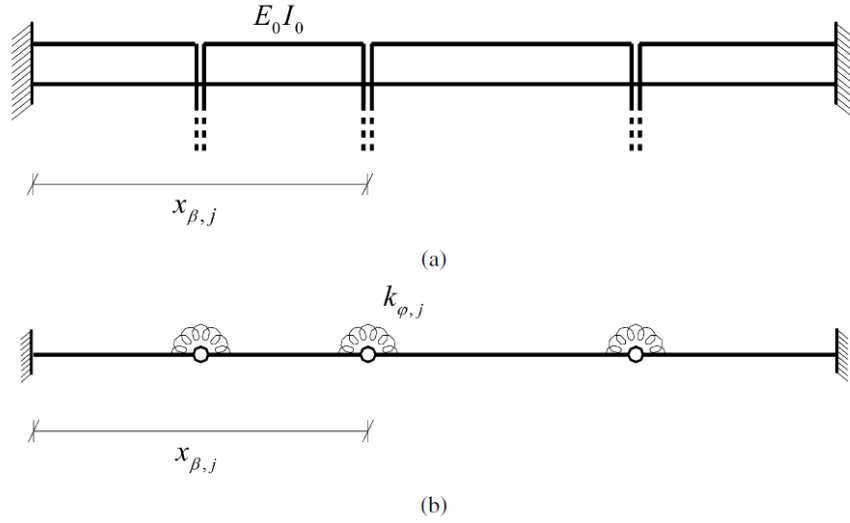


Figure 63 - (a) A beam with Dirac's delta singularities in the flexural stiffness, correspondent to (b) a beam with internal hinges and rotational springs with stiffnesses $k_{\phi,i}$ [BC07] .

For simplicity, by considering the dimensionless coordinate $\xi = x/L$, and indicating with the apex $[]^I$ the differentiation with respect to ξ , the governing differential equations of the Timoshenko beam, by accounting for the singularities introduced, take the form in eq.s (6.3) and (6.4):

$$\left[\left[1 - \sum_{j=1}^{n_\beta} (\beta_j - \beta_{j-1}) U(\xi - \xi_{\beta_j}) \right] \left[1 - \sum_{i=1}^{n_\gamma} \gamma_i \delta(\xi - \xi_{\gamma_i}) \right] \varphi'(\xi) \right]^I =$$

$$= b r^2 H(\xi) \left[1 - \sum_{i=1}^{n_\gamma} \gamma_i' \delta(\xi - \xi_{\gamma_i}) \right] [u'(\xi) + \varphi(\xi)] - m(\xi) \quad (6.3)$$

$$b r^2 \left[\left[1 - \sum_{j=1}^{n_\beta} (\beta_j' - \beta_{j-1}') U(\xi - \xi_{\beta_j}) \right] \left[1 - \sum_{i=1}^{n_\gamma} \gamma_i' \delta(\xi - \xi_{\gamma_i}) \right] [u'(\xi) + \varphi(\xi)] \right]^I = -q(\xi) \quad (6.4)$$

The equations previously written are expressed in terms of:

$u(\xi) = v(\xi)/L$ dimensionless deflection;

$q(\xi) = \frac{\bar{q}(\xi)}{E_0 I_0} L^3$ dimensionless transversal load;

$m(\xi) = \frac{\bar{m}(\xi)}{E_0 I_0} L^2$ dimensionless bending moment load;

and others parameters:

$$\gamma_i = \frac{\bar{\gamma}_i}{L}, \gamma'_i = \frac{\bar{\gamma}'_i}{L}, \beta_j = \frac{\bar{\beta}_j}{L}, \beta'_j = \frac{\bar{\beta}'_j}{L};$$

$$b = \frac{G_0}{E_0}; r^2 = L^2 \frac{A_0}{I_0}.$$

By making use of suitable integration procedure, the previously eq.s (6.3) and (6.4) give the rotation the following expressions of the rotation and the normalised deflection derivatives in eq.s (6.5) and (6.6):

$$\varphi'(\xi) = \left[1 + \sum_{j=1}^{n_\beta} \beta_j^* U(\xi - \xi_{\beta_j}) \right] \left[-q^{[2]}(\xi) - m^{[1]}(\xi) + b_1 \xi + b_2 \right] \left[1 + \sum_{i=1}^{n_\gamma} \lambda_{\gamma_i} \delta(\xi - \xi_{\gamma_i}) \right] \quad (6.5)$$

$$u'(\xi) = \left[1 + \sum_{j=1}^{n_\beta} \beta_j^* U(\xi - \xi_{\beta_j}) \right] \left[-\frac{q^{[1]}(\xi)}{br^2} + \frac{b_1}{br^2} \right] \left[1 + \sum_{k=1}^{n_\varepsilon} \lambda_{\varepsilon_k} \delta(\xi - \xi_{\varepsilon_k}) \right] - \varphi(\xi) \quad (6.6)$$

where the following additional parameters have been defined:

$$\beta_j^* = \frac{\beta_j}{1 - \beta_j} - \frac{\beta_{j-1}}{1 - \beta_{j-1}}, \beta_j'^* = \frac{\beta_j'}{1 - \beta_j'} - \frac{\beta_{j-1}'}{1 - \beta_{j-1}'}, b_2 = -2c_3, b_1 = -6c_4 \quad (6.7)$$

Integration of eq.s (6.5) and (6.6), in view of the integration rules of the distributions and after simple algebra, leads to the following explicit expression for the rotation function $\varphi(\xi)$ in eq. (6.8),

$$\varphi(\xi) = c_2 d_2(\xi) + c_3 d_3(\xi) + c_4 d_4(\xi) + d_5(\xi) \quad (6.8)$$

and the normalized deflection in eq. (6.9):

$$u(\xi) = c_1 f_1(\xi) + c_2 f_2(\xi) + c_3 f_3(\xi) + c_4 f_4(\xi) + f_5(\xi) \quad (6.9)$$

where the integration constants c_1, c_2, c_3, c_4 can be given as function of the nodal displacements, by imposing the proper boundary conditions. In case of a clamped-clamped beam subjected to

imposed end displacements, the integration constants are $u(\xi=0) = u_1$, $\varphi(\xi=0) = -\varphi_1$, $u(\xi=1) = u_2$, $\varphi(\xi=1) = -\varphi_2$.

The latter lead to the following integration constants:

$$\begin{aligned}
 c_1 &= u_1 \\
 c_2 &= \varphi_1 \\
 c_3 &= -\frac{d_4(1)}{\omega} u_1 - \frac{d_4(1) + f_4(1)}{\omega} \varphi_1 + \frac{d_4(1)}{\omega} u_2 + \frac{f_4(1)}{\omega} \varphi_2 \\
 c_4 &= -\frac{d_3(1)}{\omega} u_1 + \frac{d_3(1) + f_3(1)}{\omega} \varphi_1 - \frac{d_3(1)}{\omega} u_2 + \frac{f_3(1)}{\omega} \varphi_2 \\
 \omega &= f_3(1)d_4(1) - f_4(1)d_3(1)
 \end{aligned} \tag{6.10}$$

$$\begin{aligned}
 d_2(\xi) &= -1 \quad ; \\
 d_3(\xi) &= -2\xi - 2\sum_{j=1}^{n_\beta} \beta_j^* (\xi - \xi_{\beta_j}) U(\xi - \xi_{\beta_j}) - 2\sum_{i=1}^{n_\gamma} \lambda_{\gamma_i}^* U(\xi - \xi_{\gamma_i}) \quad ; \\
 d_4(\xi) &= -3\xi^2 - 3\sum_{j=1}^{n_\beta} \beta_j^* (\xi^2 - \xi_{\beta_j}^2) U(\xi - \xi_{\beta_j}) - 6\sum_{i=1}^{n_\gamma} \lambda_{\gamma_i}^* \xi_{\gamma_i} U(\xi - \xi_{\gamma_i}) \quad ; \\
 d_5(\xi) &= -q^{[3]}(\xi) - m^{[2]}(\xi) - \sum_{i=1}^{n_\gamma} \lambda_{\gamma_i}^* \left[q^{[2]}(\xi_{\gamma_i}) + m^{[1]}(\xi_{\gamma_i}) \right] U(\xi - \xi_{\gamma_i}) + \\
 &\quad - \sum_{j=1}^{n_\beta} \beta_j^* \left[\left(q^{[3]}(\xi) + m^{[2]}(\xi) \right) - \left(q^{[3]}(\xi_{\beta_j}) + m^{[2]}(\xi_{\beta_j}) \right) \right] U(\xi - \xi_{\beta_j})
 \end{aligned} \tag{6.11}$$

The apex $^{[j]}$ indicates a primitive of order j of the relevant function.

$$\begin{aligned}
 f_1(\xi) &= 1 & ; & & f_2(\xi) &= \xi \\
 f_3(\xi) &= \xi^2 + \sum_{j=1}^{n_\beta} \beta_j^* (\xi - \xi_{\beta_j})^2 U(\xi - \xi_{\beta_j}) + 2 \sum_{i=1}^{n_\gamma} \lambda_{\gamma_i}^* (\xi - \xi_{\gamma_i}) U(\xi - \xi_{\gamma_i}) \\
 f_4(\xi) &= \xi^3 + \sum_{j=1}^{n_\beta} \beta_j^* (\xi^3 - 3\xi_{\beta_j}^2 \xi + 2\xi_{\beta_j}^3) U(\xi - \xi_{\beta_j}) + 6 \sum_{i=1}^{n_\gamma} \lambda_{\gamma_i}^* \xi_{\gamma_i} (\xi - \xi_{\gamma_i}) U(\xi - \xi_{\gamma_i}) + \\
 &\quad - 6 \frac{\xi}{b r^2} - 6 \sum_{j=1}^{n_\beta} \frac{\beta_j^*}{b r^2} (\xi - \xi_{\beta_j}) U(\xi - \xi_{\beta_j}) - 6 \sum_{k=1}^{n_\varepsilon} \frac{\lambda_{\varepsilon_k}^*}{b r^2} U(\xi - \xi_{\varepsilon_k}) \\
 f_5(\xi) &= q^{[4]}(\xi) + m^{[3]}(\xi) + \sum_{j=1}^{n_\beta} \beta_j^* \left[(q^{[4]}(\xi) + m^{[3]}(\xi)) - (q^{[4]}(\xi_{\beta_j}) + m^{[3]}(\xi_{\beta_j})) \right] U(\xi - \xi_{\beta_j}) + \quad (6.12) \\
 &\quad + \sum_{i=1}^{n_\gamma} \lambda_{\gamma_i}^* \left[q^{[2]}(\xi_{\gamma_i}) + m^{[1]}(\xi_{\gamma_i}) \right] (\xi - \xi_{\gamma_i}) U(\xi - \xi_{\gamma_i}) + \\
 &\quad - \frac{q^{[2]}(\xi)}{b r^2} - \sum_{j=1}^{n_\beta} \frac{\beta_j^*}{b r^2} \left[q^{[2]}(\xi) - q^{[2]}(\xi_{\beta_j}) \right] U(\xi - \xi_{\beta_j}) - \sum_{k=1}^{n_\varepsilon} \frac{\lambda_{\varepsilon_k}^*}{b r^2} q^{[1]}(\xi_{\varepsilon_k}) U(\xi - \xi_{\varepsilon_k}) + \\
 &\quad - \sum_{j=1}^{n_\beta} \beta_j^* \left[q^{[3]}(\xi_{\beta_j}) + m^{[2]}(\xi_{\beta_j}) \right] (\xi - \xi_{\beta_j}) U(\xi - \xi_{\beta_j})
 \end{aligned}$$

The generalized deformations functions $\chi(\xi)$ and $\gamma(\xi)$, in absence of external loads and without slope discontinuities as the ones illustrated in Figure 63, take the form of eq.s (6.13) and (6.14):

$$\varphi'(\xi) = \chi(\xi) = \left[1 + \sum_{j=1}^{n_\beta} \beta_j^* (\xi - \xi_{\beta_j}) U(\xi - \xi_{\beta_j}) \right] (-2c_3 - 6c_4 \xi) \quad (6.13)$$

$$\gamma(\xi) = \left[1 + \sum_{j=1}^{n_\beta} \beta_j^* (\xi - \xi_{\beta_j}) U(\xi - \xi_{\beta_j}) \right] \left(-\frac{6c_4}{b r^2} \right) \quad (6.14)$$

Eq.s (6.13) and (6.14) are derived from eq.s (6.8) and (6.6) with the simplifications written above; it is useful to specify that for the forward calculations the hypothesis made above are taken into account.

Recovering the sectional equilibrium equations of the Timoshenko beam in the dimensionless domain it is possible to write:

$$\begin{aligned}
 M(\xi) &= E(\xi) I(\xi) \chi(\xi) \\
 V(\xi) &= G(\xi) A(\xi) \gamma(\xi)
 \end{aligned} \quad (6.15)$$

Comparing eq.s (6.13), (6.14) with eq. (6.15) it is immediate to recognize that

$$\begin{aligned} M(\xi) &= -2c_3 - 6c_4\xi \\ V(\xi) &= -6c_4 \end{aligned} \tag{6.16}$$

Eq.s (6.16) represent the normalised bending moment and shear function in the dimensionless domain of the Timoshenko beam. Using the integration constants of equation (6.10) it is now possible to obtain the internal nodal forces in case of a clamped–clamped beam subjected to imposed end displacements.

Combining eq.s (6.10) and (6.16) the internal end forces can be obtained:

$$\begin{aligned} V_1 = -V(0) &= 6 \left[\frac{d_3(1)}{\omega} u_1 + \frac{d_3(1) + f_3(1)}{\omega} \varphi_1 - \frac{d_3(1)}{\omega} u_2 - \frac{f_3(1)}{\omega} \varphi_2 \right] \\ V_2 = V(1) &= -6 \left[\frac{d_3(1)}{\omega} u_1 + \frac{d_3(1) + f_3(1)}{\omega} \varphi_1 - \frac{d_3(1)}{\omega} u_2 - \frac{f_3(1)}{\omega} \varphi_2 \right] \\ M_1 = M(0) &= -2 \left[-\frac{d_4(1)}{\omega} u_1 - \frac{d_4(1) + f_4(1)}{\omega} \varphi_1 + \frac{d_4(1)}{\omega} u_2 + \frac{f_4(1)}{\omega} \varphi_2 \right] \\ M_2 = -M(1) &= 2 \left[\frac{-d_4(1) + 3d_3(1)}{\omega} u_1 - \frac{d_4(1) + f_4(1) - 3d_3(1) - 3f_3(1)}{\omega} \varphi_1 \right. \\ &\quad \left. + \frac{d_4(1) - 3d_3(1)}{\omega} u_2 - \frac{3f_3(1) - f_4(1)}{\omega} \varphi_2 \right] \end{aligned} \tag{6.17}$$

6.1.2 Closed-form calculation of the Timoshenko stiffness matrix terms

Eq.s (6.17) can be used in order to obtain the stiffness matrix terms of a Timoshenko beam finite element. Each row/column of the stiffness matrix represents the force that comes up in the i th degrees of freedom for an unit imposed displacement in the j th degrees of freedom with the other degrees of freedom displacements equal to zero. Figure 64 exposes the case of an unit imposed displacement $u_1 = 1$ with $\varphi_1 = u_2 = \varphi_2 = 0$.

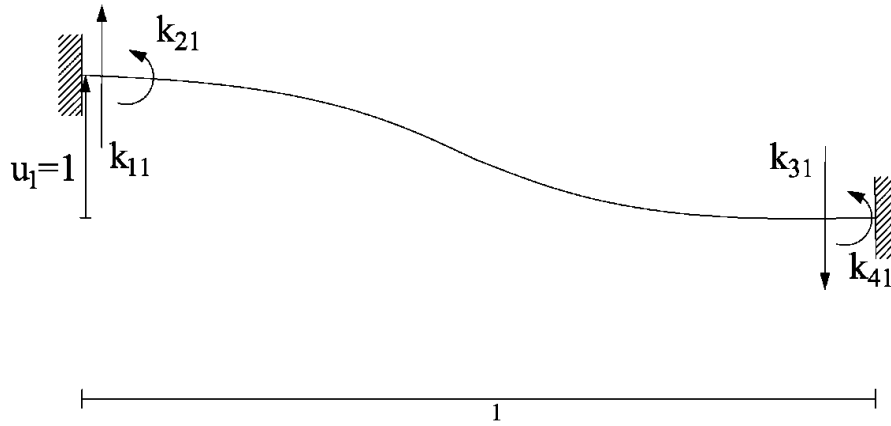


Figure 64 – First row/column stiffness matrix derivation.

For this case the end forces are:

$$\begin{aligned}
 V_1 &= -V(0) = 6 \frac{d_3(1)}{\omega} = k_{11} \\
 V_2 &= V(1) = -6 \frac{d_3(1)}{\omega} = k_{31} \\
 M_1 &= M(0) = 2 \frac{d_4(1)}{\omega} = k_{21} \\
 M_2 &= -M(1) = 2 \frac{-d_4(1) + 3d_3(1)}{\omega} = k_{41}
 \end{aligned} \tag{6.18}$$

Analogously all the terms of the stiffness matrix can be obtained.

6.1.3 Beam finite element with discontinuities

Finally, it is possible to determine the stiffness matrix \mathbf{K}_b that relates the nodal displacements \mathbf{u} to the nodal forces \mathbf{S} as shown in Figure 65 just using the definition of stiffness matrix terms.

Under the hypothesis that the axial load is omitted eq. (6.19) shows the previous relation.



Figure 65 – Finite element's dof [RAP12].

$$\mathbf{S} = \mathbf{K}_b \mathbf{u} \quad (6.19)$$

where

$$\mathbf{u} = [u_1, \varphi_1, u_2, \varphi_2]^T \quad (6.20)$$

$$\mathbf{S} = [V_1, M_1, V_2, M_2]^T \quad (6.21)$$

For convenience the corresponding dimensional expression of \mathbf{S} is written in eq. (6.22)

$$\hat{\mathbf{S}} = [\hat{V}_1, \hat{M}_1, \hat{V}_2, \hat{M}_2]^T = [V_1 L^2, M_1 L, V_2 L^2, M_2 L]^T \quad (6.22)$$

Analogously, in dimensional terms, the stiffness matrix is written in eq. (6.23)

$$\begin{bmatrix} V_1 L^2 \\ M_1 L \\ V_2 L^2 \\ M_2 L \end{bmatrix} = E_0 I_0 \begin{bmatrix} k_{11} & k_{12} & k_{13} & k_{14} \\ k_{21} & k_{22} & k_{23} & k_{24} \\ k_{31} & k_{32} & k_{33} & k_{34} \\ k_{41} & k_{42} & k_{43} & k_{44} \end{bmatrix} \begin{bmatrix} u_1 / L \\ \varphi_1 \\ u_2 / L \\ \varphi_2 \end{bmatrix} \quad (6.23)$$

where the terms are listed in eq. (6.24):

$$\begin{aligned} k_{11} &= 6 \frac{d_3(1)}{\omega} & k_{12} &= 6 \frac{f_3(1) + d_3(1)}{\omega} & k_{13} &= -6 \frac{d_3(1)}{\omega} & k_{14} &= -6 \frac{f_3(1)}{\omega} \\ k_{21} &= 2 \frac{d_4(1)}{\omega} & k_{22} &= 2 \frac{d_4(1) + f_4(1)}{\omega} & k_{23} &= -2 \frac{d_4(1)}{\omega} & k_{24} &= -2 \frac{f_4(1)}{\omega} \\ k_{31} &= -6 \frac{d_3(1)}{\omega} & k_{32} &= -6 \frac{f_3(1) + d_3(1)}{\omega} & k_{33} &= 6 \frac{d_3(1)}{\omega} & k_{34} &= 6 \frac{f_3(1)}{\omega} \\ k_{41} &= 2 \frac{-d_4(1) + 3d_3(1)}{\omega} & k_{42} &= -2 \frac{d_4(1) + f_4(1) - 3d_3(1) - 3f_3(1)}{\omega} & k_{43} &= 2 \frac{d_4(1) - 3d_3(1)}{\omega} & k_{44} &= 2 \frac{f_4(1) - 3f_3(1)}{\omega} \end{aligned} \quad (6.24)$$

6.2 Formulation

The key aspect of this finite element formulation is that the generalized functions and their applications in frame elements analysis can be a feasible alternative to the standard spread plasticity approach presented in section 3.1.3. Moreover, it solves some shortcomings; in fact, by means of generalized functions, the differential equations that govern the problem are integrated analytically and then its solution is known in terms of both kinematic and static quantity on the entire domain without adding nodes inside the element.

The stiffness matrix presented in section 6.1.3 is rewritten in eq. (6.25) for convenience. The latter can be specialized to reflect the behaviour of a structural element, where the development of the plastic zones in any position corresponds to a reduction of both the characteristics of rigidity and resistance using sectional constitutive laws.

$$\begin{bmatrix} V_1 L^2 \\ M_1 L \\ V_2 L^2 \\ M_2 L \end{bmatrix} = E_0 I_0 \begin{bmatrix} k_{11} & k_{12} & k_{13} & k_{14} \\ k_{21} & k_{22} & k_{23} & k_{24} \\ k_{31} & k_{32} & k_{33} & k_{34} \\ k_{41} & k_{42} & k_{43} & k_{44} \end{bmatrix} \begin{bmatrix} u_1 / L \\ \varphi_1 \\ u_2 / L \\ \varphi_2 \end{bmatrix} \quad (6.25)$$

The model has three distributed discontinuity as shown in Figure 66. It needs to be specified that Dirac's delta singularities like the one shown in Figure 63 are not implemented in the present formulation, it means that only distributed discontinuity are considered. The symbols $\xi_{\beta 1}$ & $\xi_{\beta 2}$ represent the end segments affected by value of bending moment higher than the yielding value M_y .

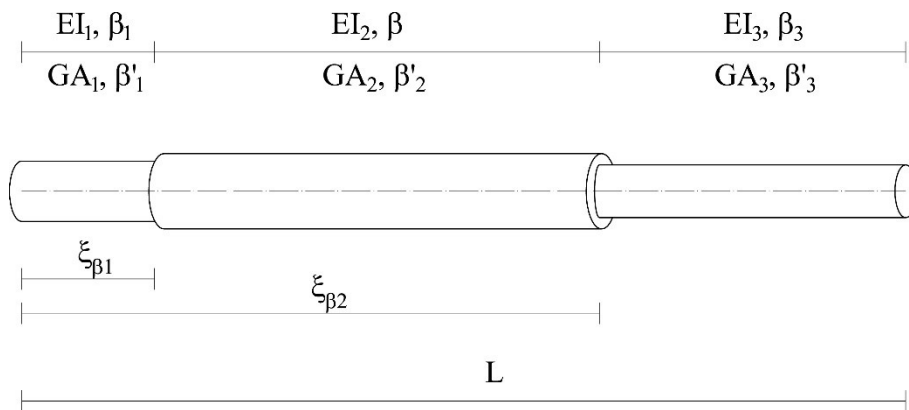


Figure 66– The proposed finite element.

The symbols shown in Figure 66 are defined in the following:

1. EI_i, GA_i , are the reference stiffnesses respectively for flexure and shear; with $i=1,2,3$.
2. M_y, V_y are the yielding and cracking values of resistance for flexure and shear respectively.
3. EI_t, GA_t are the tangent stiffnesses respectively for flexure and shear. The axial component is taken so far elastic.
4. $\xi_{\beta 1}, \xi_{\beta 2}$ are the dimensionless distances of the discontinuity.
5. $\beta_1, \beta_2, \beta_3$ are the parameters that reproduce the intensity of the flexural discontinuity and are defined as follows:

$$\beta_i = 1 - \frac{EI_t}{EI} \quad \text{with } i=1,2,3.$$

6. $\beta'_1, \beta'_2, \beta'_3$ are the parameters that reproduce the intensity of the shear discontinuity and are defined as follows:

$$\beta'_i = 1 - \frac{GA_t}{GA} \quad \text{with } i=1,2,3.$$

All parameters ranging from point 4 to 6 in the previous list vary during the analysis as soon as the member pass beyond the elastic range. In other words, the tangent stiffness matrix of the element in eq.(6.26) is a function of all these parameters:

$$K_T^e = K_T^e(EI_i, M_y, GA_i, V_y, \beta_i, \beta'_i, \xi_{\beta 1}, \xi_{\beta 2}) \quad \text{with } i = 1,2,3. \quad (6.26)$$

Now it remains to determine what are the constitutive models used and especially how is taken into account the flexure-shear interaction.

6.2.1 Flexure constitutive law

To define a flexural constitutive law a standard sectional analysis for RC elements is used; so that a moment curvature diagram $M-\chi$ is determined. The second step is to interpolate this diagram by introducing and defining the parameters of a non-linear constitutive model that is well suited for the purpose. The choice fell on the linear kinematic hardening law of Clough et al. [CBW65] allowing for stiffness degrading and shown in Figure 67. This model substantially depends on five parameters, in case of flexure they can be written as follows:

- Elastic stiffness $EI=K_0$,
- Yielding bending moment $M_y=F_{y+}$,
- Tangent stiffness $EI_t=rK_0$,
- Unloading stiffness $EI_u=K_u$,
- Reloading stiffness $EI_r=K_L$.

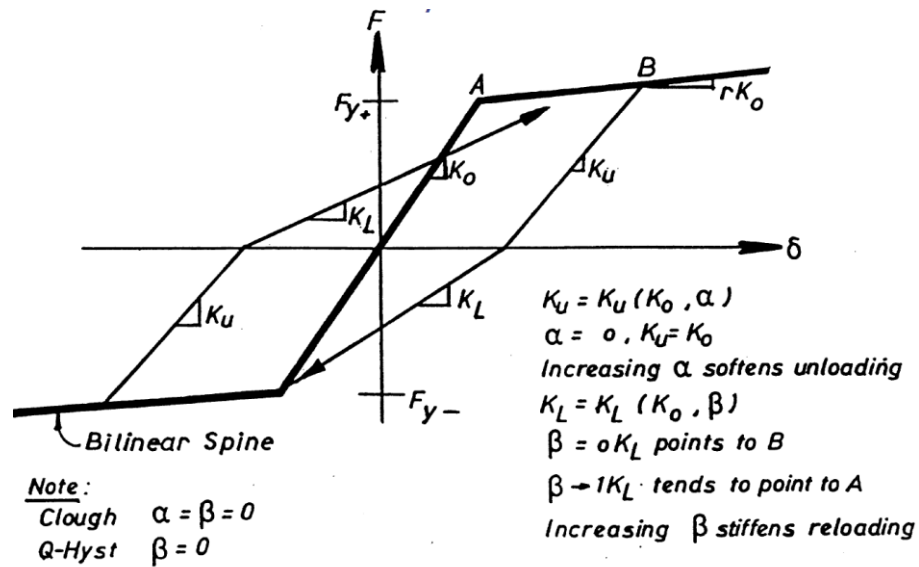


Figure 67 – Degraded hysteretic model [CBW65].

The degradation is achieved through the parameters α and β in Figure 67 respectively for the unloading branch and for the reloading branch.

6.2.2 Shear constitutive law

The shear inelastic behavior used in the analysis is defined by a hysteretic constitutive law using a sectional analysis for RC elements. The output is a phenomenological relation shear-shear strain $V-\gamma$. This diagram is a bilinear curve whose points are determined by the procedure described in [PCK07] and [SM04]. To interpolate this diagram the linear kinematic hardening law of Clough et al. [CBW65] allowing for stiffness degrading and shown in Figure 67 is used. This model substantially depends on five parameters, in case of shear they can be written as follows:

- Elastic stiffness $GA=K_0$,
- Cracking shear $V_y=F_{y+}$,
- Tangent stiffness $GA_t=rK_0$,
- Unloading stiffness $GA_u=K_u$,
- Reloading stiffness $GA_r=K_L$.

The first point of the curve is $V_y=V_{cr}$, i.e. the shear that leads to crack the section. It is obtained using eq. (6.27) by Sezen and Moehle [SM04]:

$$V_c = \frac{f_{ctm}}{L_s/h} \sqrt{1 + \frac{N}{f_{ctm} A_g}} 0.8 A_g \quad (6.27)$$

Where L_s is the shear span, h is the height of the section; f_{ctm} is the mean tensile concrete resistance, N the axial load and A_g the gross section area.

Considering the behaviour completely elastic until V_{cr} , it is possible to calculate the shear strain using eq. (6.28):

$$\gamma_s = \frac{V_{cr}}{G A_{eff}} \quad (6.28)$$

where A_{eff} is the 80% of A_g .

In order to calculate the ultimate shear resistance V_U of the section the procedure described in [PCK07] for the assessment case is used (see section 2.2.7).

Once V_U is determined, through an equivalent truss approach is possible to derive an equation that determines the shear stiffness of the section as suggested in [MCP05]:

$$k_{s,cr} = \frac{\rho_a \sin^4 \theta \cot^2 \theta}{\sin^4 \theta + n \rho_a} E_s b_w d$$

Where ρ_a is the geometric percentage of transverse reinforcement, θ is the flexure-shear crack crosses the section at an average angle to the vertical axis, n is the elastic modulus ratio, b_w is the element width and d is the effective height of the section.

So the shear strain is calculated with eq. (6.29):

$$\gamma_u = \frac{V_u}{k_{s,cr}} \quad (6.29)$$

Considering these two points it is possible to plot the V_0 - γ backbone curve (not influenced by flexure) as shown is Figure 68. It's worth to remember that the tangent stiffness GA_t is defined with these two points.

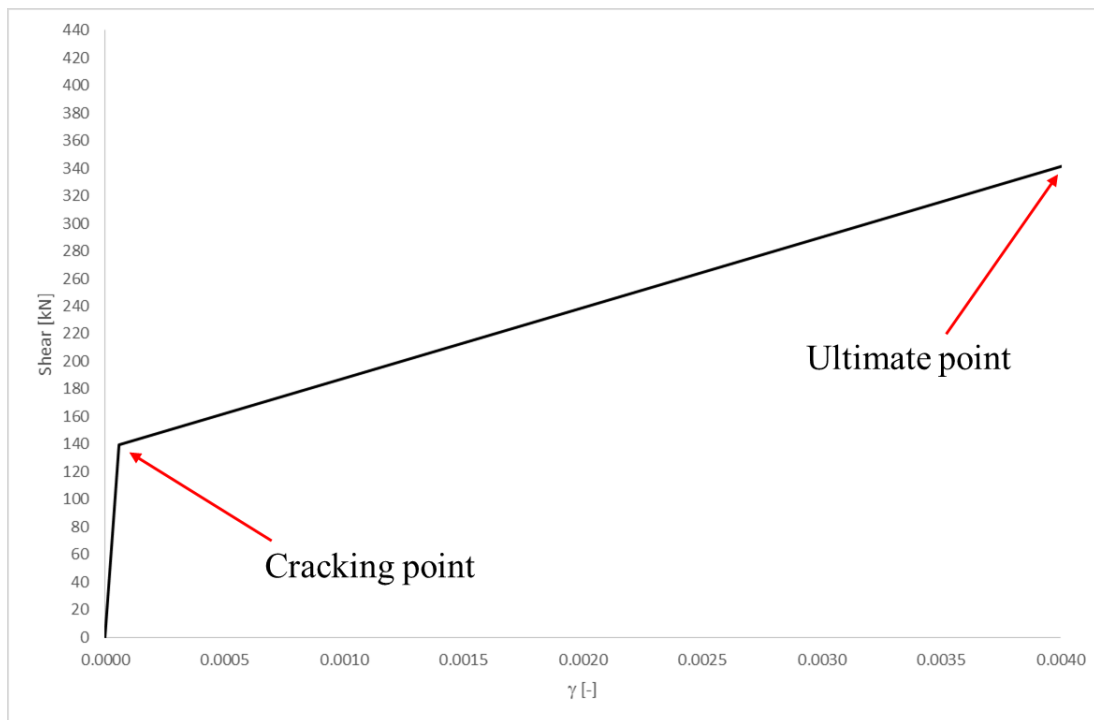


Figure 68 – V_0 - γ curve.

The unloading branch and reloading branch are governed by the parameters GA_u and GA_r respectively.

6.2.3 Flexure-Shear interaction

In the UCSD model the concrete resistance is degraded by the ductility demand of the section μ_ϕ as shown in Figure 20 through the parameter γ varying from 0.04 to 0.29 MPa.

Thus when μ_ϕ is higher than 3 the value of γ reduces and the maximum resistance decreases. For example:

$$\mu_\phi = \frac{\chi_u}{\chi_y} = 9.4 \rightarrow \gamma = 0.18 \rightarrow V_{cur} < V_0 .$$

Where V_{cur} is the current shear resistance and V_0 is the initial resistance (i.e. when $\mu_\phi < 3$).

The flexure shear interaction consists in a plastic correction procedure that always respect equilibrium between flexure and shear along the two nodes element.

The algorithm implemented in the finite element code is formed by steps below described; at each load increment:

- I. Calculate the current ductility demand μ_ϕ , the current shear resistance $V_{cur,shear}$ using eq. (2.12) and the tangent stiffness associated GA_t .
- II. Compare $V_{cur,shear}$ with the resistance coming from the integration of the flexure constitutive law $V_{cur,flexure}$.
- III. Choice the minimum between $V_{cur,shear}$ and $V_{cur,flexure}$.
- IV. Restore element equilibrium.
- V. Use the minimum above to construct the resistance forces vector at the structural level to compute the new residuum.
- VI. Repeat steps I to V until convergence is reached.

In order to describe in a more clear way the implemented code element state determination, a flowchart is illustrated in Figure 69.

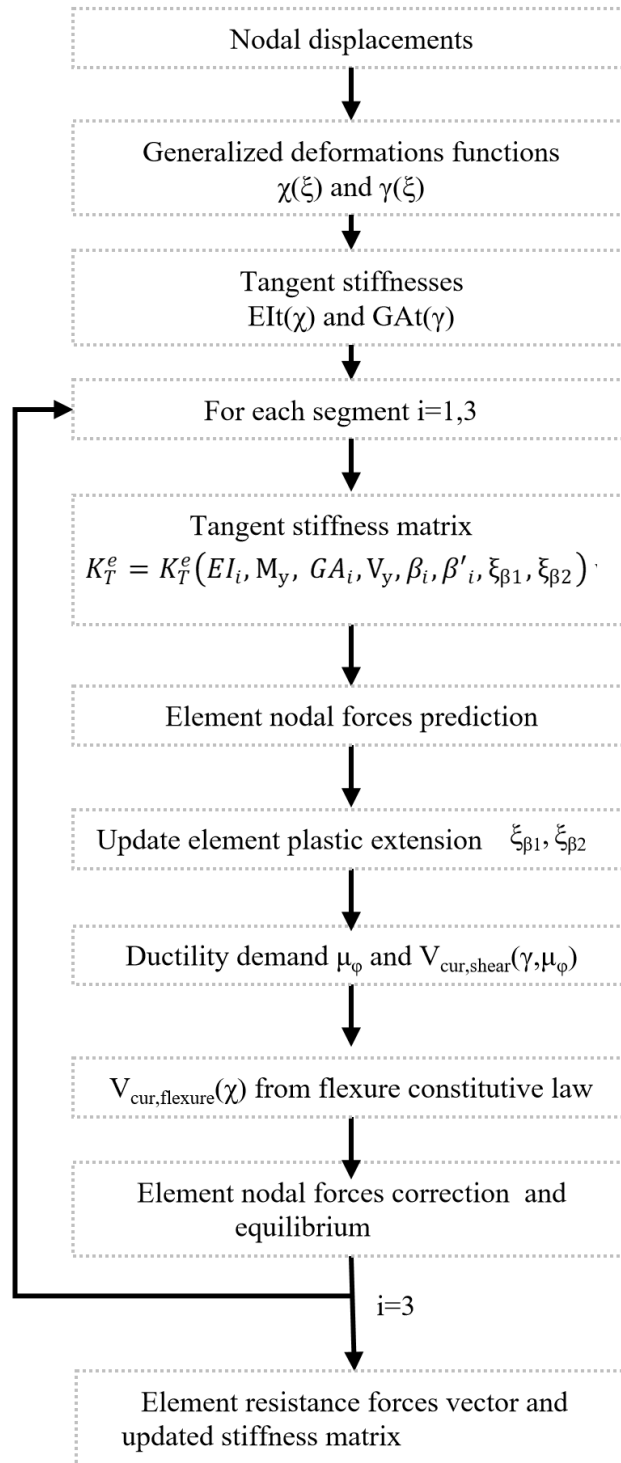


Figure 69 – Element state determination of the Timoshenko beam element

7 NUMERICAL VERIFICATIONS

7.1 Linear analysis

Before perform nonlinear analysis, it is necessary to test the finite element with a simple elastic benchmark.

7.1.1 Portal frame with an horizontal force

The stiffness distribution along the lengths are shown in Figure 70.

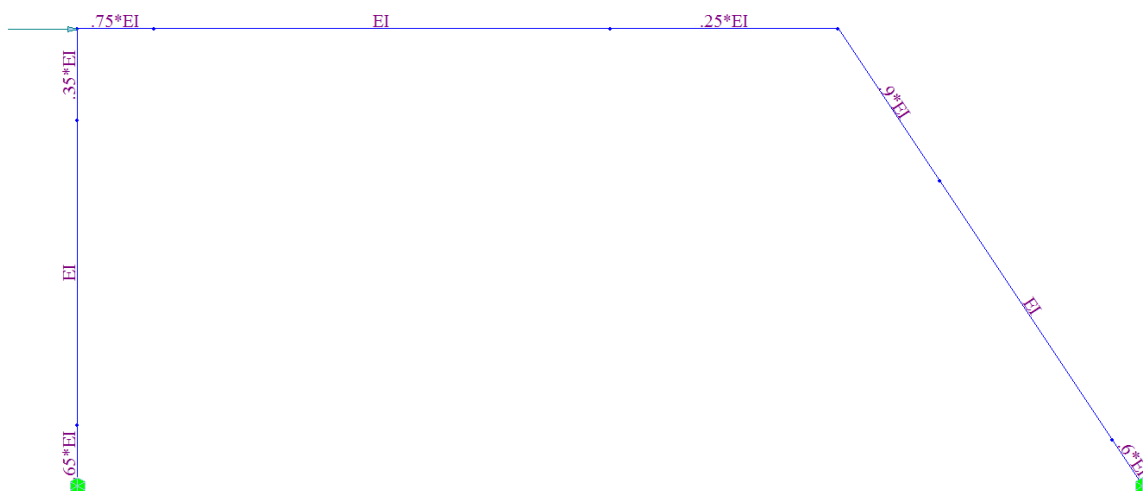


Figure 70 – Frame with discontinuities.

The reference stiffnesses are shown below:

EI	GA	EA
[Nmm ²]	[N]	[N]
900*10 ⁶	3.462*10 ⁺²	900*10 ⁶

It is worth to specify that the reduction in stiffness regards also the shear one GA.

The outputs are shown in terms of displacements and are compared with the software Midas civil.

	MIDAS	CODE
Joint=2		
U1 [mm]	757.836397	-757.772973
U3 [mm]	505.223752	505.181759
R2 [rad]	0.142078	-0.142073
Joint=8		
U1 [mm]	-757.836718	-757.772739
U3 [mm]	-0.000057	-0.0000571049790448913
R2 [rad]	-0.033655	-0.0336535148875284

Moreover the deformed shapes and the internal forces diagrams are also compared (Figure 71 - Figure 77).

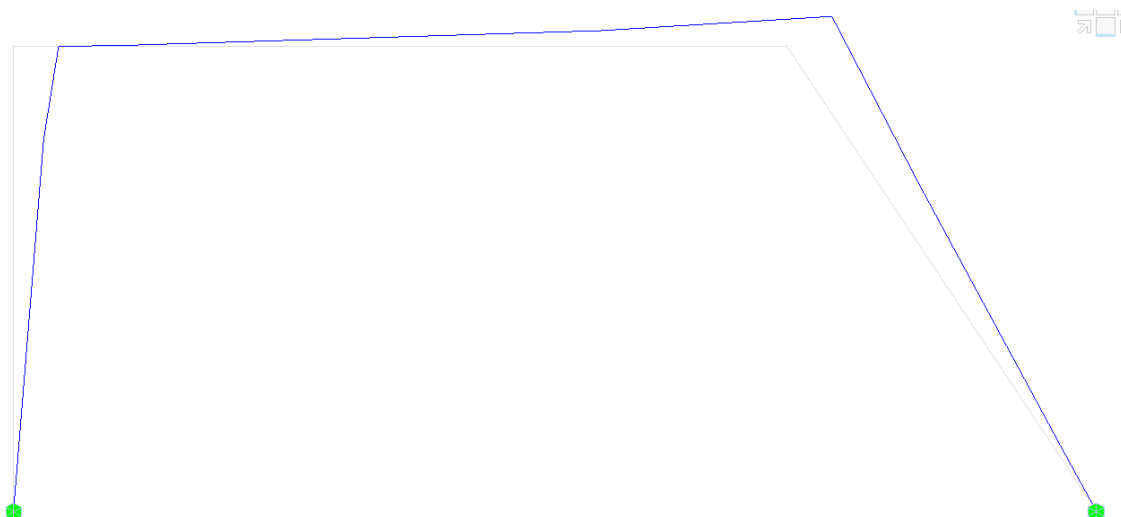


Figure 71– Deformed shape Midas.

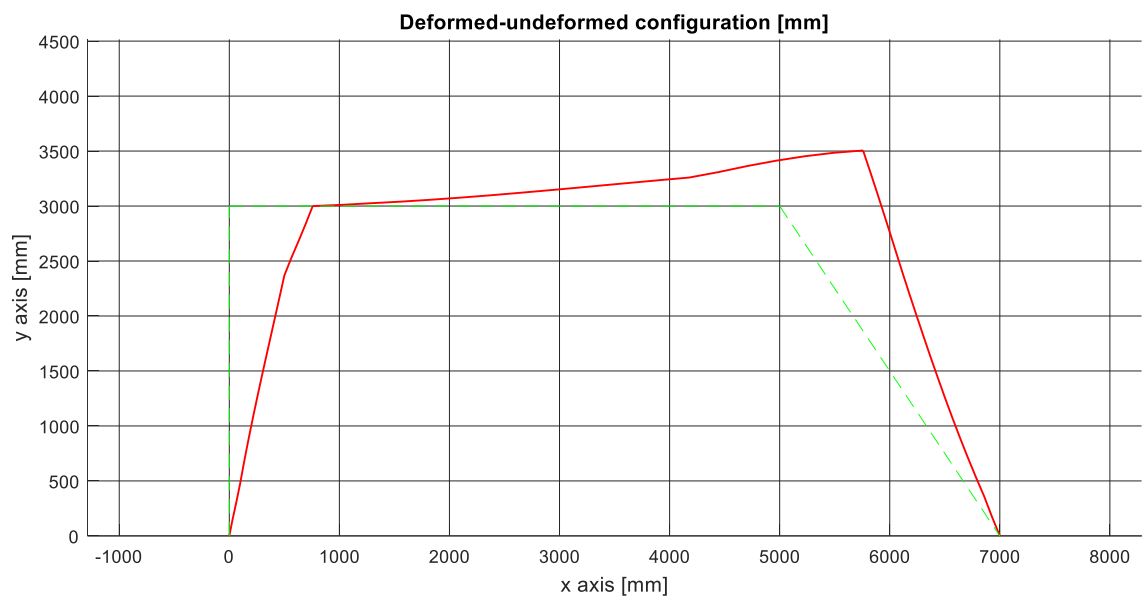


Figure 72 – Code deformed shape [mm].

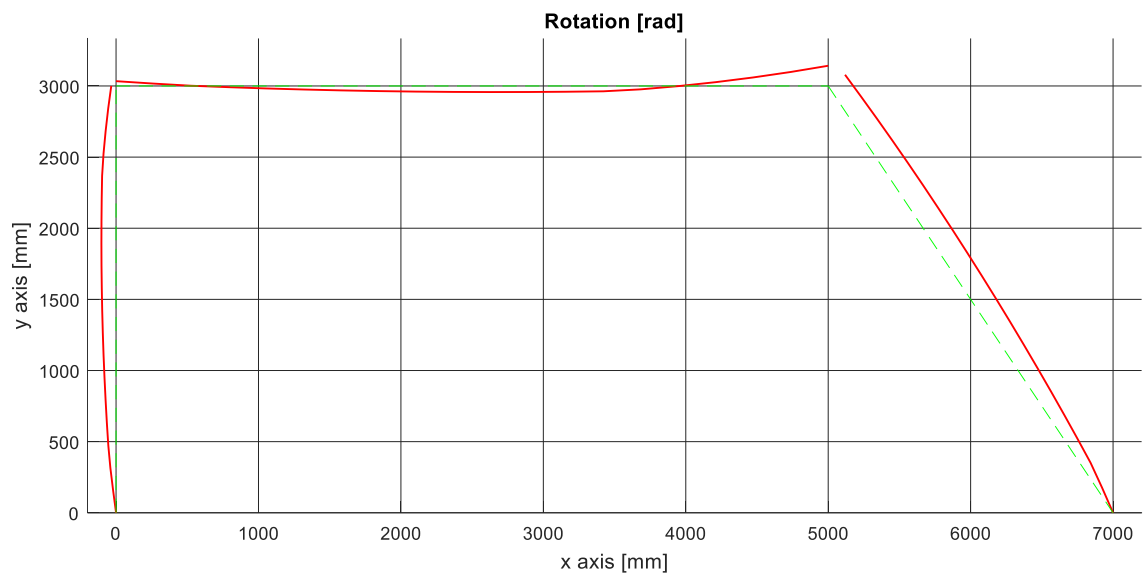


Figure 73 – Code rotations.

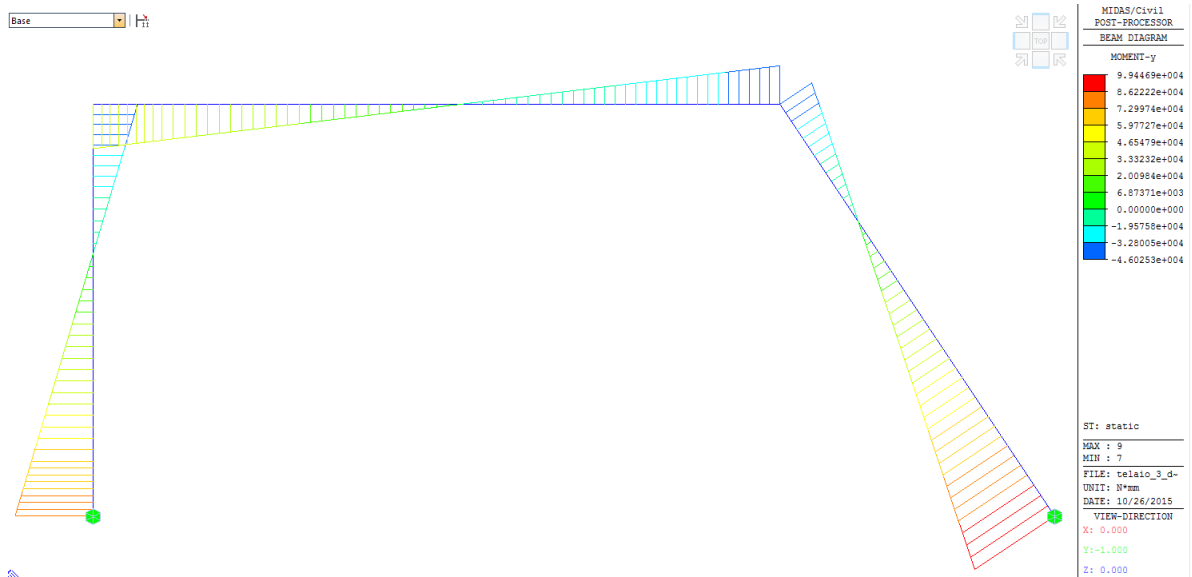


Figure 74– Bending moment diagram Midas.

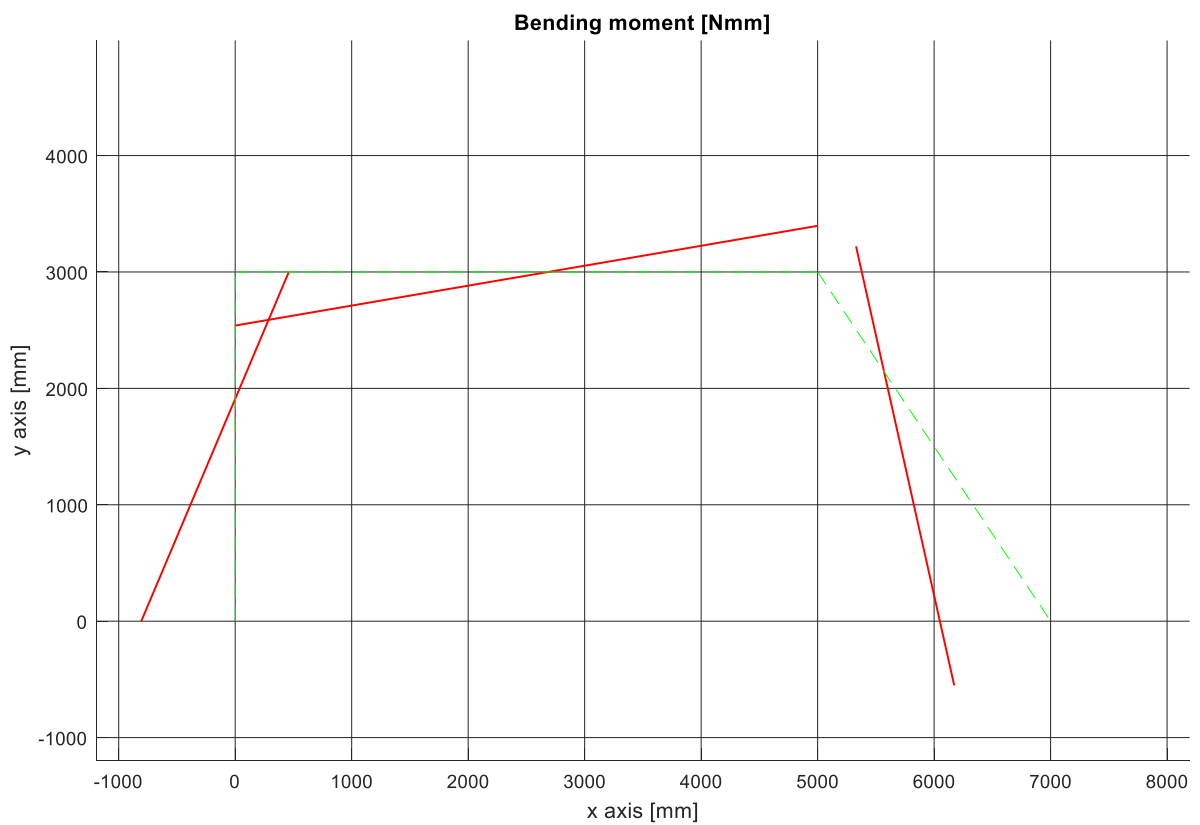


Figure 75– Code bending moment diagram.

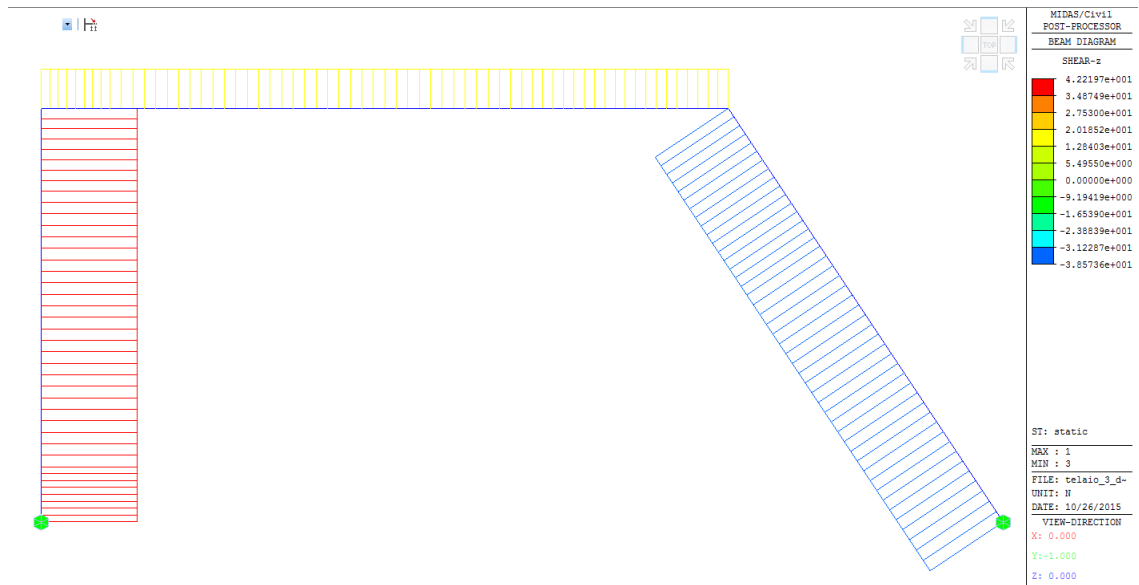


Figure 76 – Shear diagram Midas.

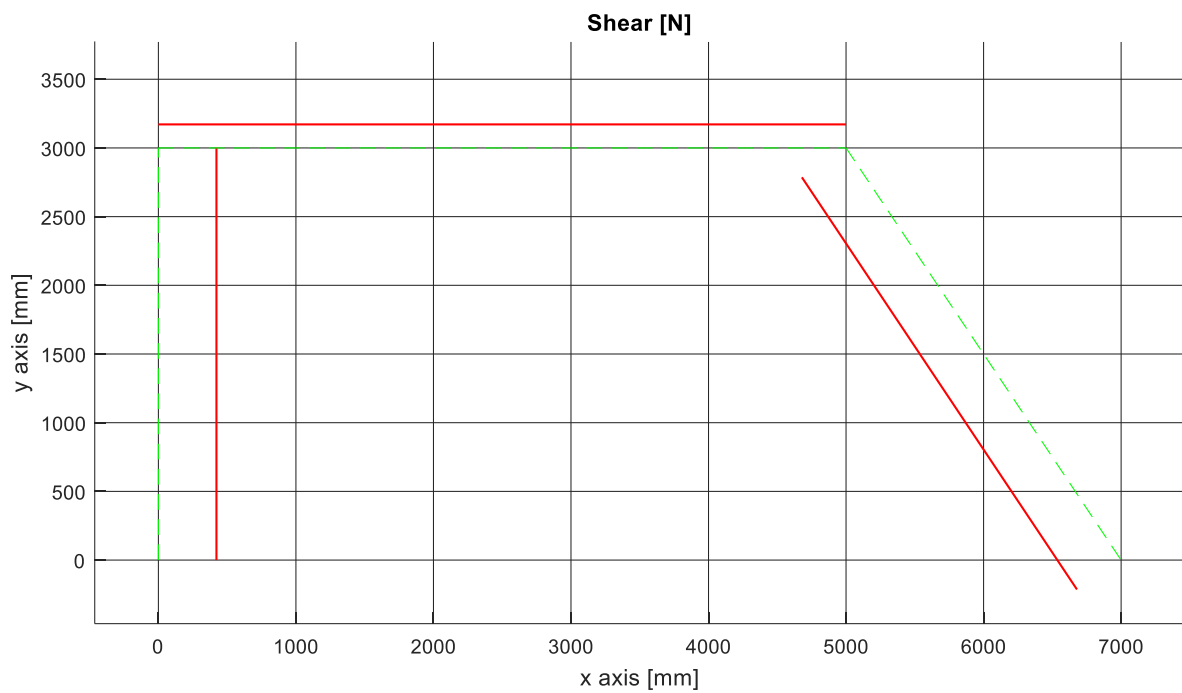


Figure 77 – Code shear diagram.

7.2 Inelastic analysis

7.2.1 Lynn 1996

The first test considered is one of the columns studied by Lynn in 1996 [LMMH96] (Figure 78). The shear aspect ratio is equal to:

$$\frac{M}{V D} = \frac{1473}{452} = 3.258$$

This means that the test is in a region where the shear-flexure interaction has to be considered; in fact the failure mode is classified as coupled.



Figure 78 – Setup of Lynn 1996 [LMMH96].

In Figure 79 are shown the reinforcement details of the column.

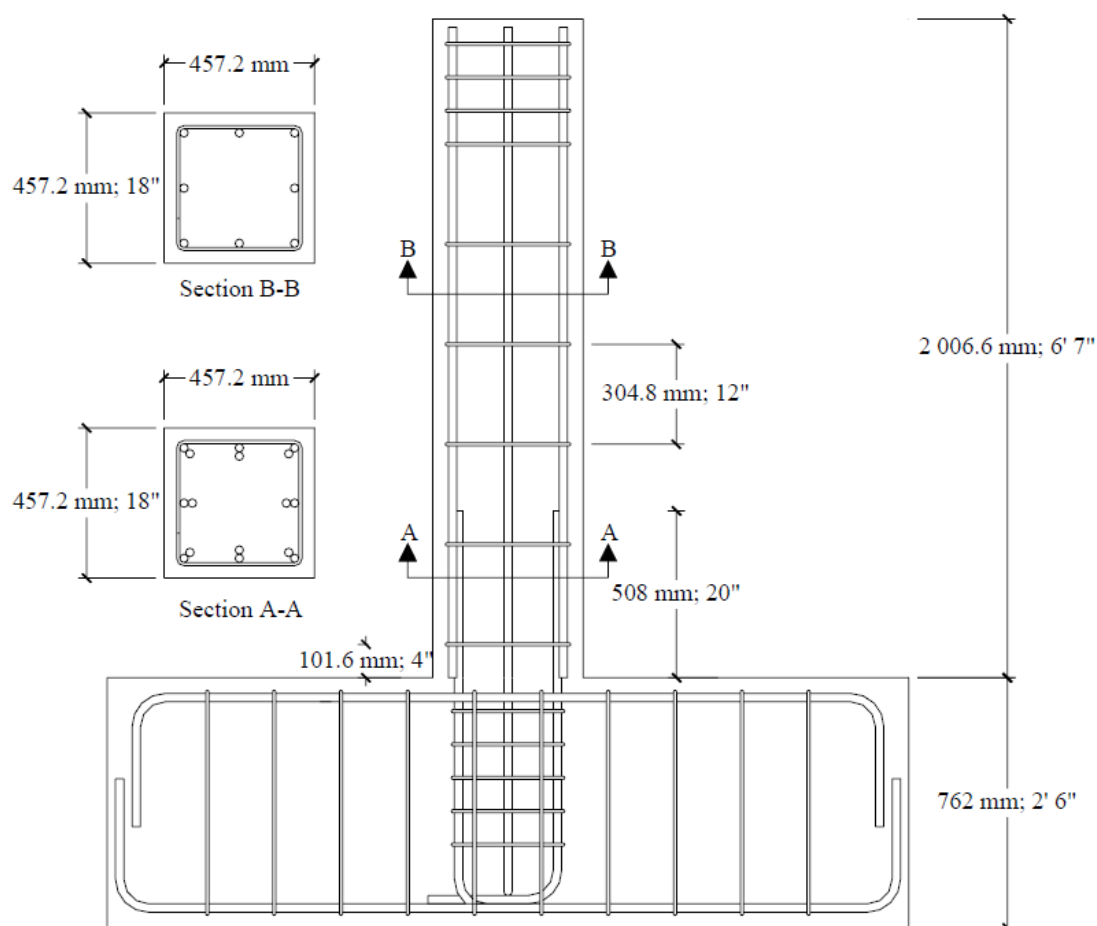


Figure 79 – Reinforcement details [LMMH96].

The test was conducted as displacement control with a linear push&pull load history.

The results are expressed in terms of force-displacement

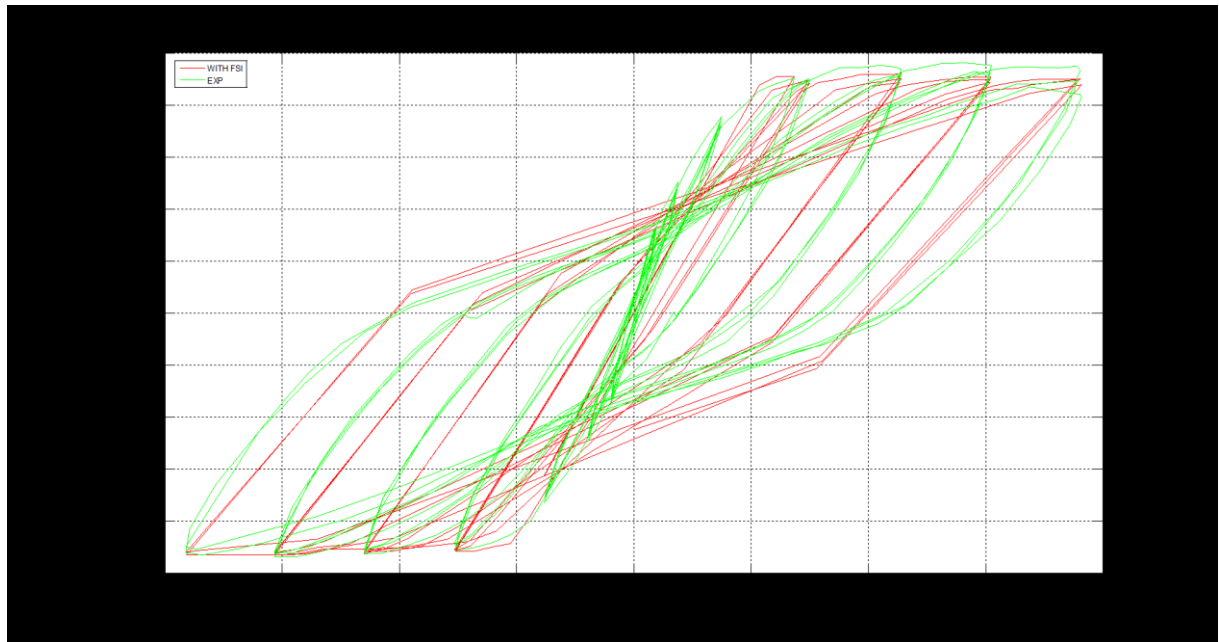


Figure 80 – Force-displacement comparison.

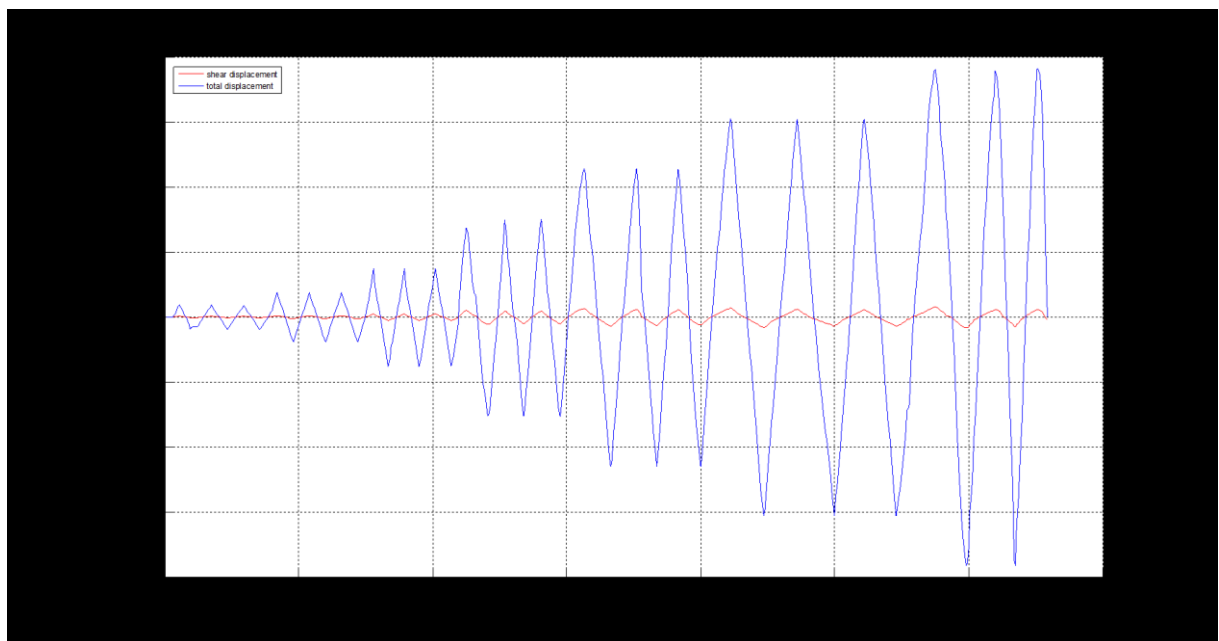


Figure 81 - Total vs displacement due to shear strain.

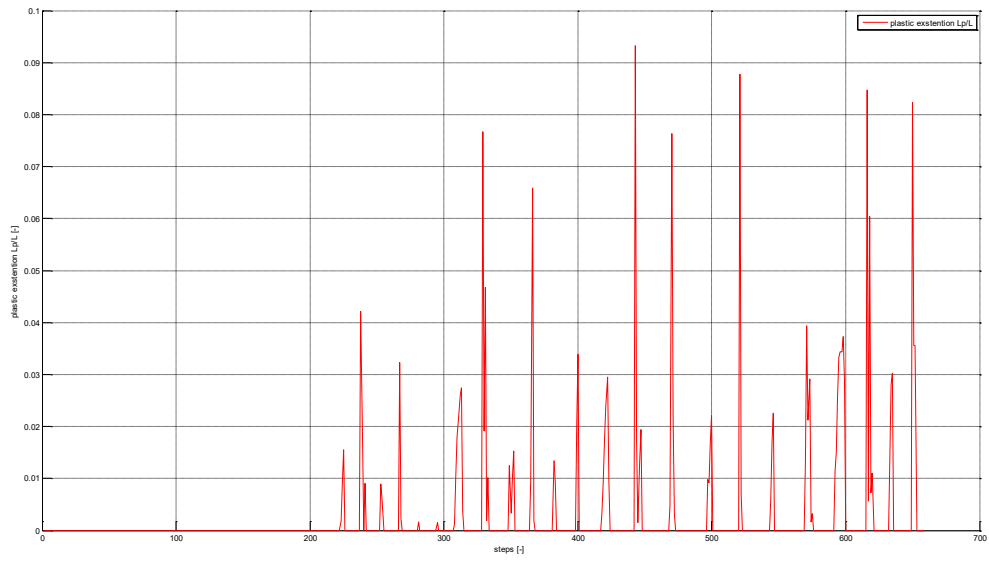


Figure 82 – Inelastic dimensionless extension zone time history.

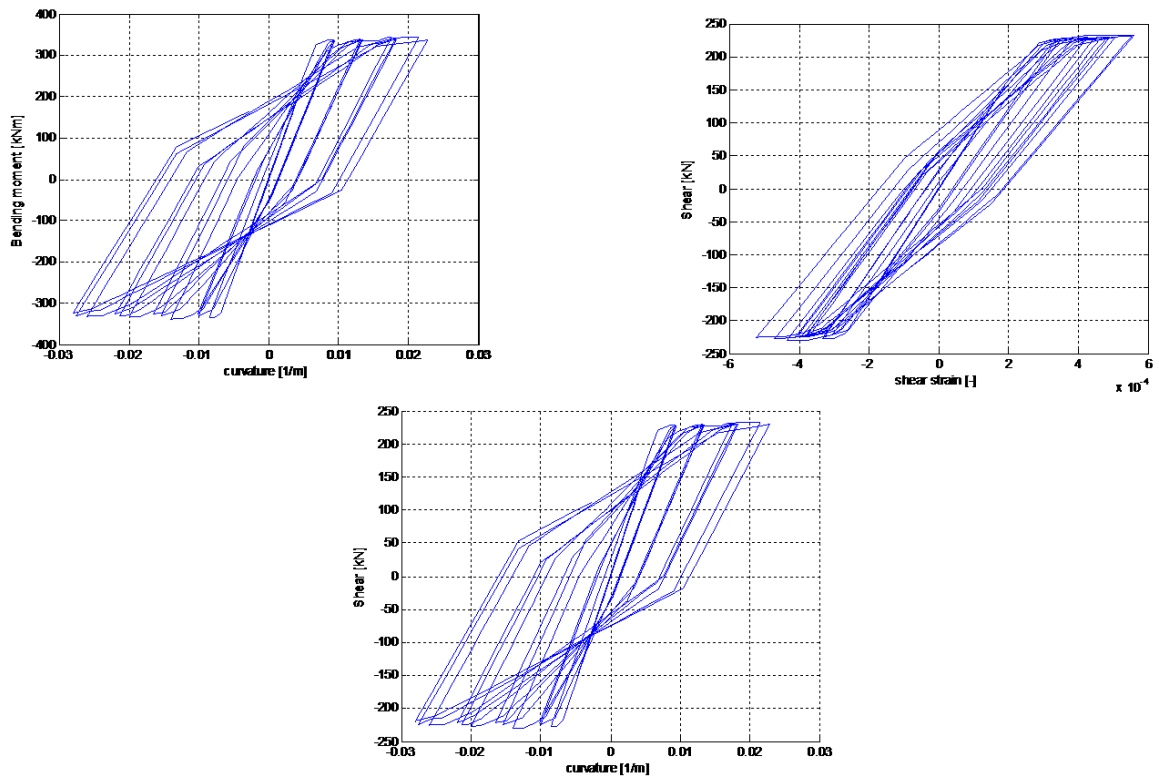


Figure 83 – Hysteretic loops quantity.

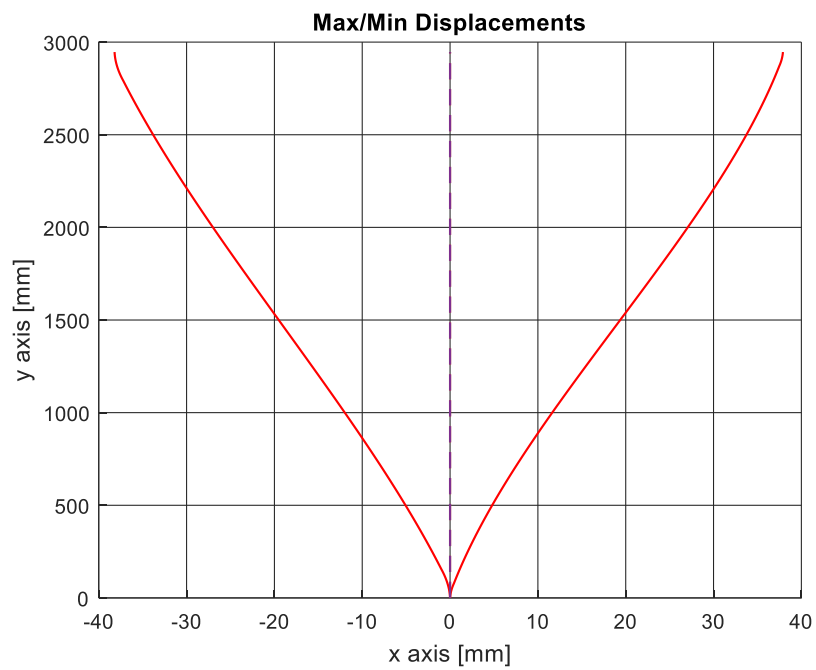


Figure 84 – Displacement functions along the element $u(\xi)$.

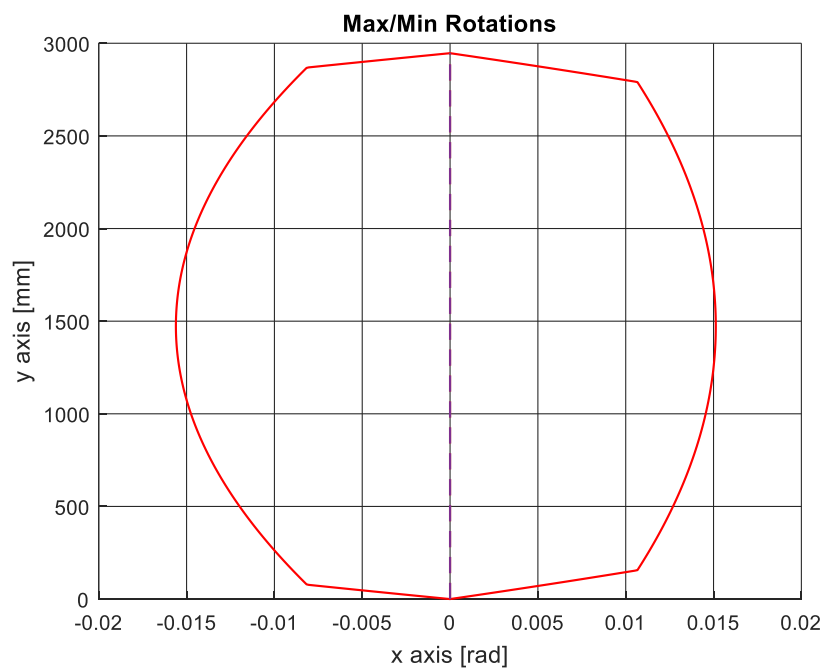


Figure 85 – Rotation functions along the element $\varphi(\xi)$.

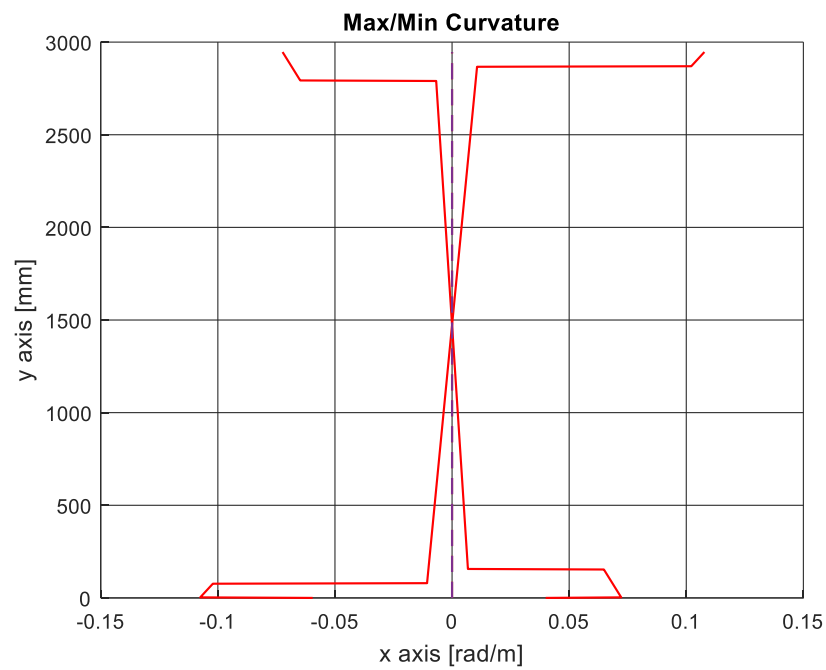


Figure 86 – Curvature functions along the element $\chi(\xi)$.

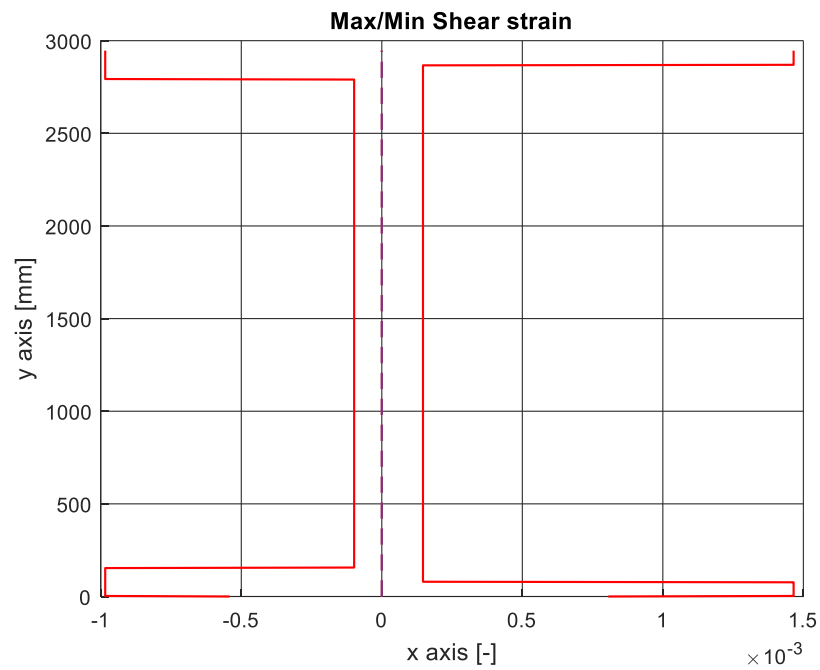


Figure 87 – Shear strain functions along the element $\gamma(\xi)$.

7.2.2 Dazio 2009

The second test considered is one of the columns studied by Dazio 2009 [DBB09] (Figure 88- Figure 91).

The shear aspect ratio is equal to:

$$\frac{M}{V D} = \frac{4560}{2000} = 2.28$$



Figure 88 – Setup of Dazio 09 [DBB09].

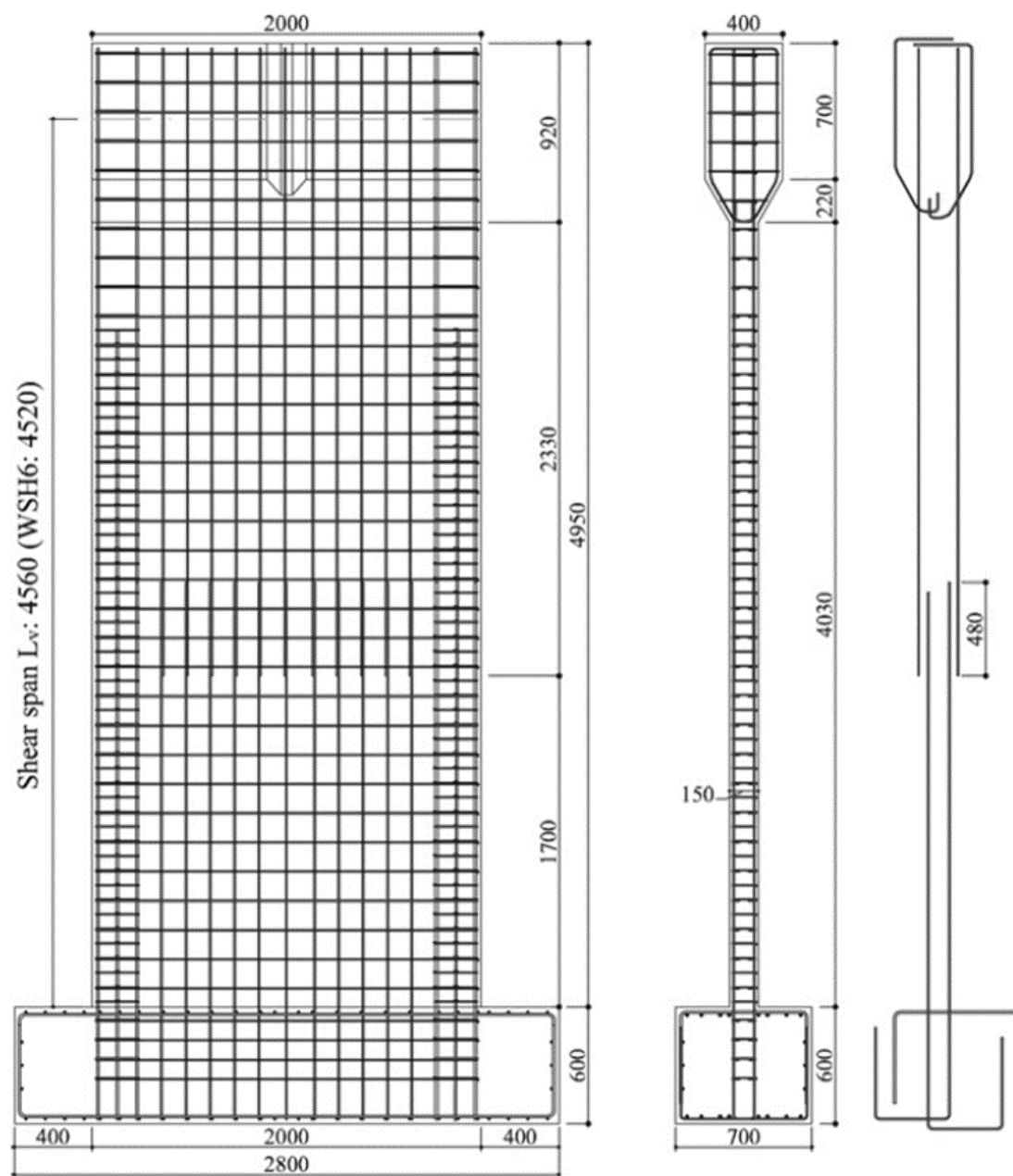


Figure 89 - Longitudinal reinforcement details [DBB09].

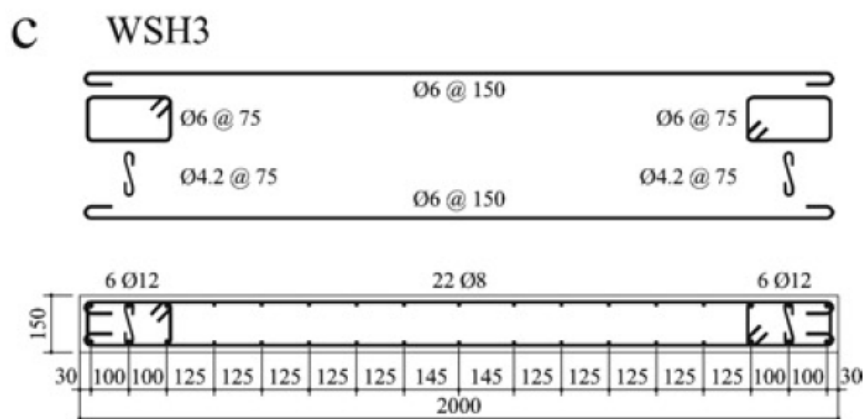


Figure 90 - Transversal reinforcement details of WSH3 [DBB09].

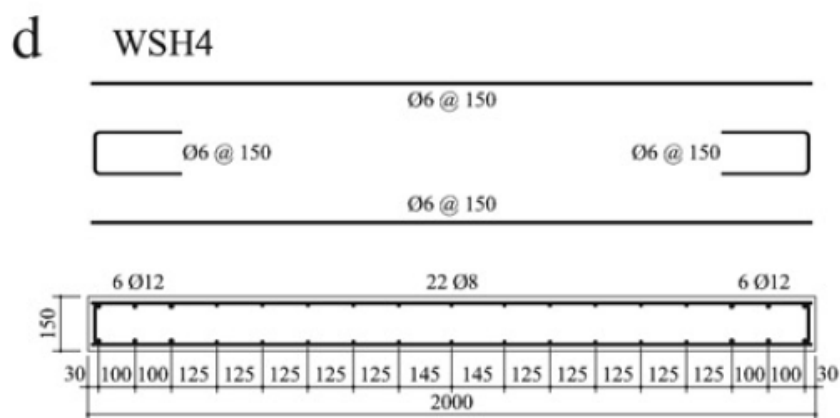


Figure 91 - Transversal reinforcement details of WSH4 [DBB09].

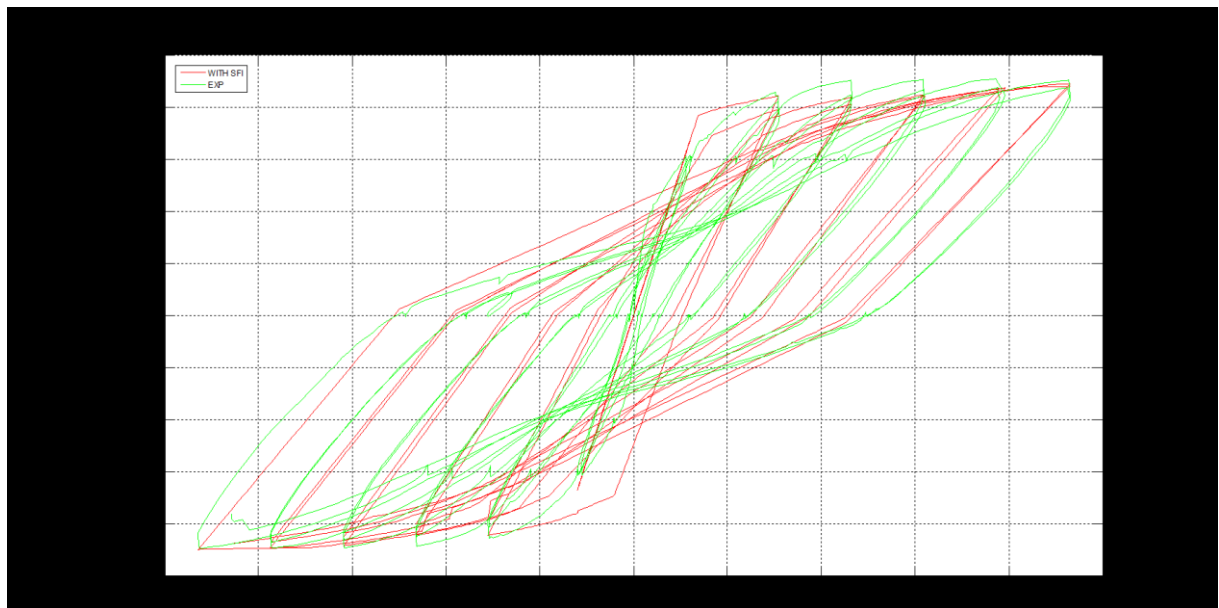


Figure 92 - Force-displacement comparison for WSH3.

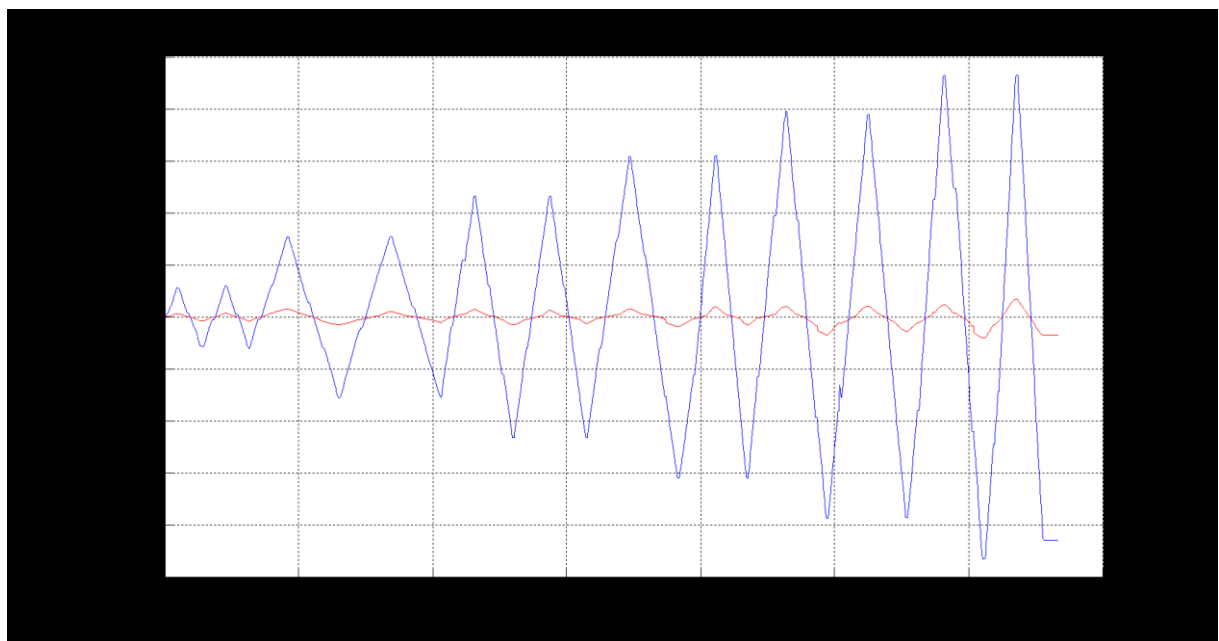


Figure 93 – Total vs displacement due to shear strain for WSH3.

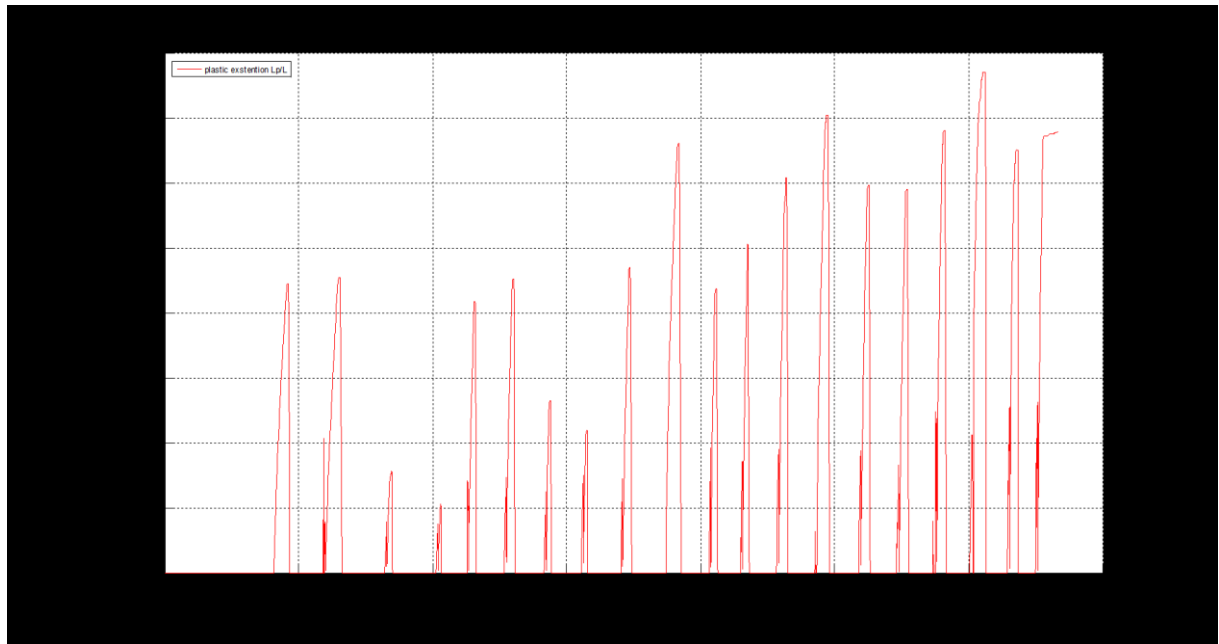


Figure 94 – Inelastic dimensionless extension zone time history for WSH3.

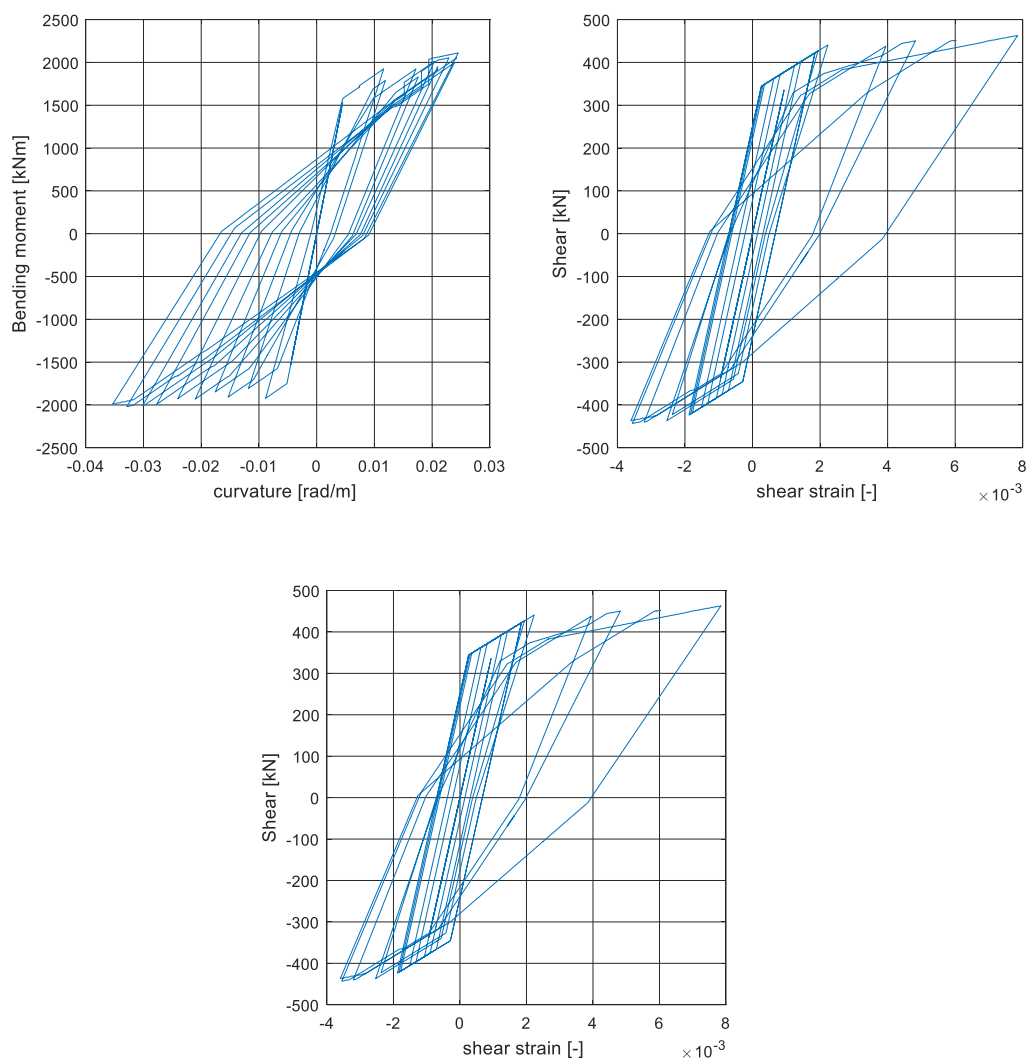


Figure 95 – Hysteretic loops quantity.

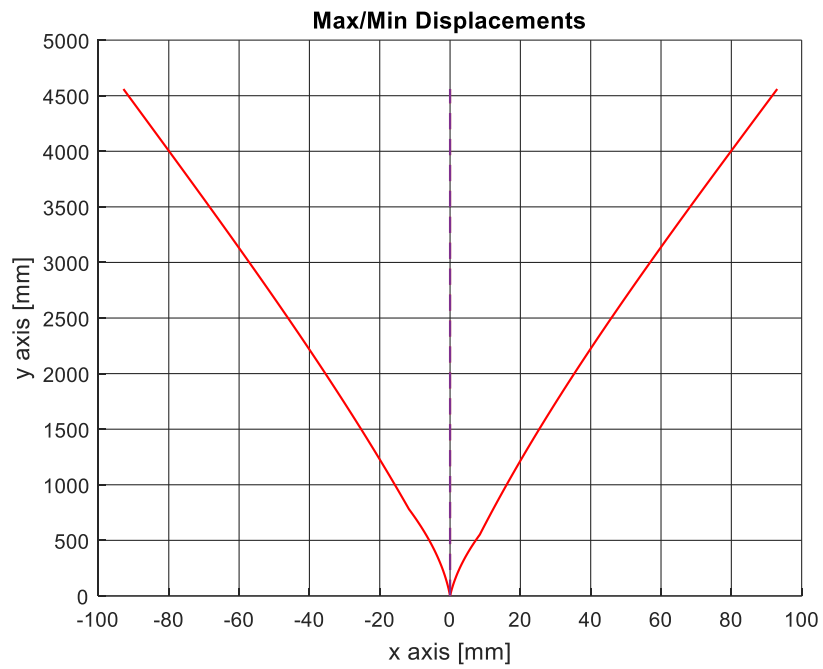


Figure 96 - Displacement functions along the element $u(\xi)$.

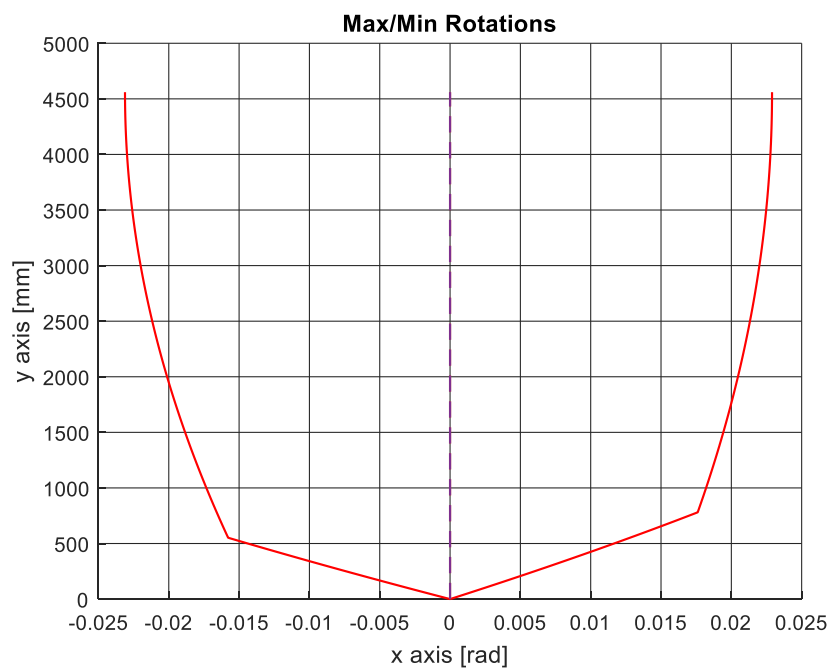


Figure 97 – Rotation functions along the element $\varphi(\xi)$.

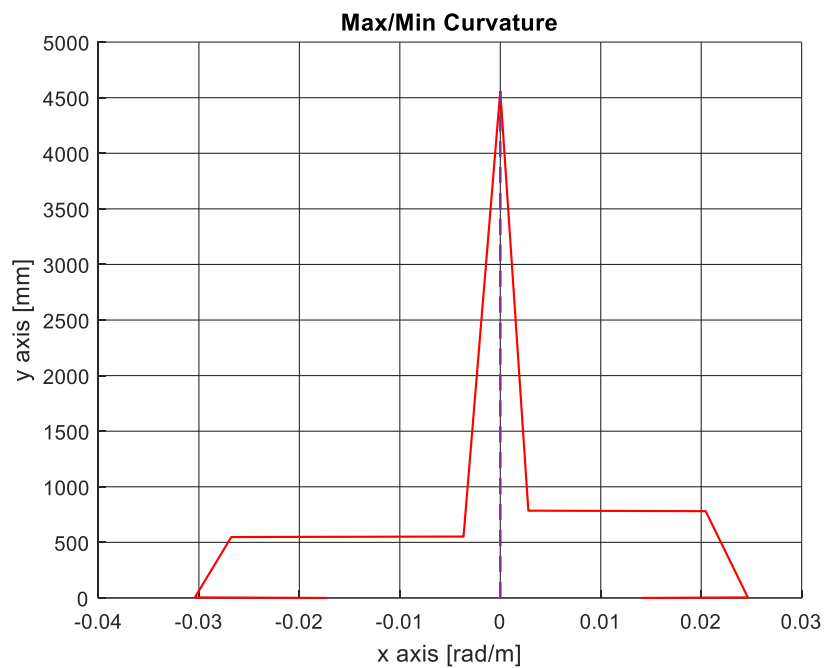


Figure 98 – Curvature functions along the element $\chi(\xi)$.

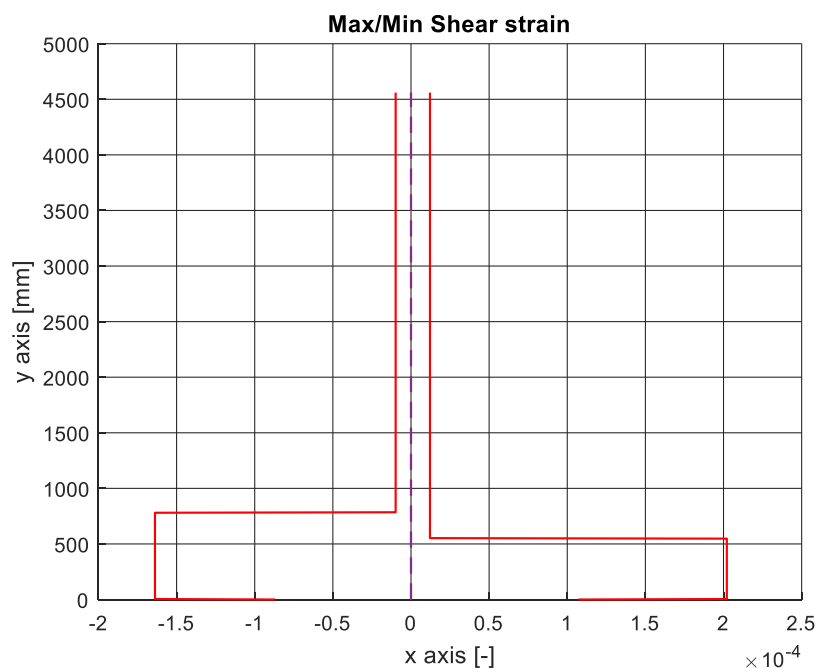


Figure 99 – Shear strain functions along the element $\gamma(\xi)$.

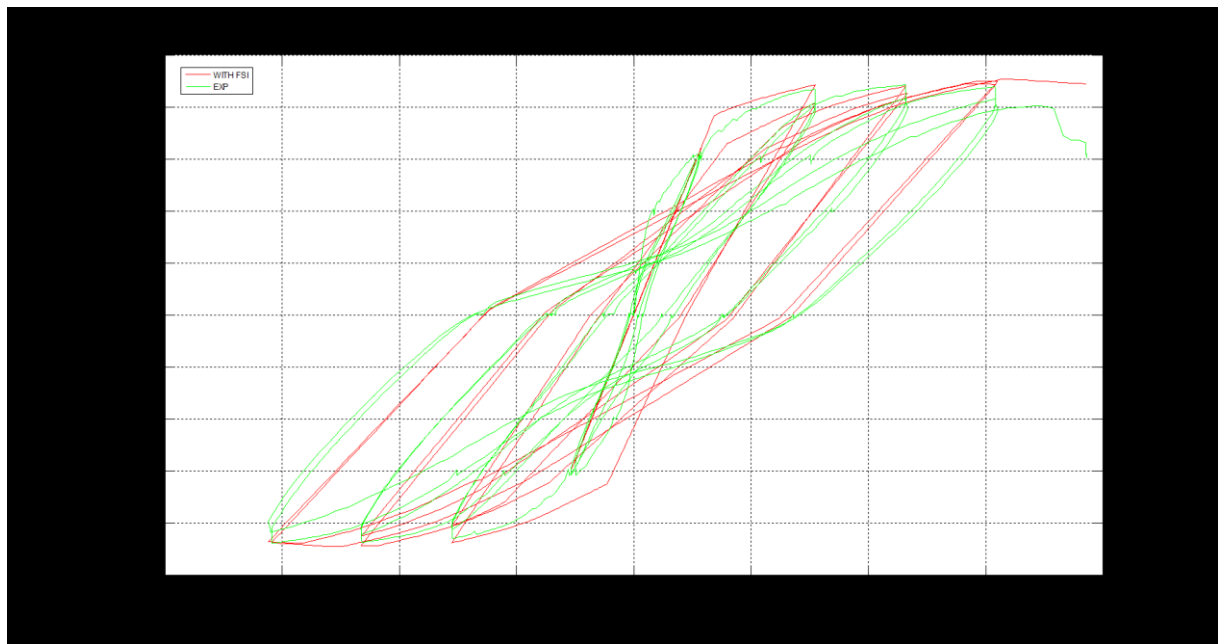


Figure 100 - Force-displacement comparison for WSH4.

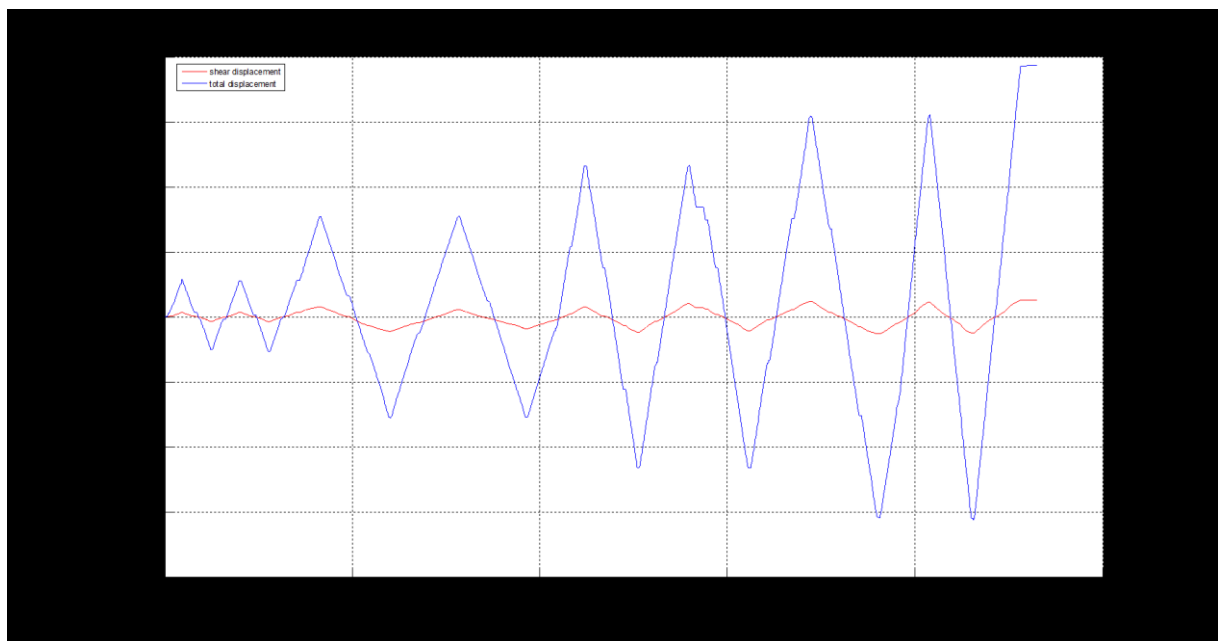


Figure 101 - Total vs displacement due to shear strain for WSH4.

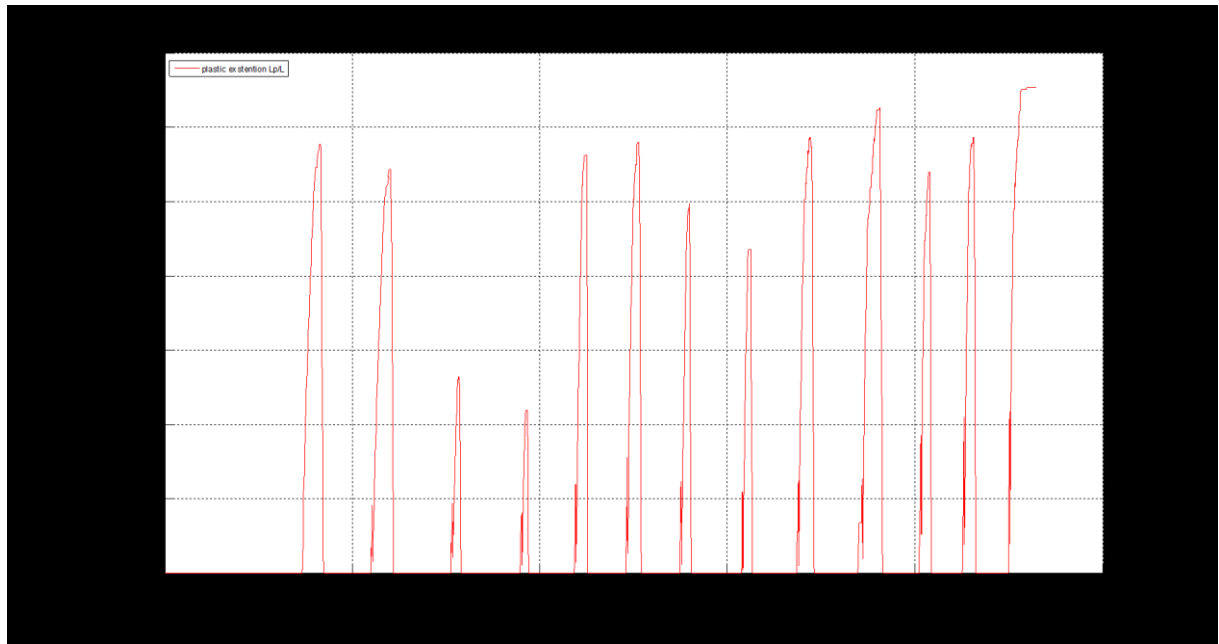


Figure 102 – Inelastic dimensionless extension zone time history for WSH4.

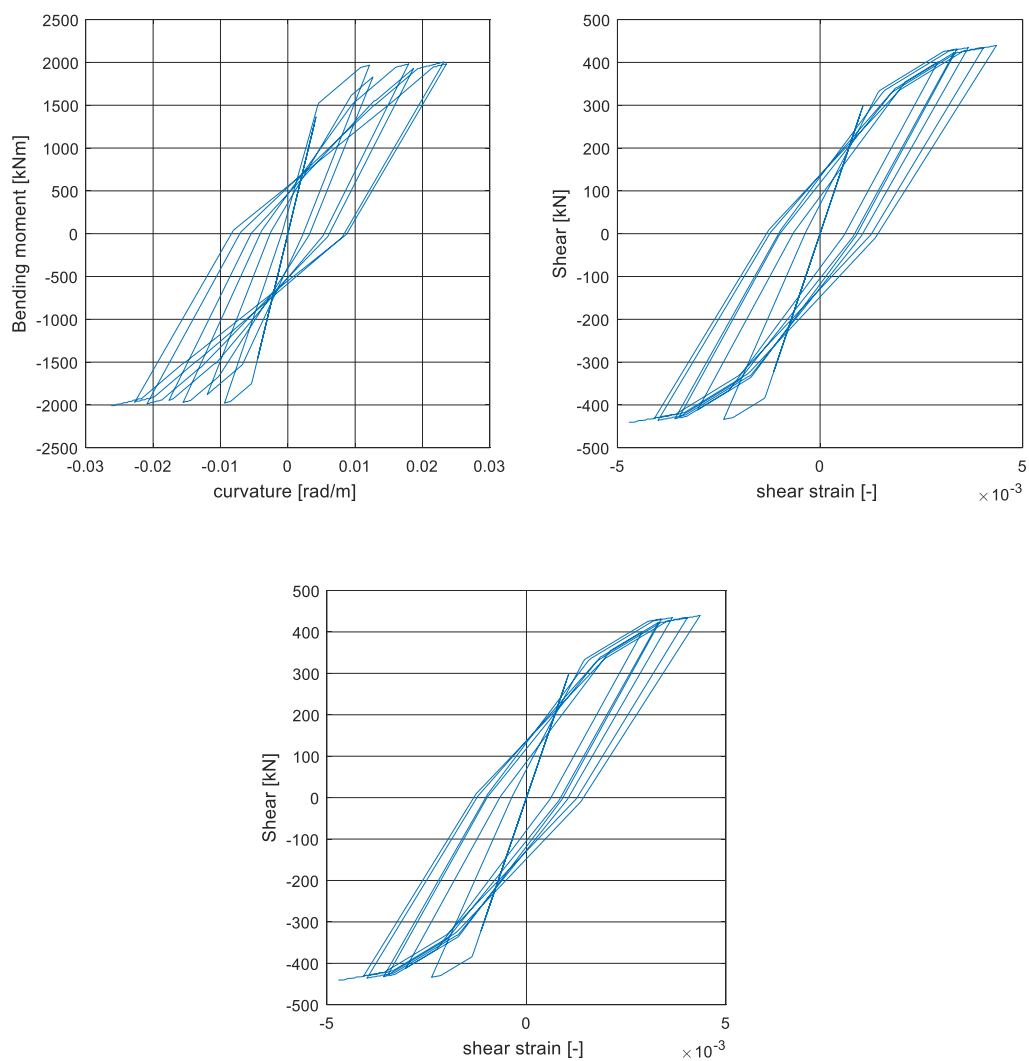


Figure 103 – Hysteretic loops quantity.

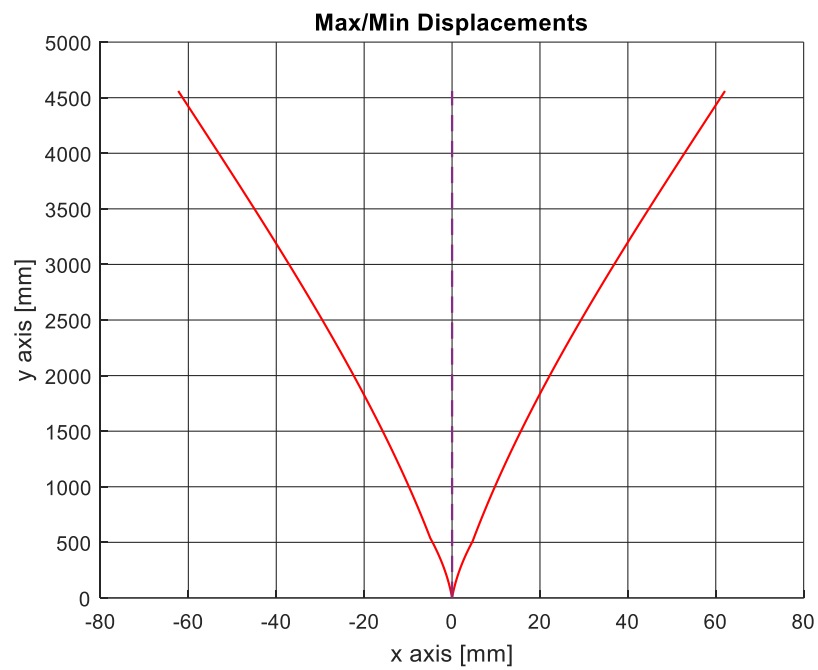


Figure 104 - Displacement functions along the element $u(\xi)$.

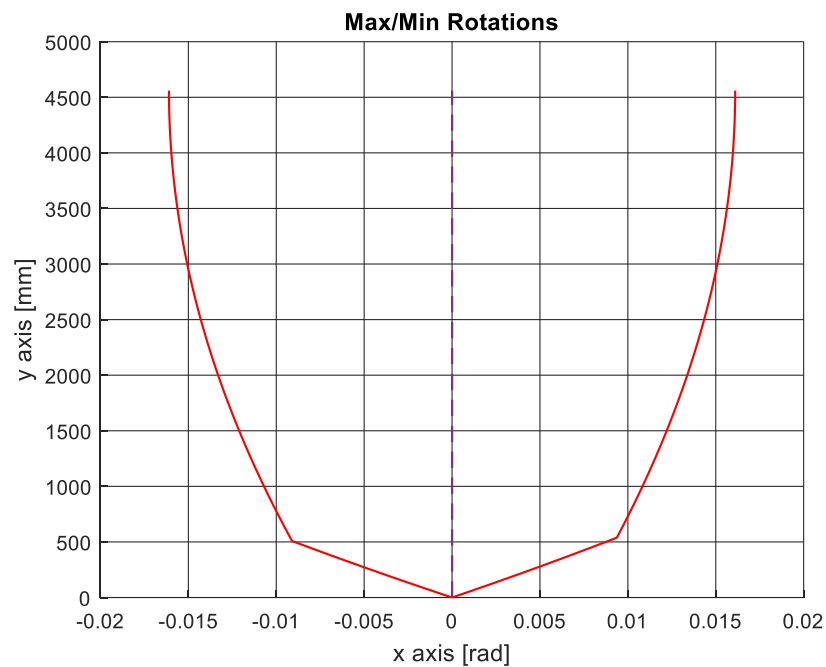


Figure 105 – Rotation functions along the element $\varphi(\xi)$.

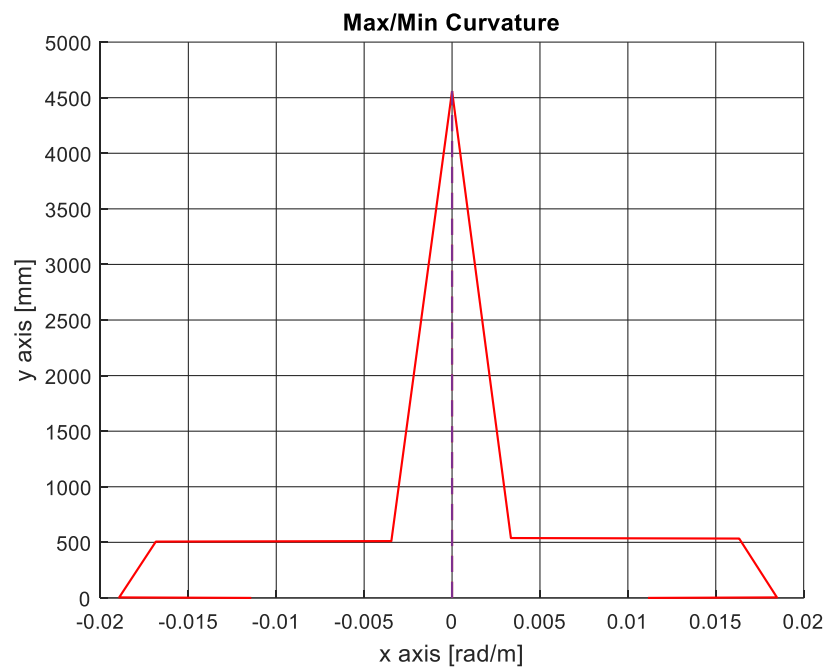


Figure 106 – Curvature functions along the element $\chi(\xi)$.

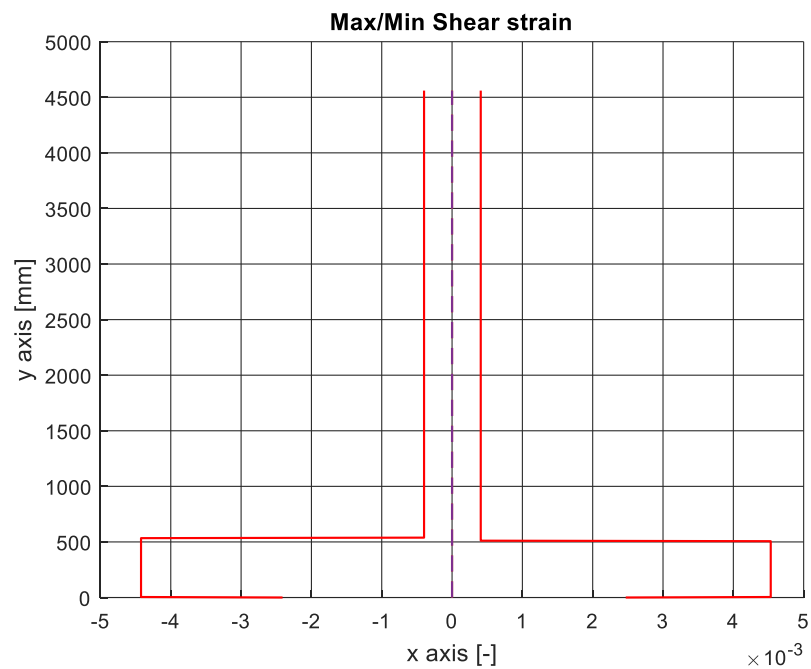


Figure 107 – Shear strain functions along the element $\gamma(\xi)$.

7.2.3 Duong 2007

This single-bay, two-storey frame (Fig. 14a) was tested by Duong et al. at University of Toronto [DSV07]. The frame was subjected to a single loading cycle but only the forward half will be compared. During the experiment, a lateral load was applied to the second storey beam in a displacement controlled fashion, while two constant axial loads of 420 kN each were applied throughout the testing procedure to simulate the axial load effects of upper storeys (Figure 108- Figure 111).

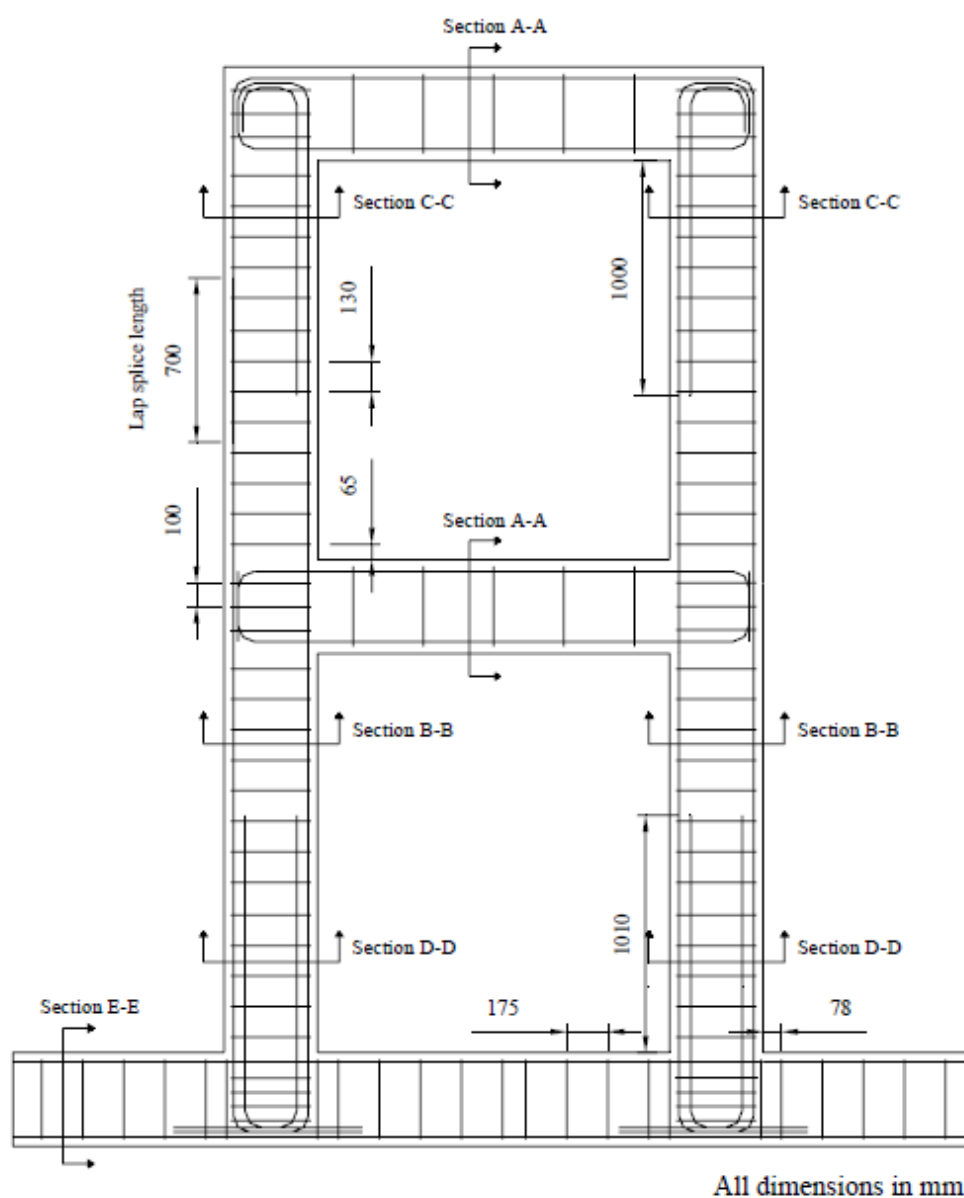


Figure 108 – Frame Reinforcement Layout [DSV07].

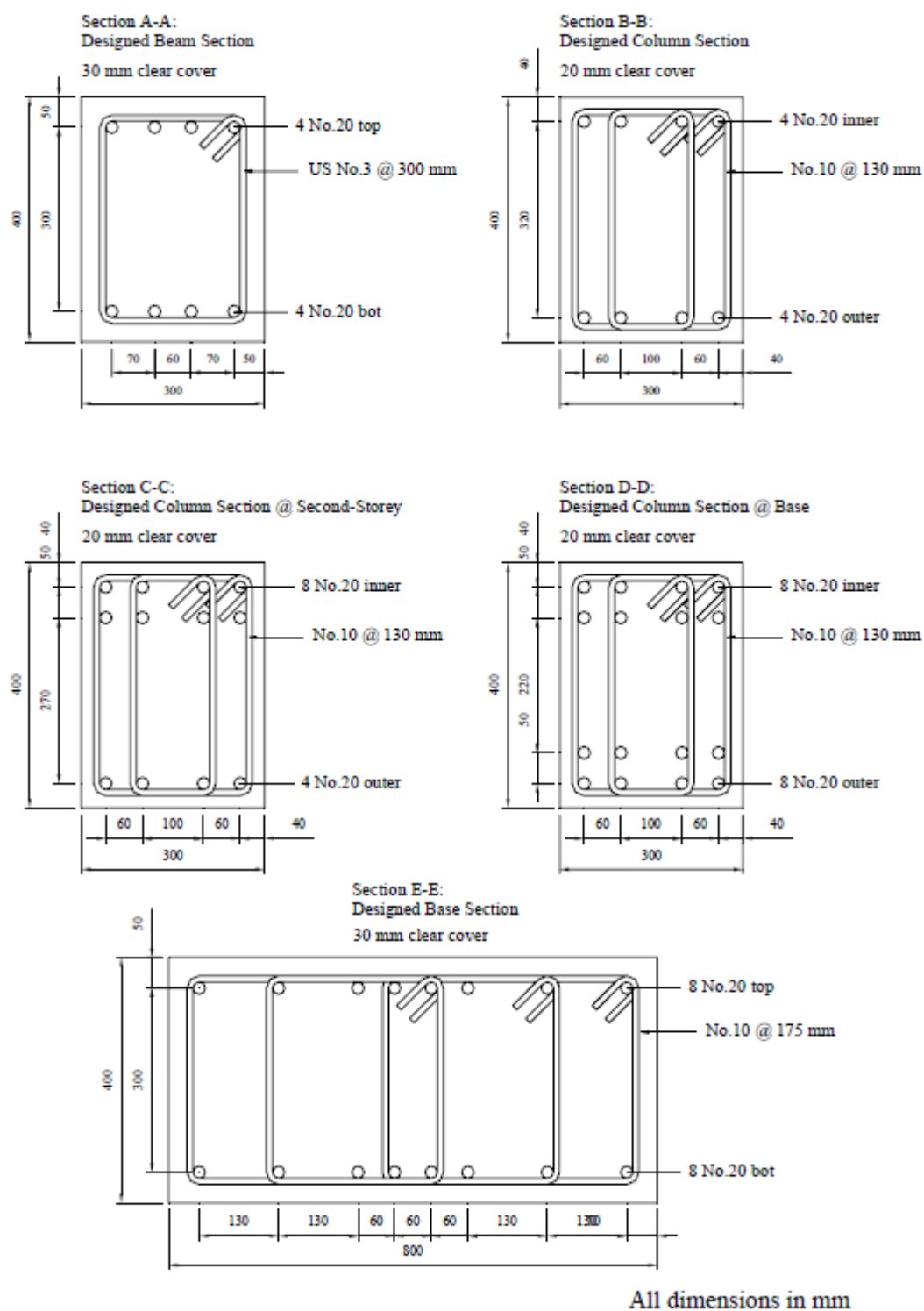


Figure 109 – Designed frame cross-sections [DSV07].



Figure 110 – Full steel and partial formwork assembly [DSV07].



West Elevation



North East Elevation

Figure 111 – Test setup [DSV07].

The Comparison of this test will be conducted in two phases; In the first phase will be considered:

- The numerical solution of the commercial software Midas/Gen with concentrated plasticity with 2 different lengths of the equivalent plastic hinge L_p/L .
- The numerical code solution without considering the FSI.
- The experimental response.

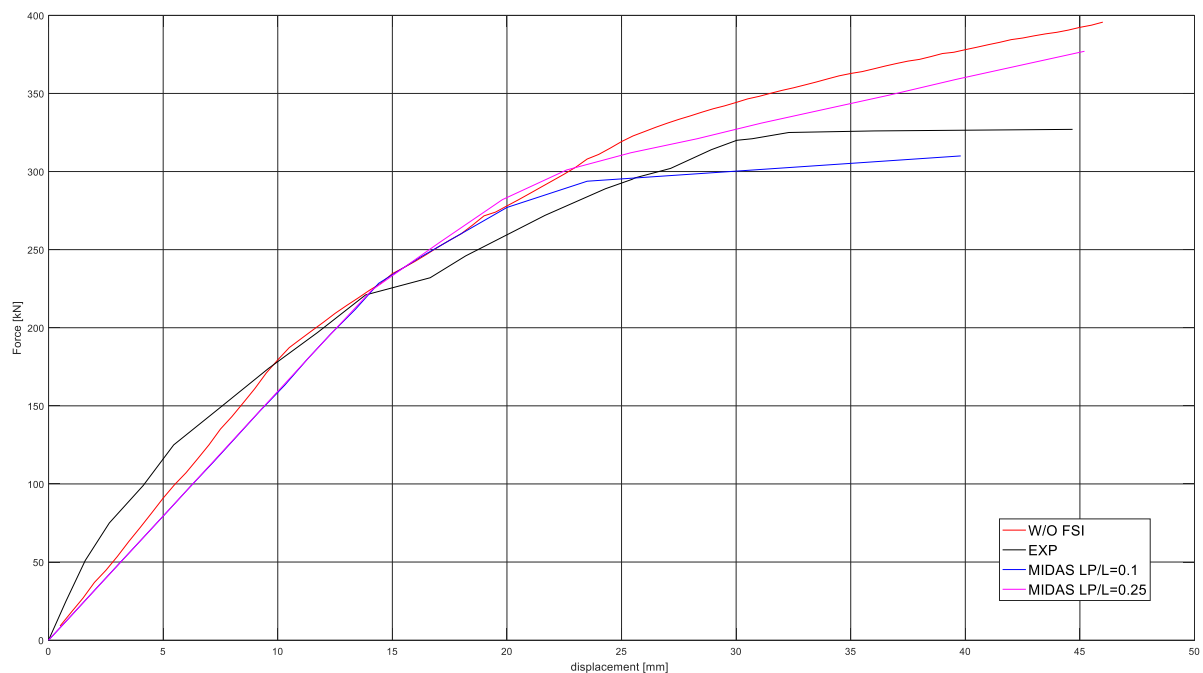


Figure 112 – Force-displacement comparison.

The second phase comprises the following responses:

- The numerical solution of the commercial software Midas/Gen with distributed plasticity.
- The numerical code solution with considering the FSI.
- The experimental response.

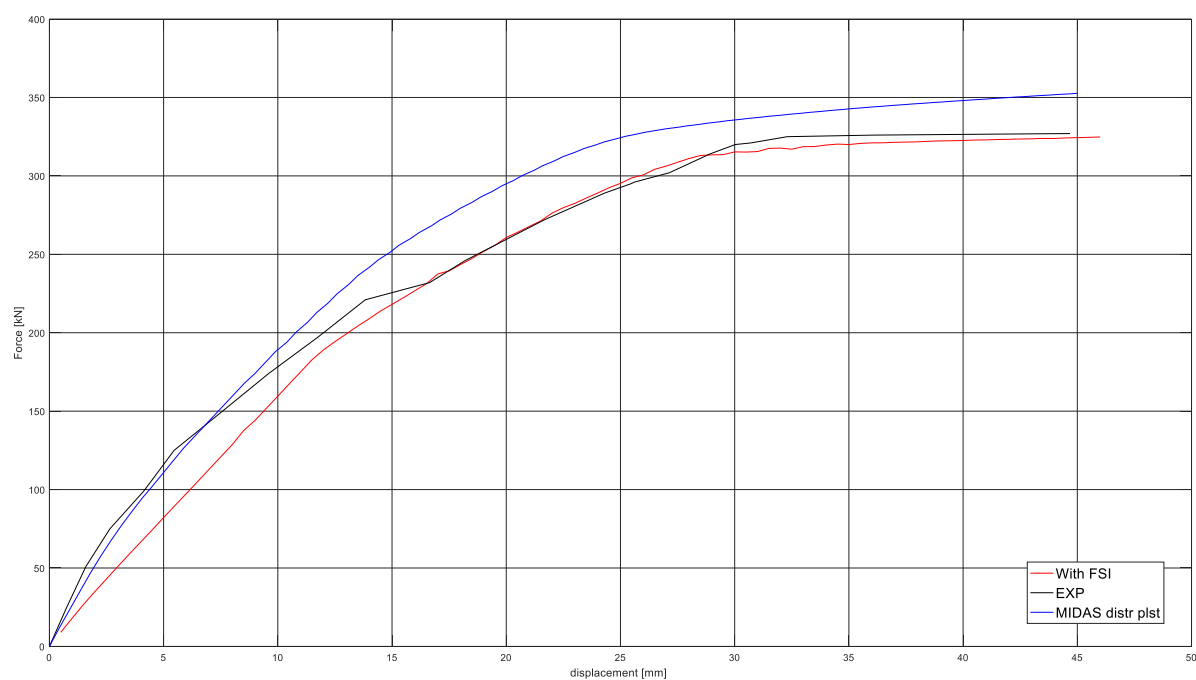


Figure 113 - Force-displacement comparison.

For this second phase, the frame deformed configuration is plotted for different load steps and different extensions of plasticity as shown in Figure 114 to Figure 117.

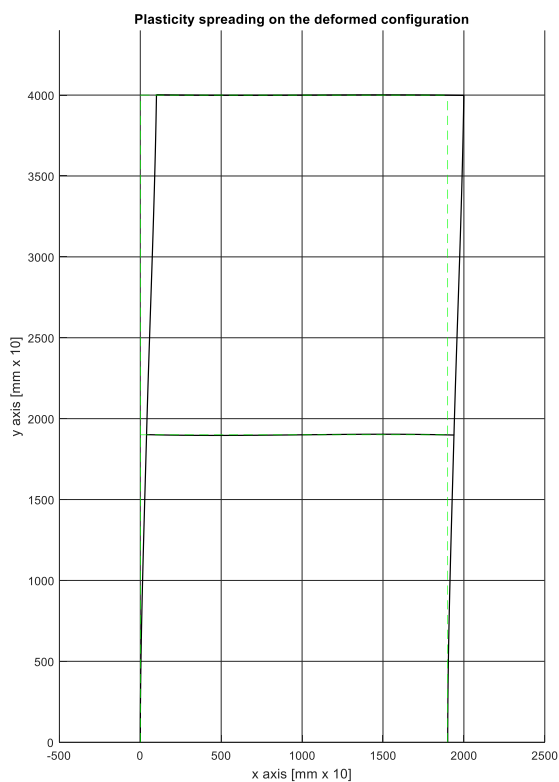


Figure 114 – Load step 40.

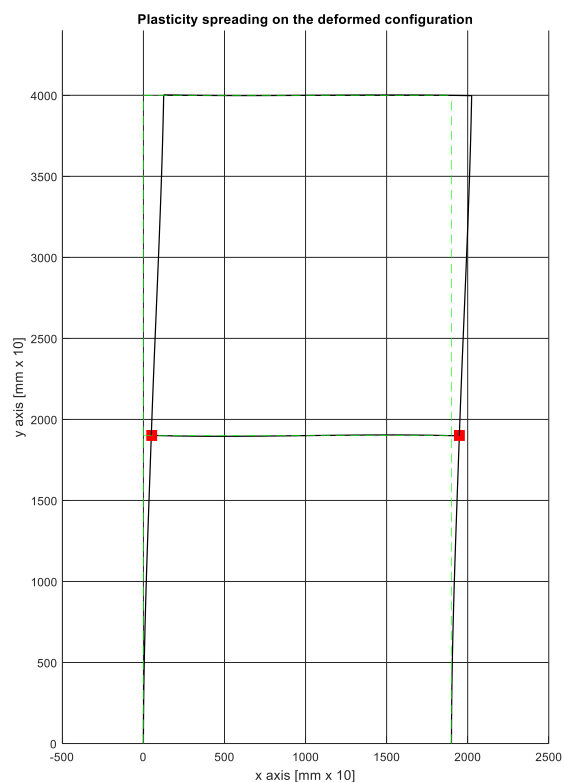


Figure 115 – Load Step 60.

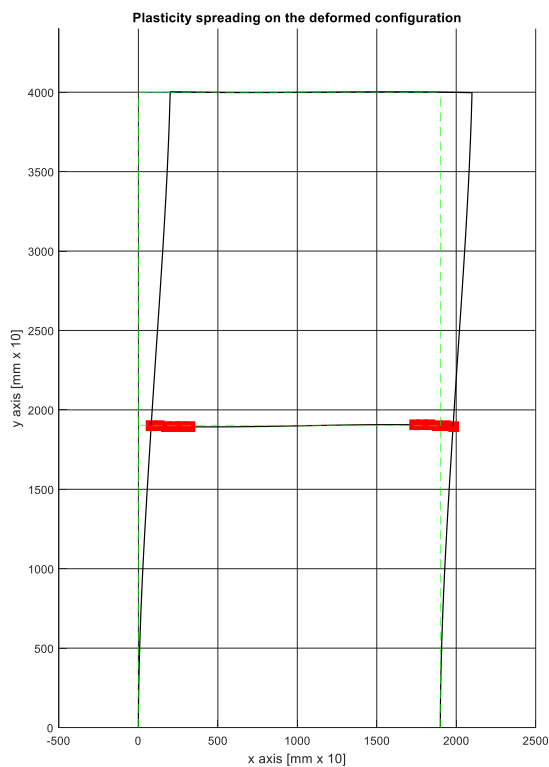


Figure 116 – Load step 80.

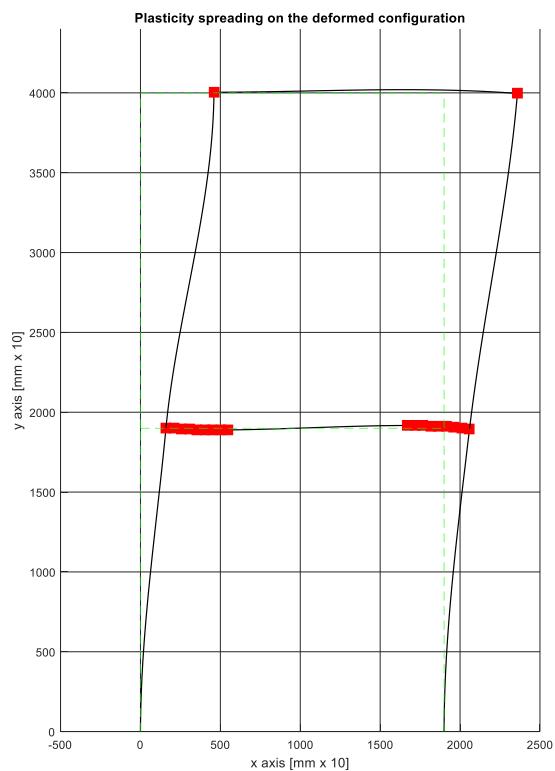


Figure 117 – Load step 92.

It is important to underline that the experimental report confirms that the only member that experienced flexural yielding are the two beam; this fact can be justified considering the great amount of reinforcement in the columns.

Of course, all the members presented flexure and shear cracking with width varying from 0.6 to 4 mm, the beam at the first storey had the wider cracked extension.

The following results are expressed in terms of member diagram and shown both static and kinematic quantities (Figure 118 to Figure 121).

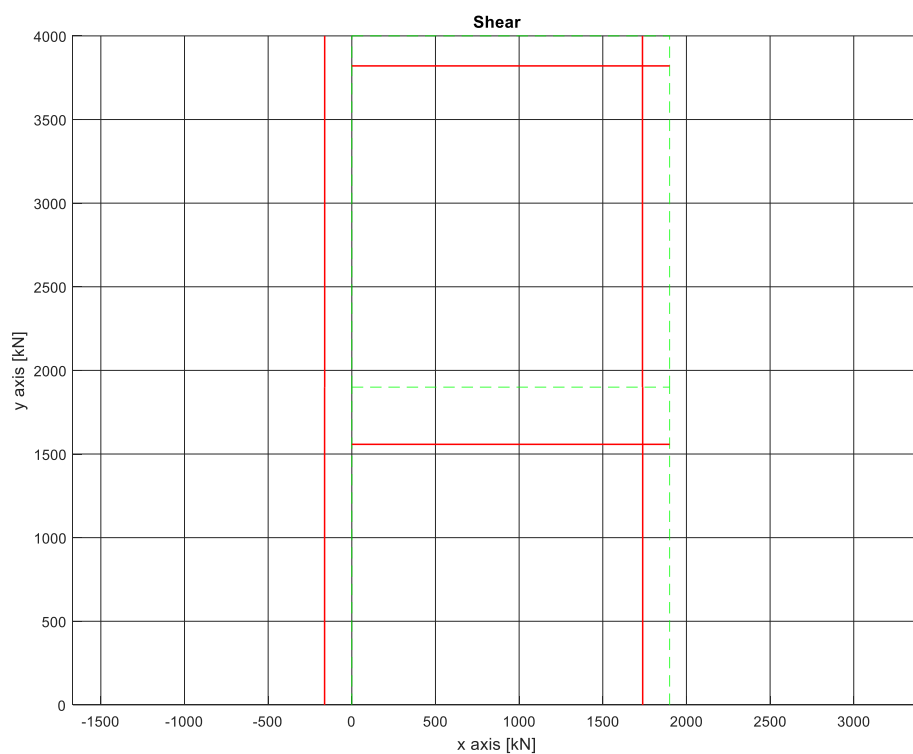


Figure 118 – Shear force diagram.

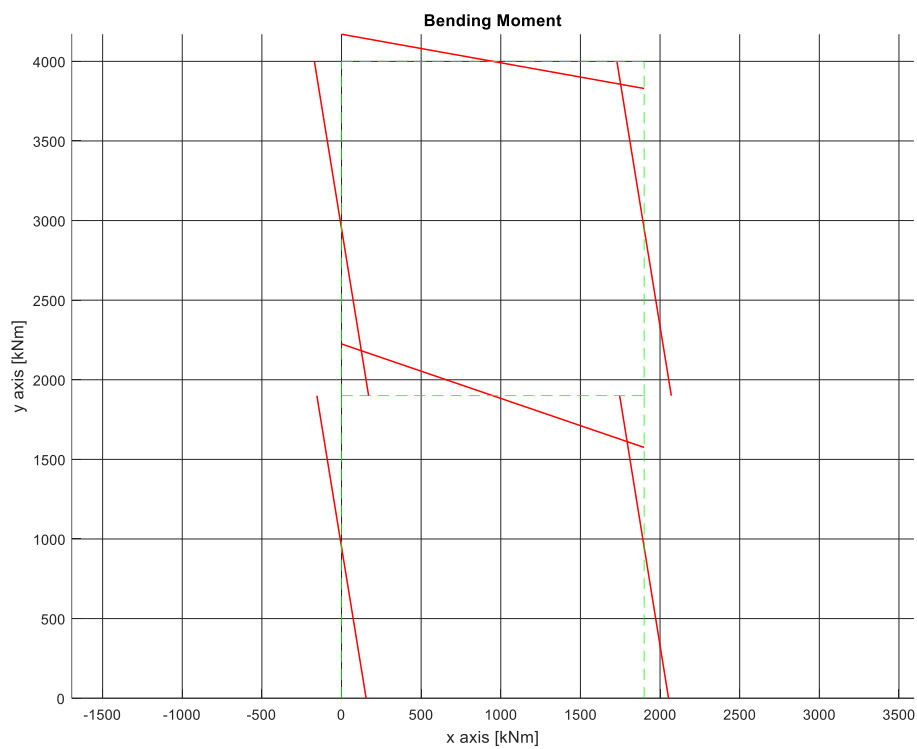


Figure 119 – Bending moment diagram.

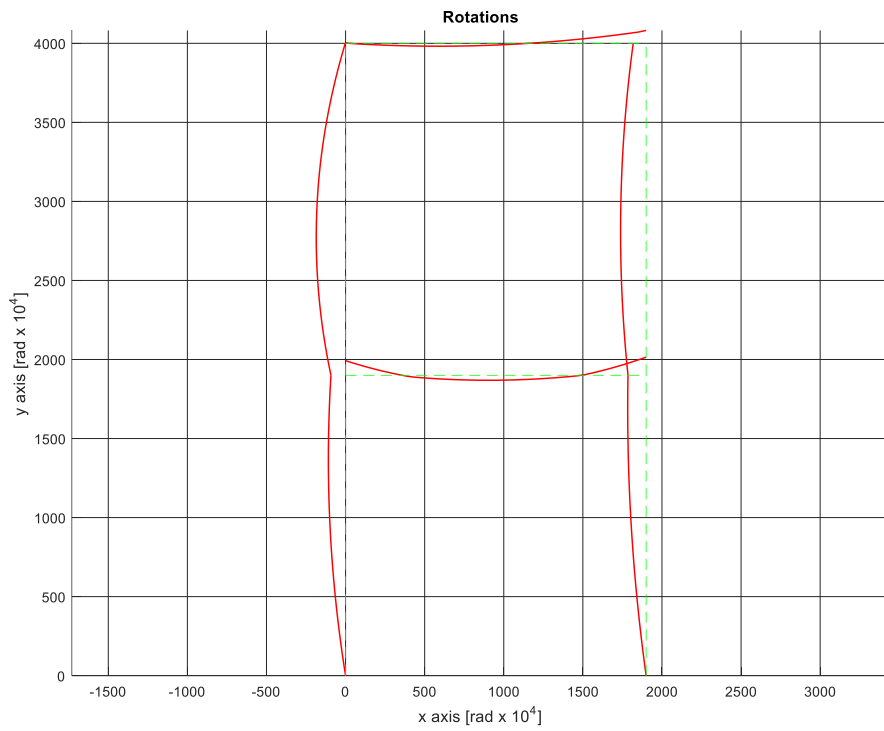


Figure 120 Rotation functions along the element $\phi(\xi)$.

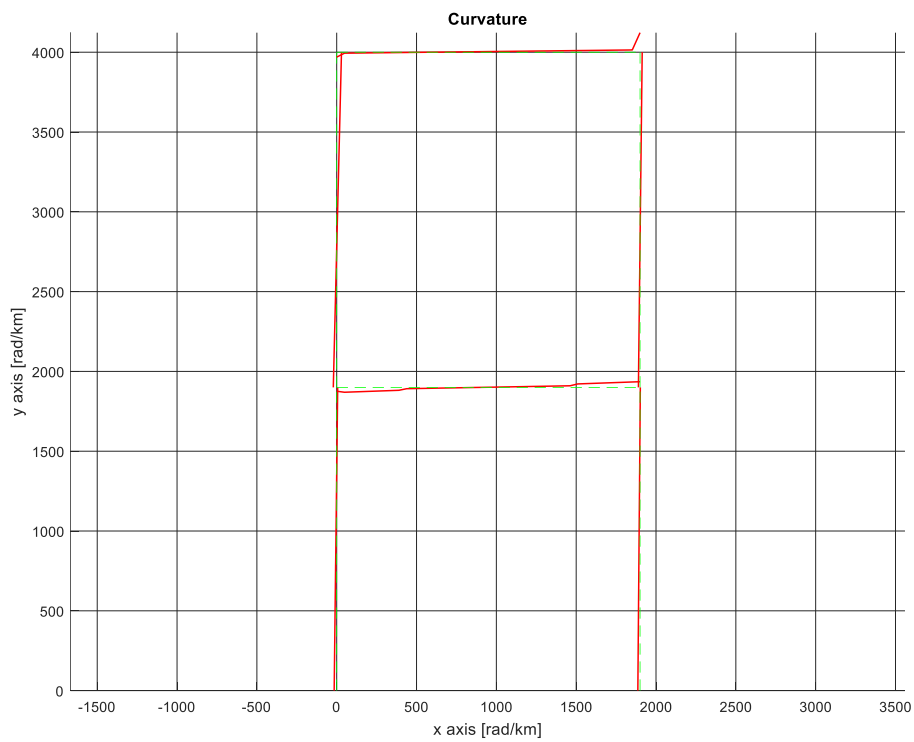


Figure 121 – Curvature functions along the element $\chi(\xi)$.

8 CONCLUSIONS

The spread plasticity approach is a great evolution of the concentrated plasticity models, and as such helps to improve results especially in cyclic non-linear analysis.

A distributed plasticity model with a fiber discretization has the advantage to be self consistent from a P - M_z - M_y interaction but the model computational complexity, especially in the case of accounting for flexure-shear interaction, is a disincentive in terms of its implementation in other structural analysis packages. In fact, the stress state and the materials fiber constitutive matrix must be numerically evaluated for each fiber and for each load step. From this point of view the spread plasticity model has a convenient computational cost, because the constitutive laws are expressed in terms of sectional quantities.

The spread plasticity model is classically formulated using the principle of virtual work in order to determine the element flexibility matrix and this is equivalent to imposing equilibrium in the nodes (in the solution the stiffness matrix is used). As in every finite element method, the outputs that are obtained are nodal quantities and it is not always possible to know what happens within the nodes. The stress recovery phase is in fact quite complex and also knowing the kinematic quantities (displacement, rotations, curvature and shear strain) within the finite element beyond the elastic limit is not in general obtainable. Hence, there are alternatives methods that are not using the principle of virtual work, the one presented in section 6.1.1 makes use of the theory of distributions to solve the Timoshenko beam differential equations that directly govern the structural problem.

In other words adopting only Heaviside's distributions functions to model abrupt, both flexural and shear, stiffness discontinuities of the beam (see equations (6.2)) , it is possible to lead to the exact closed-form solution because it is based on the differential equation associated (strong formulation). This alternative approach is the base of the proposed finite element.

The advantages of using this kind of approach are multiples; for example, the number of segments in which the development of plastic deformation is allowed are arbitrary (without adding nodes). This implies the possibility to have a plastic deformation not only in the extremal segments of the element as in the case of the classic spread plasticity approach.

The effects of distributed loads can be taken into account explicitly, without using the concept of equivalent nodal forces. All the static and kinematic quantities are known through the entire domain; see for example equations (6.8), (6.9), (6.13) and (6.14).

The new frame element is composed by two sectional constitutive models, one for flexure and one for shear, that can interact by means of an empirical relation that relates curvature demand and shear strength degradation.

The flexure–shear model is verified against experimental tests on RC rectangular columns and walls. Comparisons with experimental results on these shear-sensitive elements shows relatively good agreement.

Nevertheless, numerical complications are encountered, associated to the post-peak strength degradation that it is not fully captured if the shear strength degradation is dominant in the experimental test. Therefore, it seems that both at the element and sectional level additional improvements are required.

In particular, at element level, a linear flexibility distribution (see Figure 37c) instead of a piecewise should be formulated in order to catch in a better way the curvature scattering illustrated in Figure 24. At sectional level, the possibility to integrate also a nonlinear axial constitutive law is under the study, especially considering a coupling with flexure. In fact, so far the considered benchmarks have an axial load kept constant throughout the experimental test. Finally, it is recognized that further work and developments are still very much required with the intention to find a more consistent sectional constitutive laws capable to couple flexure, shear and axial load.

REFERENCES

- [AF66] Armstrong, P. J. and Frederick, C. O., “A Mathematical Representation of the Multiaxial Bauschinger Effect”. CEGB Report, RD/B/N731, Berkeley Nuclear Laboratories, 1966.
- [AU03] Auricchio F. Nonlinear finite element analysis. Class Notes, ROSE School, Pavia, Italy, 2003.
- [AW86] Al-Haddad MS, Wight JK. “Feasibility and consequences of moving beam plastic hinging zones for earthquake resistant design of R/C buildings.” Report No. UMCE 86–1. The University of Michigan, Ann Arbor, Michigan, 1986.
- [BC05] Biondi B., Caddemi S., 2005. “Closed form solutions of Euler- Bernoulli traves with singularities”. *International Journal of Solids and Structures* 42, 3027–3044.
- [BC07] Biondi B., Caddemi S., 2007. “Euler–Bernoulli beams with multiple singularities in the flexural stiffness”, *European Journal of Mechanics A/Solids* 26 (2007) 789–809.
- [BO85] Bazant, Z. P. and Oh, B. H. “Microplane model for progressive fracture of concrete and rock,” *Journal of Engineering Mechanics*, ASCE 111(4), 559–582, (1985).
- [CBW65] Clough, R.W., Benuska, K.L. and Wilson, E.L. (1965). "Inelastic Earthquake Response of Tall Buildings", *Proceedings, Third World Conference on Earthquake Engineering*, New Zealand, Vol. 11, New Zealand National Committee on Earthquake Engineering.
- [CCC13] Caddemi, S., Calì, I., Cannizzaro, F. “Closed-form solutions for stepped Timoshenko beams with internal singularities and along-axis external supports”, *Arch. Appl. Mech.* 83(4), pp 559–577 (2013).
- [CCCR13] Caddemi, S., Calì, I., Cannizzaro, F. & Rapicavoli D. “A novel beam finite element with singularities for the dynamic analysis of discontinuous frames”, *Arch. Appl. Mech.* 83 (10), pp. 1451-1468 (2013).
- [Ced08] Cedolin L. :” Handouts of the course “Structural Design” at the Polytechnic of Milan, Milan, Italy, 2008.

- [CF06] Christopoulos, C. and Filiatrault, A.: “Principles of Passive Supplemental Damping and Seismic Isolation”, IUSS Press, Pavia, 480pp, 2006.
- [Che68] Cheung Y. K.: “The Finite Strip Method in the Analysis of Elastic Plates with two Opposite Simply Supported Ends”, Proc. Inst. Civ., England, 1968.
- [CJ65] Clough RW, Johnston SB. “Effect of stiffness degradation on earthquake ductility requirements.” In Transactions of Japan earthquake engineering symposium p. 227–232, Tokyo; 1966.
- [CM97] Collins, M.P., and Mitchell, D. (1991), Prestressed Concrete Structures, Prentice-Hall, Inc., Englewood Cliffs, N.J., pp. 766; 1997.
- [CNTC08] Ministero delle Infrastrutture e dei Trasporti: “Circolare 2 febbraio 2009, n. 617. Istruzioni per l'applicazione delle «Nuove norme tecniche per le costruzioni» di cui al decreto ministeriale 14 gennaio 2008. (GU n. 47 del 26-2-2009 - Suppl. Ordinario n.27)”, GAZZETTA UFFICIALE Serie generale - n. 47, Roma, Italy, 447 pp, 2009.
- [DSV07] Duong KV, Sheikh FJ, Vecchio F. Seismic behaviour of shear critical reinforced concrete frame: experimental investigation. ACI Struct J 2007;104(3):304–13.
- [Cok+02] Cook R. D., Malkus D. S. , Plesha M. E., Witt R. J.: “Concepts and Applications of Finite Element Analysis”, John Wiley & Sons Inc., Madison, University of Wisconsin, 2002.
- [CPP07] Ceresa, P.; Petrini, L.; Pinho, R. “Flexure-shear fiber beam-column elements for modeling frame structures under seismic loading - State of the art”, Journal of Earthquake Engineering, bf 11:46-88, 2007.
- [CPPS09] Ceresa, P.; Petrini, L.; Pinho, R. and Sousa, R. “A fibre flexure-shear model for seismic analysis of RC-framed structures”, Earthquake Engineering and Structural Dynamics, 38: 565-586, 2009.
- [DBB09] Dazio, A., Beyer, K., Bachmann, H., ”Quasi-static cyclic tests and plastic hinge analysis of RC structural walls”. Engineering Structures, Volume 31, Issue 7, Pages 1556–1571, July 2009.
- [Dol+10] Dolce, M., Ponzo, F.C., Di Cesare, A., Arleo, G: ”Progetto di edifici con isolamento sismico” , IUSS Press, Pavia, 210pp, 2010.
- [EC02_1] EN 1992-1-1:2004. Eurocode 2 : “Design of concrete structures”. Part 1-1: General rules and rules for buildings. CEN.
- [EC02_2] EN 1992-2:2006. Eurocode 2 : “Concrete bridges”. Part 2: Design and detailing rules. CEN.
- [EC08_1] EN 1998-1:2005. Eurocode 8 : “Design of structures for earthquake resistance”. Part 1: General rules, seismic actions and rules for buildings. CEN.

- [EC08_2] EN 1998-2:2005. Eurocode 8 : “Design of structures for earthquake resistance”. Part 2: Bridges. CEN.
- [EC08_3] EN 1337-3:2005. Eurocode 8 : “Structural bearings”. Part 3: Elastomeric bearings. CEN.
- [ECH91] Hambly E. C.: “Bridge Deck Behaviour”, Taylor & Francis, 2nd Edition, London, December 1990.
- [FEMA273] FEMA: “NEHRP guidelines for the seismic rehabilitation of buildings” FEMA 273. Washington D.C.: [Federal Emergency Management Agency], 1997.
- [FPB83] Filippou F.C., Popov E.P., Bertero V.V. "Effects of bond deterioration on hysteretic behaviour of reinforced concrete joints," Report EERC 83-19, Earthquake Engineering Research Center, University of California, Berkeley, 1983.
- [GIB67] GIBERSON, M. F. “The response of nonlinear multi-story structures subjected to earthquake excitation, Earthquake Engineering Research Laboratory” California Institute of Technology, EERL Report, Pasadena, CA, 1967.
- [GPB05] Grant D.N., Blandon C.A., Priestley M.J.N.: “Modelling Inelastic Response in Direct Displacement-Based Design”. Rose School, Report 2005/03, IUSS Press, Pavia, 2005.
- [IDA96] Valles RE, Reinhorn AM, Kunnath SK, Li C, Madan A. “IDARC2D version 4.0: a program for the inelastic damage analysis of buildings.” Technical Report NCEER-96-0010, University at Buffalo, State University of New York, 1996.
- [IW89] Ibrahimbegovic A., Wilson E.L.: “Simple Numerical Algorithms for Mode Superposition Analysis of Discrete System with Non-Proportional Damping”, Journal of Computers and Structures, 33, 523-532, 1993.
- [KP73] Kent, DC Park, R. “Flexural Members with Confined Concrete”, Proceedings ASCE, vol.97, No ST7, July 1971, pp 1969-1990.
- [KR89] Kunnath SK, Reinhorn AM. Inelastic three-dimensional response analysis of reinforced concrete structures subjected to seismic loads. Technical Report No. NCEER-88-0041, University at Buffalo, The State University of New York, 1989.
- [LC78] Loo Y. C., Cunes A. R.: “The Finite Strip Method in Bridge Engineering”, Viewpoint Publication (now E. & F.N. Spon), England, London, 1978.
- [LW03] Lee, J.Y., and F. Watanabe (2003). “Shear Deterioration of Reinforced Concrete Beams Subjected to Reversed Cyclic Loading,” ACI Structural Journal, Vol. 100, No. 4, pp. 480–489.
- [LMMH96] Lynn A, Moehle JP, Mahin S, Holmes W. “Seismic evaluation of existing reinforced concrete building columns”. Earthquake Spectra 1996; 12(4):715–739.

- [LR88] Lee D. J., Richmond B.: “Bridges”, L.S. Blake, Guildford, 1988.
- [MA98] Martinelli, L. [1998] “Modellazione di pile di ponti in C. A. a travata soggetti ad eccitazione sismica,” PhD Thesis, Dipartimento di Ingegneria Strutturale, Politecnico di Milano, Milano, Italy.
- [MB89] Malerba PG, Bontempi F. “Analisi di Telai in Cemento Armato in presenza di non linearità meccaniche e Geometriche”. Studi e ricerche - Politecnico di Milano, 1989.
- [MCPP05] Miranda, P.A. Calvi G.M., Pinho, R., Priestley M.J.N., “Displacement based assessment of rc columns with limited shear resistance”, Rose research report No. 2005/04, IUSS Press, Pavia, 153pp, 2005.
- [MD12] Midas/Gen 2012 ver. 3.1, Integrated Analysis and Design System for Buildings and General Structures.
- [MID15] MIDAS/Civil: ” Analysis for Civil Structures”, Analysis manual.
- [MK08] Mergos, P.E., Kappos, A.J., “A distributed shear and flexural flexibility model with shear–flexure interaction for R/C members subjected to seismic loading”, Earthquake Engng Struct. Dyn. 2008; 37:1349–1370.
- [MK12] Mergos, P.E., Kappos, A.J., “A Gradual Spread Inelasticity Model for R/C Beam-Columns accounting for Flexure, Shear and Anchorage Slip.” Engineering Structures, Vol. 44, pp. 94-106, 2012.
- [MB13] Mergos, P.E., Beyer, K., “Modeling Shear-flexure Interaction in Equivalent Frame Models of Slender RC Walls.” The Structural Design of Tall and Special Buildings, Vol. 23, 1171-1189, 2013.
- [MP73] Menegotto M., Pinto P.E. "Method of analysis for cyclically loaded R.C. plane frames including changes in geometry and non-elastic behaviour of elements under combined normal force and bending," Symposium on the Resistance and Ultimate Deformability of Structures Acted on by Well Defined Repeated Loads, International Association for Bridge and Structural Engineering, Zurich, Switzerland, pp. 15-22, 1973.
- [NTC08] Ministero delle Infrastrutture e dei Trasporti: “Nuove norme tecniche per le costruzioni”, GAZZETTA UFFICIALE Serie generale - n. 30, Roma, Italy, 2008.
- [OTA80] Otani S., “Nonlinear dynamic analysis of reinforced concrete building structures” Canadian Journal of Civil Engineering 1980; 7(2):333–44.
- [OTA81] Otani, S., “Hysteresis models of reinforced concrete for earthquake response analysis” Journal of the Faculty of Engineering, University of Tokyo, Series B Volume 36, Issue 2, Pages 407-441, September 1981.
- [PCK07] Priestley M.J.N., Calvi G.M., Kowalsky M.J.: “Displacement- Based Seismic Design of Structures”. IUSS Press, Pavia, Italy, 2007.

- [Po75] POWELL, G. H. 1975. Supplement to computer program DRAIN-2D, Supplement to report, DRAIN-2D user's guide, University of California, Berkeley, CA.
- [PP75] Park R., Paulay T.: "Reinforced Concrete Structures". John Wiley & Sons, 1975.
- [PP92] Paulay T., Priestley M.J.N.: "Seismic Design of Reinforced Concrete and Masonry Buildings". John Wiley & Sons, 1992.
- [PRK87] Park YJ, Reinhorn AM, Kunnath SK. IDARC: Inelastic damage analysis of reinforced concrete frame-shear wall structures. Technical Report No. NCEER- 87-0008, University at Buffalo, The State University of New York; 1987.
- [PSC96] Priestley, M.J.N., Seible, F. Calvi, G. M. "Seismic Design and Retrofit of Bridges" , Wiley, New York, 1996, 686 pp.
- [RAP12] Rapicavoli, D. "L'uso delle funzioni generalizzate per la formulazione di elementi finiti di travi non omogene ed inelastiche", PhD Thesis, Dipartimento di Ingegneria Civile, Università degli Studi di Catania, Catania, Italy, 2012.
- [RP98] Ranzo G, Petrangeli M. A fibre finite beam element with section shear modelling for seismic analysis of RC structures. *Journal of Earthquake Engineering* 1998; 2:443–473.
- [RRL12] Roh H, · Reinhorn ·AM, Lee JS. Power spread plasticity model for inelastic analysis of reinforced concrete structures *Engineering Structures* 06/2012; 39:148–161.
- [SFT96] Spacone, E.; Filippou, F. C.; and Taucer, F. F., "Fiber Beam-Column Model for Nonlinear Analysis of R/C Frames, Part I: Formulation," *Earthquake Engineering and Structural Dynamics*, V. 25, 1996, pp. 711-725.
- [SM04] Sezen H, Moehle JP. "Shear strength model for lightly reinforced concrete columns". *Journal of Structural Engineering* 2004; 130(11):1692–1703.
- [SM06] Sezen, H., and J.P. Moehle (2006). "Seismic Tests of Concrete Columns with Light Transverse Reinforcement," *ACI Structural Journal*, Vol. 103, No. 6, pp. 842–849.
- [SPP82] Scott B.D., Park R., Priestley M.J.N. "Stress-strain behaviour of concrete confined by overlapping hoops at low and high strain rates," *ACI Journal*, Vol. 79, No. 1, pp. 13-27, 1982.
- [TAK73] Takizawa H. Strong motion response analysis of reinforced concrete buildings. *Concr J Jpn Nat Council Concr* 1973; II(2):10–21.
- [Tro67] Troitsky M.S.: "Orthotropic Bridges: Theory and Design", The James F. Lincoln Arc Welding Foundation, Cleveland, Ohio, 1967.
- [TS76] Takayanagi T, Schnobrich WC. Computed behavior of reinforced concrete coupled shear walls. *Structural Research Series No. 434*, University of Illinois, Urbana, IL; 1976.

- [TW59] Timoshenko S., Woinowsky-Krieger S.: “Theory of plates and shells”, McGraw-Hill, USA, 580 pp, 1959.
- [VC86] Vecchio FJ, Collins MP. The modified compression field theory for reinforced concrete elements subjected to shear. *ACI Journal* 1986; 83(2):219–231.
- [Vec00] Vecchio FJ. Disturbed stress field model for reinforced concrete: formulation. *Journal of Structural Engineering* 2000; 126(9):1070–1077.
- [Vec99] Vecchio FJ. Towards cyclic load modelling of reinforced concrete. *ACI Structural Journal* 1999; 96(2):193–202.
- [VS04] Vecchio, F.J. and Shim, W. “Experimental and Analytical Re-examination of Classic Concrete Beam Tests”, *ASCE J. of Struct. Engrg.*, Vol. 130, No. 3, pp. 460-469, 2004.
- [WJ65] Wen RK, Janssen JG. Dynamic analysis of elasto-inelastic frames. In: *Proceedings of 3rd world conference on earthquake engineering*; 1965. p. 713–29.
- [YS01] Yavari, A., Sarkani, S., 2001. On applications of generalised functions to the analysis of Euler–Bernoulli beam-columns with jump discontinuities. *International Journal of Mechanical Sciences* 43, 1543–1562.
- [YSM00] Yavari, A., Sarkani, S., Moyer, E.T., 2000. On applications of generalised functions to beam bending problems. *International Journal of Solids and Structures* 37, 5675–5705.
- [YSR01] Yavari, A., Sarkani, S., Reddy, J.N., 2001. On nonuniform Euler–Bernoulli and Timoshenko beams with jump discontinuities: application of distribution theory. *International Journal of Solids and Structures* 38, 8389–8406.
- [Zem65] Zemanian, A.H., 1965. *Distribution Theory and Transform Analysis*. McGraw-Hill, New York.